

ADA 028850

AFRPL-TR-76-46

A STUDY OF A NOVEL ADDITIVE FOR HTPB PROPELLANT

FINAL REPORT

J. P. PETERSON
HERCULES INCORPORATED
ALLEGANY BALLISTICS LABORATORY
CUMBERLAND, MARYLAND 21502

A. G. BUTCHER
M. W. BECKSTEAD
HERCULES INCORPORATED
BACCHUS WORKS
MAGNA, UTAH 84044

JULY 1976

APPROVED FOR PUBLIC RELEASE:
DISTRIBUTION UNLIMITED

AIR FORCE ROCKET PROPULSION LABORATORY
DIRECTOR OF SCIENCE AND TECHNOLOGY
AIR FORCE SYSTEMS COMMAND
EDWARDS AFB, CALIFORNIA 93523

A0129-123-01-011

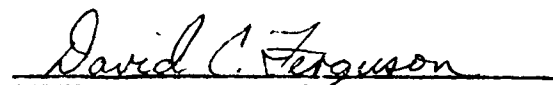
NOTICES

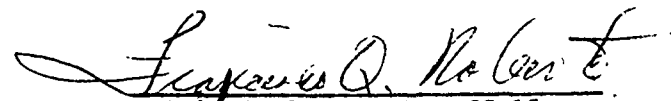
When U. S. Government drawings, specifications, or other data are used for any purpose other than a definitely related Government procurement operation, the Government thereby incurs no responsibility nor any obligation whatsoever, and the fact that the Government may have formulated, furnished, or in any way supplied the said drawings, specifications or other data, is not to be regarded by implication or otherwise, or in any manner licensing the holder or any other person or corporation, or conveying any rights or permission to manufacture, use or sell any patented invention that may in any way be related hereto.


FOREWORD

This report was submitted by Hercules Incorporated/Allegany Ballistics Laboratory, Box 210, Cumberland, Maryland 21502, under Contract FO4611-75-C-0009 with the Air Force Rocket Propulsion Laboratory, Edwards, California 93523. The work reported herein was done under the direction of Dr. J. P. Peterson with Dr. M. W. Beckstead as Principal Investigator for all acoustic stability testing and analysis. Dr. J. C. Allabashi was Project Director, and Dr. R. R. Miller was Program Manager.

This report has been reviewed by the Information Office/DOZ and is releasable to the National Technical Information Service (NTIS). At NTIS, the report will be available to the general public, including foreign nations. This report is unclassified and suitable for public release.


DAVID C. FERGUSON, 2nd Lt, USAF
Project Engineer


FRANCISCO Q. ROBERTO, GS-15
Section Chief


CHARLES R. COOKE, Chief
Solid Rocket Division

19

UNCLASSIFIED

SECURITY CLASSIFICATION OF THIS PAGE (When Data Entered)

9 Final rept.

REPORT DOCUMENTATION PAGE		READ INSTRUCTIONS BEFORE COMPLETING FORM
1 REPORT NUMBER 18 AFRPL-TR-76-46	2 GOVT ACCESSION NO.	3. RECIPIENT'S CATALOG NUMBER
4 TITLE (and Subtitle) 6 A STUDY OF A NOVEL ADDITIVE FOR HTPB PROPELLANT	5. TYPE OF REPORT & PERIOD COVERED FINAL	
7 AUTHOR(s) J. P. Peterson, Hercules/Allegany Ballistics Laboratory, and A. G. Butcher and M. W. Beckstead, Hercules/Bacchus	8. CONTRACT OR GRANT NUMBER(s) 14 PERFORMING ORG. REPORT NUMBER A0129-123-01-011	
9 PERFORMING ORGANIZATION NAME AND ADDRESS Hercules Incorporated/Allegany Ballistics Laboratory, P. O. Box 210, Cumberland, MD 21502	10 PROGRAM ELEMENT, PROJECT, TASK AREA & WORK UNIT NUMBERS 15 F04611-75-C-0009 new	
11 CONTROLLING OFFICE NAME AND ADDRESS Air Force Rocket Propulsion Laboratory Edwards, CA 93523	12 REPORT DATE 11 July 1976	
14 MONITORING AGENCY NAME & ADDRESS (if different from Controlling Office) 10 J. P. Peterson, A. G. Butcher M. W. Beckstead	13. NUMBER OF PAGES 103 12 113 p.	
16 DISTRIBUTION STATEMENT (of this Report) Approved for public release; distribution unlimited	15 SECURITY CLASS. (of this report) Unclassified	
17. DISTRIBUTION STATEMENT (of the abstract entered in Block 20, if different from Report)	15a. DECLASSIFICATION/DOWNGRADING SCHEDULE	
18 SUPPLEMENTARY NOTES		
19 KEY WORDS (Continue on reverse side if necessary and identify by block number) Graphite linters, Burn rate augmentation, HTPB composite propellant, Acoustic instability suppression		
20 ABSTRACT (Continue on reverse side if necessary and identify by block number) Experimental studies were conducted to define the utility regimes of graphite linters (chopped HMS [®] graphite fiber ranging from 50 to 200 μ) with respect to burn rate augmentation, acoustic stabilization and processing improvement in HTPB composite propellant. Linter utility regimes were defined with respect to burn rate reproducibility where the usable propellant compositional range was shown to increase as overall coarseness of the AP solids distribution increased. T-burner tests showed that linters afforded approximately the same (Continued)		

DD FORM 1 JAN 73 1473

EDITION OF 1 NOV 65 IS OBSOLETE

UNCLASSIFIED

SECURITY CLASSIFICATION OF THIS PAGE (When Data Entered)

401 824

UNCLASSIFIED

SECURITY CLASSIFICATION OF THIS PAGE(When Data Entered)

Block 20: Abstract (Continued)

amount of acoustic damping as zirconium carbide at a frequency of 1000 Hz. However, at 3800 Hz, 200 μ linters provided damping on the order of 10^2 sec⁻¹ at the 3% level. Processing improvements were demonstrated at constant burn rate by replacing a 0.7 μ fine AP fraction with 2 μ AP and graphite linters.

micrometers

10⁻⁴ s

UNCLASSIFIED

SECURITY CLASSIFICATION OF THIS PAGE(When Data Entered)

PREFACE

This report documents the results of the experimental and analysis effort to demonstrate the utility of graphite linters in HTPB composite propellant. Specific areas of interest are burn rate augmentation, acoustic stabilization, and processing improvement. The effort was supported by the Study of a Novel Additive for HTPB Propellants program (Contract No. F04611-75-C-0009) under the direction of Lt. C. S. Waterman, Formulation/Ingredients Section of the Air Force Rocket Propulsion Laboratory, Edwards Air Force Base.

TABLE OF CONTENTS

	<u>Page</u>
PREFACE	iii
I. INTRODUCTION	1
A. Assessment of the Problem of Linter Utility	1
B. Program Objectives	2
II. SUMMARY	3
III. PROGRAM PLAN	4
A. Task I - Delineation of Linter Burning Rate Augmentation	4
1. Subtask 1 - Definition of Linter Utility Regime	4
2. Subtask 2 - Mechanical Properties Optimization for Small-Scale Motor Preparation	4
3. Subtask 3 - Demonstration Motor Firings	4
4. Subtask 4 - Demonstration of Linter Utility in Iron Oxide - Catalyzed Propellants Containing Aluminum	5
5. Subtask 5 - Combustion Mechanism Study	5
B. Task II - Acoustic Instability Study	5
C. Task III - Demonstration of Processing Improvements	5
IV. TECHNICAL DISCUSSION	6
A. State-of-the-Art	6
B. Task I - Delineation of Linter Burning Rate Augmentation	7
1. Subtask 1 - Definition of Linter Utility Regimes	8
2. Subtask 2 - Mechanical Properties Optimization for Small-Scale Motor Preparation	19
3. Subtask 3 - Demonstration Motor Firings	19
4. Subtask 4 - Demonstration of Linter Utility in Iron Oxide - Catalyzed Propellants	21
5. Subtask 5 - Combustion Mechanism Study	21

TABLE OF CONTENTS (CONT.)

	<u>Page</u>
IV. (CONT.)	
C. Task II - Acoustic Instability Study	22
1. Test Data and Hardware	23
2. Correction Factors Used in Data Analysis	24
3. 1000 Hz Data	26
4. Burn Rate	28
5. Particle Damping Evaluation	28
D. Task III - Demonstration of Processing Improvements	32
V. RECOMMENDATIONS	34
VI. APPENDICES	97
A. Appendix I - Nomenclature	97
B. Appendix II - Burn Rate Correlation	100

LIST OF FIGURES

<u>Figure No.</u>	<u>Title</u>	<u>Page</u>
1	Program Milestone Chart	35
2	Influence of 400 μ Linters on Burning Rate at 2000 psia; for Double-Base and Composite Propellants - Lower Rate Range	36
3	Influence of 400 μ Linters on Burning Rate at 2000 psia; for Double-Base and Composite Propellants - Higher Rate Range	36
4	Typical Orientation Pattern for 400 μ Linters and 50 μ Coarse Solids	37
5	Typical Pressure-Time Trace for Center-Perforated Composite TPC Using 50 μ Coarse Solids and 400 μ Linters	37
6	Typical Random Distribution of 3% 50 μ Linters with 50 μ Coarse Solids	38
7	Typical Pressure-Time Trace for Center-Perforated Composite TPC Using 50 μ Coarse Solids with 50 μ Linters at 3% Concentration	38
8	Influence of Linter Length on Burning Rate	39
9	Effect of Frequency on Particulate Damping for Graphite Linters	40
10	Linter Length Distribution for Nominal 50 μ Linters	41
11	Linter Length Distribution for Nominal 90 μ Linters	42
12	Linter Length Distribution for Nominal 150 μ Linters	43
13	Linter Length Distribution for Nominal 200 μ Linters	44
14	Diagram Showing Location of Slices for Microscopic Examination	45
15	Photographs Showing Random Linter Orientation in Propellant 2L-150-9 (50X Magnification)	46
16	Photographs Showing Preferential Linter Orientation in Propellant 2L-150-1 (50X Magnification)	47
17	Linter Utility Regimes for Fixed Fine Oxidizer Size (2 μ) and Total Oxidizer Surface Mean Diameter (4.9 μ)	48

<u>Figure No.</u>	<u>Title</u>	<u>Page</u>
18	Linter Utility Regimes for Fixed Fine Oxidizer Size (2μ) and Total Oxidizer Surface Mean Diameter (5.6μ)	49
19	Linter Utility Regimes for Fixed Fine Oxidizer Size (2μ) and Total Oxidizer Surface Mean Diameter (8.0μ)	50
20	Linter Utility Regimes for Fixed Fine Oxidizer Size (0.7μ) and Total Oxidizer Surface Mean Diameter (1.7μ)	51
21	Linter Utility Regimes for Fixed Fine Oxidizer Size (0.7μ) and Total Oxidizer Surface Mean Diameter (2.4μ)	52
22	Linter Utility Regimes for Fixed Fine Oxidizer Size (0.7μ) and Total Oxidizer Surface Mean Diameter (4.5μ)	53
23	Rate Versus Linter Length for Composition NA-2Lxx-3 (Highest Augmented Rate with Most Reliable Random Linter Orientation is NA-2L90-3) at 1% Linter Concentration	54
24	Rate Versus Linter Length for NA-.7Lxx-4 at 1% Linter Concentration	54
25	Burn Rate Results (Strands and TPC's) for Demonstration Motor Propellant and the Corresponding Base Case Propellant	55
26	Pressure-Time Trace for TPC Demonstration Motor (Nominal 400 psia)	56
27	Pressure-Time Trace for TPC Demonstration Motor (Nominal 750 psia)	57
28	Pressure-Time Trace for TPC Demonstration Motor (Nominal 1000 psia)	58
29	Pressure-Time Trace for TPC Demonstration Motor (Nominal 1600 psia)	59
30	Pressure-Time Trace for TPC Demonstration Motor (Nominal 2100 psia)	60

<u>Figure No.</u>	<u>Title</u>	<u>Page</u>
31	Typical Orientation Pattern in Vertical Web Cross-Section of TPC Motor for 200 μ Linters (Rate Marginal) in Composition NA-2L200-6(2)	61
32	T-Burner Hardware Test Configurations for VATB and End Burner Testing	62
33	Relation of Pulse Decay Measurements to Total Mass Burned, Data Taken at 4000 Hz in End Burner Hardware	63
34	Uncorrected α as a Function of Area Ratio for Mix NA-2L200-8(3)M	64
35	Burn-Out Decay Measurements Showing Increased Losses as a Function of Mass Burned	65
36	Loss Variation During Burning for 1.5 Area Ratio Samples. Data from Two Tests Each from Mixes NA-2L90-8(3) and NA-2L200-8(3)M	66
37	Final Adjusted α Versus Area Ratio Data; NA-2L200-8(3)M, 1000 Hz, 1000 psia	67
38	Final Adjusted α Versus Area Ratio Data; NA-2L90-8(3)M, 1000 Hz, 1000 psia	68
39	Computer Calculated Curves for Pressure Coupled NA-2L00-8 Baseline Propellant Test Data	69
40	Computer Calculated Curves for Velocity Coupled NA-2L00-8 Baseline Propellant Test Data	70
41	Computer Calculated Curves for Pressure Coupled NA-2L00-6M Baseline Propellant Test Data	71
42	Computer Calculated Curves for Velocity Coupled NA-2L00-6M Baseline Propellant Test Data	72
43	Pressure Coupled and Velocity Coupled Response Variations as Affected by Linter Variation	73
44	Effects of Linter Variation on Burn Rate at 1000 psia, 1000 Hz	74
45	Particle Damping as a Function of Frequency Showing Linter Variation Effects	75

<u>Figure No.</u>	<u>Title</u>	<u>Page</u>
46	Effects of Linter Variation on Particle Damping	76
47	Flow Profile and Travel Distance in Burner Chambers of Different Lengths Showing Relation to Acoustic Velocity Mode Shape	77
48	Particle Damping Efficiency for 90μ and 200μ Linter Lengths	78
49	Comparison of Damping Characteristics of Linters, ZrC and Al_2O_3 at 1000 Hz, 1000 psia	79

LIST OF TABLES

<u>Table No.</u>	<u>Title</u>	<u>Page</u>
1	Ammonium Perchlorate Properties	80
2	Binder Composition	81
3	Compositions and Results for 1-Pt Mixes Containing 2 μ Fine AP Fraction	82
4	Compositions and Results for 1-Pt Mixes Containing 0.7 μ Fine AP Fraction	83
5	Burn Rate Results for Composition NA-2L90-3	84
6	Burn Rate Results for Composition NA-.7L90-4	85
7	Tailoring UFAP Composition to Obtain Low Pressure Exponent	86
8	Results of First 5-Gallon Mix for Composition NA-2L90-3(3)M	87
9	Results of Second 5-Gallon Mix for Composition NA-2L200-6(2)	88
10	Linter Utility in Iron Oxide Results	89
11	Compositions for Combustion Mechanism Studies	90
12	Propellant Ingredients	91
13	Computer Analysis Results of 1000 Hz Data	92
14	Burn Rate Changes as Measured from T-Burner Data	93
15	Particle Damping Characteristic Data	94
16	Processing Improvement Results	95

SECTION I

INTRODUCTION

Recently, Hercules discovered that the addition of small amounts of graphite linters (chopped graphite fiber having nominal lengths ranging from 50 to 400 μ) to composite propellant produced a very dramatic increase in burning rate of propellants with base rates ≥ 0.25 -0.30 in./sec. This rate augmentation effect was discovered during studies of the influence of linters on acoustic instability where the linters are also advantageous in reducing instability. Prior to this work, linters also had been shown to be effective in augmenting the rate of crosslinked double-base (XLDB) and gun propellants. Recent Hercules IR&D work has shown that, in addition to augmenting burning rate and reducing acoustic instability, linters also improve composite propellant mechanical properties and, through a wide choice of solids distributions, permit more easily processed propellant slurries to be made at a given burning rate.

A. Assessment of the Problem of Linter Utility

Because graphite linters display large values of length/diameter (diameter approximately 7.5 μ), the potential exists for preferential orientation during flow of an uncured propellant slurry. Ideally, a completely random linter orientation is desired in a cured propellant such that propellant burn rate is independent of burning direction. The opposite extreme, a high degree of preferential linter orientation, results in anomalous ballistic behavior in that burn rate is highly direction dependent. Burn rate in the direction of linter orientation is much higher than in the direction normal to the oriented linters.

As a direct consequence of the above characteristics, one of the major areas in need of study is burn rate reproducibility as a function of degree of linter orientation; that is, how much systematic linter orientation can be tolerated in a cured propellant such that the propellant can be used in motor applications. Closely related to this area is the influence of solids distributions on linter orientation. Thus, the initial problem addressed in this program is delineation of the influence of solids distributions on degree of linter orientation in a cured HTPB propellant and the determination in test motors. This study will define the utility of linters in solid propellant and provide a basis for studying the positive attributes of graphite linters as stated in the following objectives.

B. Program Objectives

The objective of the program was to define the utility of graphite linters 50 and 200 μ in length in solid HTPB propellants. As a corollary, areas of application studied were burn rate augmentation, acoustic instability suppression, and improved processing characteristics. Of these potential applications, the first two are of primary importance and formulations containing linters can be tailored for each of the two applications individually or in combination. Thus, burn rate augmentation and acoustic instability suppression received primary consideration in this study. The third application was sufficiently characterized to demonstrate the processing variations that are possible with linters.

SECTION II

SUMMARY

The 12-month AFRPL-sponsored program to study graphite linter utility in HTPB composite propellant yielded the following major results:

1. Linter utility regimes were defined based on one-pint scale photomicrograph results.
2. A 25% rate augmentation was obtained using 1% 200 μ linters in a randomized system.
3. A 39% rate augmentation was demonstrated using TPC motors with a 0.49 in./sec at 1000 psia composition containing 3% 200 μ linters; pressure-time traces were acceptable below 2000 psia but displayed large nonlinearity above 2000 psia.
4. A burn rate of 2.1 in./sec at 1000 psia (170% rate augmentation) was demonstrated for a 0.78 in./sec base composition containing 1% Imperial iron oxide and 3% 150 μ linters; the linters afforded 40% augmentation over the iron oxide composition without linters.
5. T-burner tests showed that graphite linters are as good as, or better than, ZrC and Al_2O_3 for damping acoustic instability at 1000 Hz. At 3800 Hz, 3% 200 μ linters produced 129 sec^{-1} of damping.
6. Processability was greatly enhanced by replacing 0.7 μ AP with 2 μ AP and graphite linters with no loss in burn rate.

SECTION III

PROGRAM PLAN

The Novel Additive for HTPB Propellants program consisted of three major tasks. The final Milestone Chart is shown in Figure 1. The 12-month program was initiated January 20, 1975 and completed on January 20, 1976 within the original budget.

A. Task I - Delineation of Linter Burning Rate Augmentation

Task I was designed to examine linter orientation and burn rate augmentation in five subtasks.

1. Subtask 1 - Definition of Linter Utility Regime

Subtask 1, the nucleus of Task I, was a fundamental study in which linter orientation was examined in a broad range of compositions at the one-pint scale such that compositional regimes (solids distributions) could be defined for linter utility. The purpose of the subtask was to define the AP distributions which would produce essentially random orientation of linters having a given length. The gross composition of 86 wt. % AP and 1 wt. % graphite linters was used. This solids level permitted a wide range of solids size distributions to be processed. Linter orientation was assessed by visual examination of photomicrographs of key areas of the cured propellant grain (i.e., areas where orientation is most likely to occur) and by burn rate reproducibility of strands cut from cured grain extremities.

2. Subtask 2 - Mechanical Properties Optimization for Small-Scale Motor Preparation

The objective of this subtask was to adjust binder stoichiometry at the one-pint mix scale to develop mechanical properties sufficient for ten-pound charge (TPC) demonstration motors in Subtask 3.

3. Subtask 3 - Demonstration Motor Firings

This subtask was designed to demonstrate graphite linter containing propellant utility in ten-pound charge (TPC) demonstration motors. One five-gallon mix was planned for each of two candidate compositions. The goal of this effort was the generation of TPC pressure-time traces covering a nominal pressure range of 500 to 2000 psia.

4. Subtask 4 - Demonstration of Linter Utility in Iron Oxide - Catalyzed Propellants Containing Aluminum

The objective of this subtask was a demonstration of a 2 in./sec at 1000 psia propellant using Imperial iron oxide and graphite linters as burn rate augmentors. The work was done at the one-pint scale.

5. Subtask 5 - Combustion Mechanism Study

This subtask was planned to examine the burning surface of linter-containing propellants in a microwindow bomb test apparatus using high-speed color motion picture photography to record the test.

B. Task II - Acoustic Instability Study

The influence of graphite linters on acoustic growth and damping was evaluated in end-burning, extended-area, and velocity-coupled T-burner tests. These tests were conducted at the Hercules/Bacchus facility under the direction of Dr. M. W. Beckstead. Eight smokeless composite formulations were planned for testing. Two linter lengths (designated long and short) were examined at three linter concentrations where the third concentration was zero, corresponding to a base case. In addition, two iso-rate (constant burning rate) formulations were studied. One case involved a composition change of a long linter-containing propellant such that the burning rate at 1000 psia was equivalent to the rate of one of the short linter-containing propellants above. The second iso-rate study involved a similar change in a short linter-containing propellant such that the burning rate was the same as that of one of the original long linter-containing propellants above.

Extended area tests were conducted at a pressure of 1000 psia and a frequency of 1000 Hz using three different area ratios. Standard tests (end-burning grains) were conducted at 1000 psia over a frequency range of 1000 to 4000 Hz.

C. Task III - Demonstration of Processing Improvements

Task III was designed to show that graphite linters can be used to enhance propellant slurry processability. The effort consisted of replacing a 0.7 μ fine AP size fraction with 2 μ AP and graphite linters such that burn rate was held constant and slurry viscosity was decreased. In addition, the inherent problems of UFAP were eliminated.

SECTION IV

TECHNICAL DISCUSSION

This section of the final program report on the use of graphite linters in HTPB propellants begins with a brief review of the linter utility state-of-the-art prior to the program. Following the state-of-the-art discussion is a detailed presentation, by task, of the results generated during the 12-month AFRPL-sponsored program.

A. State-of-the-Art

This section is a summary of the state-of-the-art of graphite linter applications prior to the start of the novel additive program.

Graphite linters are short lengths of HMS[®] graphite fiber which can readily be prepared in the length range of 50 to 400 μ . Above a base rate of 0.25-30 in./sec, the addition of 1% linters produces significant increases in burning rate as shown in Figures 2 and 3. The degree of augmentation has been shown to be independent of the type of propellant used (i.e., composite or double-base) and depends only on the base or unaugmented propellant burning rate. The linters used to generate the data in Figures 2 and 3 had a nominal number average length of 400 μ in the cured propellant. Motor firings and photomicrographs of microtomed slices of cured propellant revealed that the 400 μ linters were selectively oriented parallel to directions of propellant slurry flow during casting operations. Figure 4 shows the degree of orientation while Figure 5 shows the irregular nature of the ten-pound charge (TPC) motor pressure-time trace. Prior to this program, Hercules' IR&D studies had conclusively established that linter lengths less than or equal to the coarsest filler diameter will not orient when there is a sufficient concentration of coarse filler particles (\sim 25% by weight 50 μ coarse filler for 50 μ linters). Figure 6 shows the randomness of 50 μ linters while Figure 7 shows the resultant flat pressure-time behavior of the TPC motor. The maximum length for random orientation, however, will be a complex function of both coarse filler size and concentration, and these tradeoffs must be established to realize the full augmentation potential of linters. Since it has been established that increased linter length increases the degree of augmentation (Figure 8), maximization of linter length is important and constitutes the major technical challenge for practical utilization of linters as rate augmentors. Thus, a large portion of the current program experimental effort was designed to deal with this area.

Work in the area of acoustic instability prior to the current program has shown that chopped graphite linters do act as sources of particulate damping. Small T-burner studies were conducted at Hercules/Bacchus using a 1.5-inch-diameter burner where cylindrical grains of varying areas were

used. Particulate damping coefficients were found by extrapolating measured acoustic growths to zero area. Tests were conducted at 500 psia on a propellant containing 1% graphite linters of approximately 400 μ length. Particulate damping versus frequency is shown in Figure 9. Theoretical calculations (Dobbins-Tempkin model) showed that the linters, on a weight basis, are comparable in effectiveness to spherical particles of the same diameter as the cross-sectional diameter of the linters. This observation suggests that the linters have not been consumed appreciably within the zone in which they are effective.

While these results are encouraging, it is recognized that they are by no means conclusive proof that linters eliminate acoustic instability in rocket motors. Multiple rounds must be fired to establish statistical significance and, preferably, it should be ascertained whether the motors can be pulsed into instability to check for nonlinear effects.

Motion picture photography of past motor firings using linter-containing propellants showed that the linters had no effect on smoke characteristics. Thus, it is concluded that the linters have essentially been consumed before they reach the exit plane. Previous tests with other particulate materials at the 1% level suggest that, even at this low level, an effect on plume transparency would be seen if particulates were present.

The benefits of linters in the area of slurry processing had not been studied in detail prior to the current program. However, latitude exists in the solids distributions incorporated into a propellant when linters are used to adjust burning rates. This makes possible significant changes in slurry viscosities at constant burn rate.

The benefits to be gained from using graphite linters to augment burn rate, stabilize motors, and enhance slurry processability, combined with the need for more complete characterization of the methods of linter incorporation, form the basis of the program outlined in Section III. A discussion of the program results is presented in the following paragraphs.

B. Task I - Delineation of Linter Burning Rate Augmentation

It has already been noted that graphite linters may be useful in a broad range of solid propellants. These include high-performance composite propellants (metalized), smokeless composite propellants, high-performance crosslinked double-base (XLDB) propellants, smokeless XLDB propellants, and conventional casting powder double-base propellants. Of these types of propellants, the smokeless composite propellants are the likely systems for initial evaluation of graphite linters. Interest arises because smokeless composite propellants display acoustic instability problems and are, in general, lower in burning rate because of the

unavailability of a smokeless burning rate accelerator. Thus, graphite linters, which do not contribute to exhaust smoke at the 1% level, provide a unique additive approach for the simultaneous or individual control of problems in this family of propellants.

The smokeless composite propellant has an added advantage in this type of study because it is the basic building block from which all other composite propellants (having a specified binder) are derived. Thus, it provides a sound baseline evaluation of graphite linters and results may be readily extended to more complex formulations. Limited exploratory work was planned to show that such extension is feasible and to demonstrate the advantages of graphite linters in more complex (metalized compositions containing other rate catalysts) formulations. A solids loading of 86% was chosen because it is realistic for smokeless formulations and is still low enough to allow processing latitude.

To provide maximum applicability of graphite linters, the areas of rate augmentation and suppression of acoustic instability were studied in detail. Firstly, with respect to burning rate, the combination of linter length and AP size distribution was studied to determine maximum rate augmentation without preferential orientation of the linters during slurry casting. It has already been discussed (Section IV-A) that a careful choice of AP size distribution and linter length will yield a random linter orientation. The intent of this task was to optimize the system and determine the range of solids distributions which will randomize, or nearly randomize, graphite linters having a given length. Secondly, in Task II, the linter lengths which produced rate augmentation and random or nearly random orientation were evaluated with respect to acoustic instability, such that the ability to simultaneously augment rates and suppress acoustic instability could be characterized. Evaluation of rate augmentation and acoustic stability constituted the major program effort. Sufficient data were generated in Task III to permit a preliminary evaluation of linters as a tool for improving processing. Processing improvement is particularly valuable in high rate propellants.

1. Subtask 1 - Definition of Linter Utility Regimes

Because of the importance of incorporating linters into a propellant in a manner that will augment burning rate while maintaining flat pressure-time traces, this area comprised the first portion of the program. Since this area forms the foundation for later work, it necessarily involved more experimental work and proportionately more time.

The major experimental work of this subtask consisted of preparing 96 one-pint mixes where the first 48 formulations contained 2 μ fine AP and the second 48 formulations contained 0.7 μ fine AP (UFAP). The total AP level was 86 wt. %. Linter level was 1 wt. %. Linter lengths of

50, 90, 150, and 200 μ were evaluated. Each length was incorporated into a series of 12 AP solids distributions for the 2 μ fine AP series and into a series of 12 AP solids distributions for the UFAP series.

The nominal AP size fractions, lot numbers, and average sizes (surface mean diameter, d_{32}^* , and volume mean diameter, d_{43}^*) are given in Table 1. These lots of AP were prepared or gathered at the start of the program in sufficient quantity for the entire program to provide continuity.

The binder composition used is given in Table 2. Use of this binder resulted in processable end-of-mix viscosities and good mechanical properties for the cured propellants in most cases. The NCO/OH ratio is 0.92.

The graphite linters used in the program are characterized by cumulative plots of number percent greater than versus linter length. The plots are shown in Figures 10 through 13 for the nominal 50, 90, 150, and 200 μ lengths, respectively. As indicated in the above plots, linter length is represented by the 50 percentile point for a given length distribution.

A complete tabulation of compositions and results is given in Tables 3 and 4. Table 3 represents the 48 formulations containing 2 μ fine AP and Table 4 represents the 48 formulations containing UFAP.

Viscometric results are presented as m and n' defined by the power law constitutive equation:

$$\tau_s = m \dot{\gamma}^{n'} \quad (1)$$

where: τ_s = shear stress, dyne/cm²

$\dot{\gamma}$ = shear rate, sec⁻¹

m = consistency index, g sec ^{$n'-2$} /cm = poise for $n' = 1.0$

n' = flow behavior index, dimensionless.

The magnitude of m is equal to apparent viscosity at a shear rate of 1.0 sec⁻¹. The apparent viscosity can readily be calculated at any other shear rate using:

*Defined in Table I.

$$\eta_{app} = \tau \dot{\gamma}^{n'-1} \quad (2)$$

where: η_{app} = apparent Newtonian viscosity, poise

The magnitude of n' indicates the departure of the propellant slurry from Newtonian behavior. The usual range of n' is from 1.0 (Newtonian behavior) to approximately 0.2 (pseudoplastic behavior).

A complete review of the power law equation is given in Reference (1).

Strand burn rates are reported at three pressures (room temperature) of 500, 1000, and 2000 psia. The results consist of average values of two strands for 500 and 2000 psia, whereas three strands were averaged at 1000 psia. The randomness of the linters is reflected in the % disparity obtained at each pressure by subtracting the lowest strand burn rate from the highest, dividing the difference by the highest value, and multiplying the result by 100. The testing was designed to examine the most extreme cases of potential linter orientation. This was done by selectively cutting burn rate strands from the top, middle, and bottom of the nominal 4 x 4 x 1-inch cured grain from a one-pint mix. For the 500 and 2000 psia firings, one strand was fired from the top of the grain and one was fired from the bottom of grain (see Figure 14 for location of top and bottom). In the 1000 psia case, an additional strand was fired from the middle of the grain. Thus, large values of % disparity indicate regions of various stages of flow orientation of the linters. Conversely, small values of % disparity (less than approximately 9%) indicate random orientation since regions of different flow patterns produce similar burn rates.

Also reported in Tables 3 and 4 are the values of n and c for the pressure range of 500 to 2000 psia. n and c are defined by:

$$r_b = cP^n \quad (3)$$

where: r_b = burn rate, in./sec

P = pressure, psia

n = burn rate pressure exponent, dimensionless

c = burn rate/pressure constant of proportionality,
in.²ⁿ⁺¹/lbⁿsec

(1) Peterson, J. P., Bulletin of the 4th JANNAF Characterization Meeting, CPIA, Publication No. 225, August 1974, pp. 1-10.

Because of the importance of screening for randomly oriented systems at the one-pint scale, the burn rate results were complemented by photomicrographs of five key areas in the cured propellant. These key areas are: (1) adjacent to a glass slide over which the propellant flowed during casting (most rigorous test for orientation), (2) at the Teflon spacer/propellant block interface near the bottom of the grain, (3) at the same interface near the top of the grain, and (4) and (5) at the top of the propellant grain near each side. These areas are depicted in Figure 14 and, based on prior experience, are believed to be the best areas for characterizing degree of linter orientation. Because the photomicrograph method of assessing linter orientation is an absolute method, the approach has been used as the primary indicator of degree of orientation and thus has precedence over the burn rate disparity approach.

Mechanical property data were generated using a strain rate of 0.74 in./in.-min at temperatures of -65°, 77°, and 165°F. The test specimen is a 4-inch Modified JANNAF Type C dogbone. The results for initial modulus, E_0 , and maximum tensile strength, σ_m , are expressed in terms of initial sample cross-sectional area. Elongation values are reported as ϵ_m , the strain at maximum stress, and ϵ_b , the strain at the point of sample breakage.

The notation, NA-2Lxx-y, has the following meaning: NA signifies novel additive in reference to the program; 2 indicates the size of the fine AP size fraction (μ); Lxx indicates the linter length (μ) used where xx is 50, 90, 150, or 200 μ ; y indicates the position in a given series (1 through 12) where a series is defined by the fine AP size and linter length. Thus, NA-2L90-3 signifies the third composition studied in a series where 2 μ fine AP and 90 μ linters are used in this novel additive program. By analogy NA-.7Lxx-y refers to the 0.7 μ fine AP series.

As mentioned earlier, the screening of propellants containing 1% linters was accomplished using two separate criteria: photomicrographs and strand burn rates. Recall that the objective is to determine solids distributions which permit linters to be incorporated into a propellant such that linter orientation is random. That is, any preferential orientation due to flow of the slurry is undesirable as unstable ballistic behavior is a likely result.

a. Linters Orientation Analysis

The photomicrograph criterion used to assess linter orientation in cured propellant grains is illustrated by the typical photomicrographs of two propellants shown in Figures 15 and 16 for compositions NA-2L150-9 and NA-2L150-1, respectively. The numbers associated with each photograph refer to the location of the area in the propellant grain as given in Figure 14. Figure 15 represents a randomly oriented system as evidenced by lack of orientation in each of the five photographs. This is

the requirement for complete randomness used throughout the program. In contrast, Figure 16 shows a system where the linters are preferentially oriented in areas 1, 3, and 4. The requirement for declaring a system marginally acceptable is the existence of orientation in no more than two areas of areas 1, 4, and 5, with areas 2 and 3 having random orientation. A system is judged unacceptable when the marginal criterion is exceeded. Figure 16 does exceed the marginal criterion and is judged unacceptable based on photomicrograph analysis alone. Thus, the three categories used in assessing linter orientation are good (random orientation), marginal* (isolated local areas of orientation), and poor (extensive preferential orientation). This approach is currently qualitative but shows potential for becoming quantitative by using optical image analysis.

The second method used to judge the acceptability of a linter-containing propellant is based on the scatter of strand burn rate results. Strands were cut from three regions of the propellant grain shown in Figure 14: the top, middle, and bottom. The 500 and 2000 psia results were obtained by averaging the burn rates of a strand cut from the top and a strand cut from the bottom of the grain. The 1000 psia results were determined by averaging the burn rates of strands cut from the top, middle, and bottom of the grain. At each pressure, percent disparity was calculated by dividing the difference between the high and low burn rates by the high rate and multiplying the resulting fraction by 100 as stated above.

Thus, higher values of percent disparity represent systems in which linter orientation varies from region to region in the grain. A random system would burn at the same rate at all locations. The quantitative assessment of orientation is accomplished by comparing the values of percent disparity for linter-containing propellants to values normally encountered for unaugmented propellants. A percent disparity of $\leq 6\%$ has been determined to be the normal experimental scatter. This fact, combined with past experience with linter-containing propellants, has resulted in the criterion for random orientation being $\leq 9\%$ disparity at all three of the above-mentioned pressures. Disparities greater than 9% but $\leq 14\%$ for any or all of the above pressures are judged marginal and $> 14\%$ is unacceptable. Based on this approach, composition NA-2L150-9 is good and NA-2L150-1 is unacceptable (refer to Table 3).

A complete analysis of photomicrographs and strand burn rates has been made for the 96 mixes in the screening exercise, and the results are presented in Tables 3 and 4 under the heading of Orientation. The shapes of the symbols used under the heading indicate the approximate AP surface mean diameters, d_{32} . The values for the 2 μ fine AP series are:

*At this point during the execution of the program, the marginal rating was believed to be usable in motor applications. This area will be discussed in detail in Section IV-B.3.

$\bigcirc \approx 4.9 \mu$, $\square \approx 5.6 \mu$, $\Delta \approx 8.0 \mu$. For the UFAP series the values are: $\bigcirc \approx 1.75 \mu$, $\square \approx 2.5 \mu$, $\Delta \approx 4.5 \mu$. The shading of the symbols indicates degree of linter orientation. Unshaded indicates no orientation, half-shaded indicates marginal acceptability, and fully shaded implies an unacceptable system (highly oriented linters). As per the above discussion, the respective classifications are good, marginal, and poor.

The approach used to define compositions in which graphite linters can be readily used was to plot graphite linter length (50, 90, 150, and 200 μ) versus the weight median diameter of the coarse solids (AP) size fraction, d_{50} . The weight median diameter is the point representing the 50th percentile in a size distribution. A given plot was constrained by fixing the size of the fine solids size fraction and the surface mean diameter, d_{32} , of the total solids. All work was done at 86% AP as stated at the outset.

The plots of linter length versus the d_{50} of the coarse AP size fraction were intended to define three regions pertaining to linter utility: (1) a region of high burn rate reproducibility, (2) a region of poor burn rate reproducibility, and (3) a marginal region bounded by the above two extremes. Figures 15a and 16a are representative depictions of linter orientation for regions of high burn rate reproducibility (random linter orientation) and regions of poor burn rate reproducibility (preferential linear orientation), respectively. In a composition where linters are randomly oriented, the propellant burn rate is direction independent. However, for the case where linters are preferentially oriented, burn rate is dependent on the direction of burning. The burn rate in the direction of linter orientation is significantly greater than the burn rate normal to the direction of linter orientation. This latter phenomenon accounts for the poor burn rate reproducibility in compositions containing regions of oriented linters and emphasizes the need for randomizing linters in order to extract their utility on a reliable basis.

The analysis of the linter orientation results from the 96 one-pint mixes of Task I, Subtask 1 is presented as a series of plots (linter length versus d_{50} of coarse AP size fraction) in Figures 17 through 22. In the first three plots (Figures 17, 18, and 19) the size of the fine AP fraction is constant at 2 μ . In the last three plots (Figures 20, 21, and 22) the fine AP fraction size is constant at 0.7 μ . As stated earlier, the purpose of the analysis is to conveniently show which compositions have the capability of randomizing, or nearly randomizing, graphite linters.

In Figures 17, 18, and 19, the results for compositions NA-2Lxx-y (2 μ fine AP size fraction) are grouped according to the total surface mean diameter, d_{32} of the AP solids where the values of d_{32} are approximately 4.9, 5.6, and 8.0 μ , respectively. The same concept was used

in Figures 20, 21, and 22 in which compositions NA-.7xx-y were analyzed. At the time the compositional grids (Tables 3 and 4) were devised, the parameter d_{32} was assumed to correlate burn rate results for reduced smoke HTPB composite propellants. This assumption was shown not to have general validity in Appendix II. Thus, the plots at constant d_{32} do not correspond to a constant base rate (burn rate without linters). However, this fact does not detract in any way from the linter orientation assessment.

Focusing on the plot (Figure 17) representing the smaller d_{32} (4.9μ) in the 2μ fine AP composition series, several trends can be readily identified (note that the shape and shading of the symbols have the same meaning* as delineated earlier). The most notable feature of Figure 17 is the overwhelming darkened area corresponding to poor burn rate reproducibility. Since a broad range of solids distributions was covered, the conclusion is drawn that for a solids d_{32} of 4.9μ the range of compositions showing potential for motor application is quite restricted. This situation is greatly improved as d_{32} increases and will be discussed in the following paragraphs.

As regards the construction of the Figure 17 plot, as well as the similar plots in Figures 18 through 22, the location of the boundaries separating the three regions is somewhat qualitative because of the sparseness of the results.** However, this approach is consistent with the original program objective to develop broad preliminary guidelines pertaining to linter utility. The presence of more data points would more accurately fix the boundary locations, but the trends (currently the main point of interest) would remain the same.

With the above information in mind, the boundaries defining the marginal and high reproducibility regions were sketched. In the particular case of Figure 17, no data exist to support the open area. But when all the results (Figures 18 through 22) were considered, the location of the open area was felt to be a reasonable approximation. Finally, as regards linter utility in actual motor firings, the marginal region will be shown in Section IV-B.3 to be usable to a large extent.

*Open Symbol - high burn rate reproducibility (random linter orientation); good rating.
Half-Shaded Symbol - marginal reproducibility; marginal rating.
Fully Shaded Symbol - poor reproducibility (preferential linter orientation); poor rating.

**Figures 17 through 22 were based on the photomicrograph results because this method of analyzing linter orientation is thought to be the most fundamental method.

Comparing the size and location of the three regions in Figure 17 with the respective regions in Figure 18 for a d_{32} of 5.6μ and Figure 19 for a d_{32} of 8.0μ reveals a progressively larger useful area. That is, as the total solids average size increases, greater quantities of coarse AP sizes can be used. The result is a wider range of compositions which have the capability of completely or partially randomizing graphite linters. The note should be made that a small number of points do not agree with the boundaries as currently sketched. This number of points is small compared with the total, and at this stage of evolution in test procedures the few points which deviate from the suggested patterns are not unexpected.

Even though d_{32} does not completely correlate burn rate, the gross generality can be made that as the average size of the total AP solids increases, the propellant burn rate diminishes. Thus, an apparent tradeoff exists between the compositional latitudes and the magnitude of the propellant burn rate.

The conclusion drawn from Figures 17, 18, and 19 representing a 2μ fine AP size fraction is that a tradeoff among linter length and coarse solids size and amount exists for the randomization of linters for a fixed fine AP size fraction and total solids d_{32} . There appears to be a physical limitation of processability at each of two extremes. Namely, for a given linter length, the size of the coarse AP fraction can be decreased down to some critical size if, at the same time, the corresponding AP coarse fraction concentration is increased. At the other extreme, the coarse AP size can be increased to some critical size where the coarse AP concentration becomes too low or the size of the coarse AP fraction becomes too large relative to the linter length. The results of this program suggest the following approximation as regards size criticality:

$$0.3 \text{ to } 0.4 \ell \leq \text{Coarse AP Size Fraction } d_{50} \leq 2 \text{ to } 3 \ell$$

where, ℓ = linter length.

As mentioned above, processing difficulties may arise before either of the critical extremes is reached.

One method of increasing the useful range of compositions as regards linter orientation is to decrease the size of the fine AP size fraction. The results of this change are depicted in Figures 20, 21, and 22 where 0.7μ fine AP was used as opposed to the 2μ fine AP fraction discussed above. This change affords two potential advantages.

Firstly, reducing the size of the fine AP fraction at constant d_{32} permits the use of higher concentrations and/or larger sizes of the coarse AP fraction. The drastic increase in the usable region (assume for

the present that all of the marginal region is usable) of compositions is seen in Figure 22 ($d_{32} \sim 4.5 \mu$) compared with Figure 17 ($d_{32} \approx 4.9 \mu$).

Secondly, reducing the fine AP size permits lower total AP solids d_{32} 's to be formulated which produces, in general, higher burn rates. This is shown in Figures 20 and 21 for d_{32} 's of 1.7 and 2.4 μ , respectively. One disadvantage to decreasing the size of the fine AP is the resultant higher burn rate pressure exponent. However, a workable compromise can be reached and will be discussed in a later Subsection IV-B.1.c.

b. Burn Rate Augmentation Analysis

The program goal was to select the fastest burning base case oxidizer distribution which will randomly orient graphite linters. From the standpoint of burn rate augmentation, linter length should be maximized.

Analysis of the results in Tables 3 and 4 shows that only the longer linter lengths studied (150 and 200 μ) displayed significant augmentation capability at the 1% level. The 50 μ linters produced virtually no augmentation in the 2 μ fine AP series and only small augmentation in some of the 0.7 μ fine AP compositions. The 90 μ linters displayed little, if any, augmentation in the 2 μ fine AP series at the 1% level but did show some promise in the 0.7 μ fine AP series.

The 2 μ fine AP composition judged to have the greatest potential is composition NA-2Lxx-3. This composition was selected for several reasons: (1) the oxidizer distribution completely randomized 90 μ linters, (2) 150 and 200 μ linters displayed marginal acceptability, (3) the pressure exponent was acceptable (≤ 0.6) for an HTPB composite propellant, and (4) the base rate (no linters) was the highest for a composition which would randomize 90 μ linters.

The above results are displayed in Figure 23 where strand burn rates at 1000 psia are plotted versus linter length for the lengths used in this program (50, 90, 150, and 200 μ). Open symbols indicate completely random linter orientation, half-shaded symbols represent marginal acceptability, and fully shaded symbols indicate unacceptable preferential orientation. At the 1% linter level, only the composition containing 200 μ linters showed significant augmentation in rate ($\approx 12\%$) over the base case. However, higher linter concentrations would produce more dramatic rate augmentation, even for the shorter linters. This will be discussed later.

A point of major significance in Figure 23 is the small change in pressure exponent with increasing linter length. Considering the

experimental scatter, the exponents for the base case system and the 50, 90, and 150 μ linter systems have the same value (≈ 0.4) with the 200 μ linter system only slightly higher (≈ 0.5). Thus, for linter lengths of practical concern, the influence of length on pressure exponent is minimal.

To supplement the results shown in Figure 23, the composition NA-2L90-3 was modified to contain 3% linters. The results are presented in Table 5. At 3% 90 μ linters some rate augmentation is evident. Compared with the base case burn rate, approximately 9% rate increase is obtained by using 3% linters. This rate increase is real because the data scatter about the mean value is somewhat less than 4% at worst. Thus, 90 μ linters at the 3% level produce approximately the same effect as 200 μ linters at the 1% level.

Theoretical specific impulse values are also listed in Table 5. A loss of 0.5 units is calculated for 1% linter replacing binder. With an additional 2% linters replacing AP, a loss of 6.4 units is calculated. The large reduction of specific impulse is due to the lowered oxidation index when linter replaces the oxidizer. The usual mode of addition of linter is as a replacement for metal to minimize the loss of specific impulse.

The final point of significance in Table 5 is the small change in pressure exponent as linter concentration is increased. This fact, combined with the previous discussion of pressure exponent, indicates that linters do not contribute significantly to undesirable changes in pressure exponent.

The 0.7 μ fine AP series is analyzed in a manner analogous to the 2 μ fine AP series. The results are presented in Figure 24 and Table 6. Shown in Figure 24 are the results for composition NA-.7Lxx-4 which was judged to have the best oxidizer distribution in the 0.7 μ fine AP series. Relative to the measured base rate, the 50 μ linters show no augmentation. The 90, 150, and 200 μ linter augmentation increases with increasing linter length. The 50 μ linter system is completely random, the 90 and 150 μ linter systems are marginal, and the 200 μ linter system is unacceptable. This composition is attractive from the standpoint of burn rate but has the serious limitation of a high pressure exponent. This exponent is the result of the base case composition (presence of 0.7 μ AP) rather than the linters. In addition, this composition does not permit the use of 200 μ linters. Examination of Figures 23 and 24 shows that the 50 μ linter burn rate results can be considered the same as the base case.

Table 6 extends the results shown in Figure 24 by presenting results for 3% 90 μ linters. As noted previously, the pressure exponent, n , is not appreciably changed when linter concentration is increased. As regards burn rates, a combined analysis of Figure 24 and Table 6 indicates the rate for 1% 90 μ linters in composition NA-.7Lxx-4 is somewhat high. The point representing 1% 90 μ linters in Figure 24 lies above the trend

(solid curve) and when the linter concentration was increased to 3% the increase in burn rate was not as large as anticipated based on past experience. It is believed that the burn rate for the 3% 90 μ linter-containing propellant is the proper value (\approx 25% augmentation). The major point of this analysis is that significant augmentation can be obtained using practical linter concentrations and lengths. The exponent problem of UFAP propellants is addressed in the following subsection. It should be noted, in passing, that the base case UFAP composition yielded a marginal rating using the disparity criterion. This illustrates the point made earlier that the photomicrograph criterion is more reliable than the disparity criterion.

c. Control of Pressure Exponent in UFAP Propellant

The results obtained in the initial screening exercise indicate that UFAP-containing low smoke propellants suffer, in many cases, from a high pressure exponent ($n > 0.6$). This statement is supported by the results discussed in the preceding subsection.

In an effort to systematically control the pressure exponent in a UFAP-containing composition, while still utilizing the high rate attributes of UFAP, a propellant was made having the composition given in Table 7 (NA-.7L90-13).

The composition of NA-.7L90-13 was derived from NA-2L90-3 (2 μ fine AP) because of the linter-randomizing ability of NA-2L90-3. The results indicate that replacing 2 μ fine AP with UFAP (corresponding intermediate size of 20 μ AP replaced by 6 μ AP for processing considerations) produced a 12% increase (0.77 to 0.86 in./sec at 1000 psia) in burn rate with a pressure exponent of only 0.51. Thus, the use of UFAP in conjunction with linters affords potential for high burn rates without a large pressure exponent. The high exponent attribute of UFAP can be controlled to some extent while still maintaining the randomizing capability of the composition. This situation exists because the coarse solids govern linter orientation and the extremely fine solids significantly enhance pressure exponent.

Composition NA-.7Lxx-13 was also prepared using linter lengths of 150 and 200 μ at the 1% level. The results for the longer linters are given in Table 7. The 50 μ linter length was not used because of negligible rate augmentation observed in the initial screening work. The results for the longer linter lengths indicate that burn rate augmentation increases with increasing linter length up to approximately 10% for the 200 μ linters. As discussed previously, the burn rate pressure exponent increases very little as linter length is increased. From the strand burn rate results, all three linter lengths were randomly oriented.

2. Subtask 2 - Mechanical Properties Optimization for Small-Scale Motor Preparation

Six one-pint mixes were prepared to examine the influence of NCO/OH and rubber (R45M*)/plasticizer (IDP**) variations. The values of NCO/OH studied were 0.92, 0.89, and 0.85. Two rubber/plasticizer values of 2.5 and 2.2 were used at each NCO/OH. The composition employed in this study was NA-2L90-3.

Analysis of the mechanical properties corresponding to the above binder parameter ratios indicated that the NCO/OH value of 0.92 and rubber/plasticizer value of 2.5 produced the best set of mechanical properties. These NCO/OH and rubber/plasticizer values were used throughout Task I, Subtask 1. The mechanical properties E_0 , psi/ σ_m , psi/ ϵ_m , % were 650/144/28 at 165°F; 860/152/32 at 77°F; and 7900/670/16 at -65°F. Although somewhat harder than desired, these properties were quite satisfactory for the planned ten-pound charge motors of Task I, Subtask 3.

3. Subtask 3 - Demonstration Motor Firings

The objective of this subtask was to demonstrate two linter containing formulations in ten-pound charge (TPC) motors. The primary requirement was a flat pressure-time trace for pressures ranging from 500 to 2000 psia. The plan consisted of testing one composition with a good rating and one composition with a marginal rating. Thus, the question of the utility of a marginal propellant in motor applications could be answered.

The composition selected as the first candidate for scale-up to the five-gallon mixer is given in Table 8. As noted in the table, the AP level was reduced 1% relative to composition NA-2L90-3(3) which contained 87% total solids (AP and linters). This solids reduction was made because of concern for processability. The results of the program indicate that good linter-randomizing compositions are difficult to process. This occurs because the solids distributions required to randomize linters are exactly opposite the distributions required for good processability.

Even with the above modifications, the thickness of the slurry was such that the TPC motor molds did not fill properly. Thus, the casting operation was considered to be a failure and, as a result, no TPC data were obtained for a formulation with a good rating. Very likely, a small change in solids distribution could have been made which would have made the slurry

* R45M = Hydroxyl-terminated polybutadiene

** IDP = Isodecyl pelargonate

more easily processed, but this was beyond the program scope and was not pursued.

The results obtained from propellant cast into a small box are given in Table 8. As can be seen in the table, burn rate results are good and are consistent with results generated earlier in the program. However, a consistency index of 18.3 Kp and a flow behavior index of only 0.18 indicate a very thick, highly non-Newtonian slurry. A slurry having these properties flows well under a large driving force but becomes very "stiff" under conditions of gravity flow (mold filling). The risk of a failure was considered prior to making the mix and the consensus among research and processing personnel was that a reasonable chance for a successful casting existed and that the risk should be taken.

The second and final five-gallon mix of this subtask was prepared using the composition given in Table 9. This composition has a marginal rating for linter orientation. The mixing and casting were carried out successfully. The rheological (viscometric and mechanical) properties are presented in Table 9.

Five TPC motors were fired and the data were analyzed. The burn rate results are shown in Figure 25. The solid line in Figure 25 was constructed using strand burn rate measurements from both one-pound and five-gallon mix propellant. The agreement between the strand rates and the TPC results is excellent. For comparison, the base case one-pint mix strand results are given as the dashed line. A rate augmentation of 39% is shown at a pressure of 1000 psia. Pressure exponents are approximately 0.4.

The five pressure-time plots for the TPC motors are shown in Figures 26 through 30. The nominal pressures represented in the traces are 400, 750, 1000, 1600, and 2100 psia for Figures 26, 27, 28, 29, and 30, respectively. The traces for pressures below 2000 psia suggest successful full-scale motor potential. However, the 2100 psia trace displays severe nonlinearity and would not lend itself well to motor application. Thus, the conclusion is that a propellant containing marginally oriented linters has useful application for motors operating below 2000 psia.

For completeness, Figure 31 shows a typical web cross-section of a TPC grain normal to the longitudinal direction. The section covers the distance from the center port wall to the outer chamber wall. As can be seen, local isolated areas of linter orientation exist but no gross overall trends are to be found. This is the concept of a marginal formulation as regards linter orientation.

As a result of the processing failure of the composition containing randomly oriented linters, no conclusion can be drawn as regards upper operating pressure limits. The speculation is that much higher operating pressures could be used with completely randomized linters.

A summary of the results of this subtask is that approximately 40% rate augmentation with a pressure exponent less than 0.5 can be obtained using 2% graphite linters in a burn rate range greater than 0.3 in./sec for operating pressures less than 2000 psia.

4. Subtask 4 - Demonstration of Linter Utility In Iron Oxide - Catalyzed Propellant

As stated earlier, the purpose of this subtask was to show that linters can be used in conjunction with other rate augmentation additives (iron oxides, carboranes, liquid ferrocenes, etc.) to further increase burn rate or reduce cost at constant burn rate. The latter case is particularly important for the extremely expensive carboranes.

The goal in this program effort was to formulate a processable 2 in./sec at 1000 psia propellant using Imperial iron oxide and graphite linters. This goal was accomplished.

The complete set of results for this subtask is given in Table 10. The burn rate of 2.1 in./sec at 1000 psia for the composition containing 1% Imperial iron oxide and 3% 150 μ linters is 40% higher than the iron oxide composition without linters. The use of iron oxide without linters produced rate augmentation of 92% over the base case composition. The total augmentation due to the combination of iron oxide plus linters is 170%. Linter orientation was marginal.

The unusual behavior of the pressure exponent is noted but not explained. The important fact is that the linter-containing composition had only a slightly higher exponent than the base case. These exponents are recognized to be high. However, the purpose of this subtask was to demonstrate linter utility with no work proposed to adjust pressure exponent.

5. Subtask 5 - Combustion Mechanism Study

The objective of this subtask was to quantitatively assess the mechanism of burn rate augmentation due to graphite linters in composite propellant. The approach consisted of visually examining the burning surfaces of linter-containing propellants in a microwindow bomb using high-speed color motion picture photography to record the tests. Based on the

nature of the linter material (virtually all carbon) and past Hercules' cursory visual examinations of linter-containing propellant, the mechanism for rate augmentation is almost certainly mechanical in nature. That is, the propellant burning surface is increased by cone formations around the linters due to the high thermal conductivity of the linters ($\approx 70 \text{ Btu/ft-hr/ft}^2\text{°F}$). Thus, the approach used to meet the objective was to attempt to measure cone angles from the motion picture films and relate the increased surface to increased burn rate.

Tests conducted on samples containing a single layer of 200μ and 0.25-inch linters sandwiched between two 1/16-inch layers of propellant gave unsatisfactory results. The formation of conical burning surfaces around the linters did not manifest itself clearly enough to be measured. In an attempt to overcome this difficulty, a composition was prepared containing 0.1% 400μ linters. Motion picture films depicting the burning of this new formulation showed some evidence of cone formation around the linters. However, the apparent cones were not well defined and measurement of cone angles was not possible. A listing of the compositions studied in this subtask is given in Table 11.

The conclusions drawn from all the work of this subtask are that: (1) linters of 200μ length and smaller are consumed before exiting from the visible flame above the burning propellant surface, and (2) cone angles were not readily apparent because the burn rate range of the AP-HTPB base propellants studied in this program was at the lower end of the practical range for linter utility. That is, for cases of little or no burn rate augmentation, there is little noticeable cone formation around the linters.

C. Task II - Acoustic Instability Study

Task II, the Acoustic Instability Studies segment of the Novel Additives program, was completed at Hercules' Bacchus Works by the Advanced Technology and Applied Physics Research Groups. A total of 96 tests were scheduled for eight propellants. One of the propellant formulations scheduled for testing had unacceptable mechanical properties and thus was eliminated. This change reduced the total required testing, and 83 T-burner tests were conducted to acquire sufficient data for analysis purposes. A listing of these propellants is given in Table 12. Two baseline formulations were used. Variations in the weight percent and size of the graphite linter additives were made in each of the two formulations.

The objective of the acoustic analysis was to determine the effects on acoustic parameters of varying the linter size and concentration. This work included observing variations in driving and damping response of the propellant formulations, burn rate changes, and changes in response as a function of frequency. Two baseline formulations were used to determine the sensitivity of linter-related effects to formulation changes.

1. Test Data and Hardware

The test hardware used was the variable area T-burner (VATB) and an end burning T-burner. Test hardware setup schematics are shown in Figure 32. The VATB hardware was used to acquire variable area pressure-coupled and velocity-coupled data at 1000 Hz (see Figure 32a, b). The best quality data was acquired in the VATB. It is possible to use a large range of propellant sample sizes. Sample location can also be varied for specialized testing. However, the frequency range is limited between 300 and 1600 Hz. Testing at frequencies above this range requires use of the end burner hardware. Testing in this hardware is done using end burning propellant samples as shown in Figure 32c. This restricts propellant sizes to an area ratio of 1.0 or less. Area ratio is the ratio of burning propellant surface to the cross-sectional area of the burner. Data analysis of end burner tests is restricted to comparison of performance between propellants. Particle damping response is usually all that can be determined from this type of analysis.

Figure 33 shows typical end burner test data plotted as a function of mass burned. The reason for plotting the data in this manner will be explained in the next section. The variable area T-burner allows a much more flexible system. Using this system, data for pressure-coupled analysis are acquired by systematically varying the propellant sample area ratio over a range which may extend from 1.5 to 9.0. Those data are then plotted as the measured growth response α versus the test sample area ratio as shown in Figure 34. Smokeless propellants are typically tested over the range of 1.5 to 6.0. This range usually provides good spontaneous growth data, but when additives are used, pulsing is necessary at low area ratios.

To obtain velocity-coupling data, a constant area driver sample is placed in the ends of the burner, and the test sample is placed halfway between the vent and the burner end as shown in Figure 32b. The test sample is varied in size, and data are plotted with respect to the test sample area ratio. Figure 34 also shows a plot of velocity-coupled data. From these data, particle damping, pressure-coupled driving, and velocity-coupled driving of a propellant can be measured. The use of a suppression paddle inserted in the center of the burner makes it possible to stop spontaneous oscillations during the burn. Withdrawal of the paddle allows them to restart for additional growth information. Using this technique can result in up to three datum points per test. It is also possible to pulse during testing up to three times using Mark 2 Mod 0 pulsing squibs.

Test data taken for this study in both VATB and end burner hardware showed good consistency and repeatability. Where possible, repeat testing of suspicious data was conducted and a limited number of tests were repeated to verify consistency of results. For example, the data at area ratio 1.5 in Figure 34 were acquired from three separate tests.

2. Correction Factors Used in Data Analysis

Several correction factors are applied to the 1000 Hz VATB data in order to correct for nonpropellant-related influences on test data. These influences or biases are associated with three physical characteristics of the test hardware and propellant geometry. These are: (1) changes in geometry characteristics as the propellant burns, (2) changes in losses caused by residue buildup on chamber walls, and (3) changes in heat transfer during burning. Each correction is handled separately during the analysis.

Changes in geometry resulting from burning the propellant samples react with the acoustic field, causing changes in acoustic response. Correction for these changes has been modeled by Culick⁽²⁾ and is applied to test data through use of a computer program. Modifications as described by Flandro⁽³⁾ have been made to Culick's original work.

A second correction is applied to account for changes in response associated with residue buildup on the T-burner chamber walls. This data bias was first noted for aluminized double-base propellants and reported in a paper by Hercules Incorporated at the 12th JANNAF Combustion Meeting.⁽⁴⁾ Continued studies have verified that a similar effect occurs with smokeless composite and min-smoke double-base propellants. This effect has been related to the total mass burned during a test. To determine this correction for the linters propellant, test sample ratios of 1.5, 3.0, and 4.5 were used. All data were measured from the burnout decays of initially spontaneous growth tests. These decay measurements were then plotted as a function of the total mass burned during the test from which they were measured. Figure 35 shows the burnout decays from four different tests using propellant NA-2L00-8 and three tests of propellant NA-2L90-8. Data from these were plotted to show a consistency in behavior between propellants with and without linters. The difference in position of the two curves drawn in Figure 35 reflects the contribution to damping of the linters in propellant NA-2L90-8. No apparent curvature change is noted, suggesting that the linters do not affect residue losses significantly. The residue losses increase as a function of mass burned, reaching an asymptote at an area ratio of ~ 6 . The following equation is used to correct each datum point:

(2) Culick, F. E. C., Editor, T-Burner Testing of Metallized Solid Propellants, AFRPL-TR-74-28, California Institute of Technology, Pasadena, California, 1974.

(3) Flandro, G. A., "Solid Propellant Acoustic Admittance Corrections," Journal of Sound and Vibration, 36(3), 1974, pp. 297-312.

(4) Butcher, A. G., Beckstead, M. W., "Anomalous Behavior of T-Burner Test Data," Presented at 12th JANNAF Combustion Meeting by Hercules Incorporated, Magna, Utah, August 1975.

$$\alpha_c = \alpha_o - Le^{-h\Delta m} \quad (4)$$

where: α_c = corrected α
 α_o = measured growth or decay
 L = total change in losses
 h = rate of curvature change
 Δm = mass burned

This corrects the data to a maximum loss condition. Since this is an asymptotic condition, small inaccuracies in determining the actual asymptotic value will not strongly influence overall data corrections. Correction to the intercept value at $\Delta m = 0$ where the slope is a maximum is undesirable because the same small inaccuracy at this point could result in very significant correction differences.

A third correction is made to the data to account for changes involved with heat transfer characteristics occurring during burning. This change affects the small area ratio tests, resulting in a decrease in losses experienced during burning. Figure 36 shows 1.5 area ratio data from two tests each for mixes NA-2L90-8(3) and NA-2L200-8M(3) plotted as a function of the product of mass burned and the time from ignition where α was measured. This heat transfer change has been observed only with smokeless propellants. It probably exists with aluminized propellants but is masked by heavy smoke residue accumulations on the burner walls. Correction for the heat transfer changes is made in a similar manner as with residue buildup corrections discussed earlier. The behavior of the data again indicates an exponential change of the form:

$$\alpha = \alpha_c - He^{-ht\Delta m} \quad (5)$$

where: α_c = corrected α for mass residue only
 H = total heat transfer change
 ht = curvature
 Δm = mass burned
 t = time α was measured

This correction is applied to each datum point to correct it to a non-transient asymptotic condition.

The end burner data show a dependence on the time α is measured during burning. Separate effects of residue and heat transfer changes cannot be isolated because of the limited area ratio range possible in the end burner hardware. It is therefore impossible to make detailed and specific corrections to these data. However, since a consistent behavior in α with respect to the time of acquisition during firing is indicated in Figure 33, a procedure was adopted for analysis of these data. All end burner data at 4000 Hz and 2200 Hz were plotted as α versus mass burned. The slope of the data was assumed to be linear over the range in question and all α values used for comparative analysis were taken where the slope intersected the value of $\dot{m} = 0.2$. This value was selected arbitrarily; however, most propellants tested did have a datum point close to this value.

Although similar behavior has been observed with other propellants, the correction values above are exclusive to the linters-containing propellants tested in the VATB and end burner hardware systems. Sufficient information has not yet been compiled to generalize these corrections to other conditions or propellant formulations.

3. 1000 Hz Data

Acoustic response characteristics for the 1000 Hz data were determined from tests conducted in the VATB hardware. The response characteristics being measured were pressure-coupled driving (B_g), velocity-coupled driving (Rv^i), and particle damping (α_{pd}). Data plots of α versus area ratio for two of the propellants tested are shown in Figures 37 and 38. The α values plotted in these figures have been corrected for mass residue losses, heat transfer characteristic changes and geometry changes as discussed previously. Both the pressure-coupled and velocity-coupled data are shown. A computer analysis on each set of data was run from which values of B_g , Rv^i , and α_{pd} were determined. Table 13 lists the results of the analysis including the variation explained which is a measure of the relative statistical confidence of the calculated values. The computer-calculated theoretical curves for each set of data are shown in Figures 39 and 42. Data points were not included to preserve clarity of the plots. Figures 39 and 41 show the pressure-coupled response curves of each propellant in the NA-2L00-8 and NA-2L00-6M baseline series, respectively. Figures 40 and 42 show the corresponding velocity-coupled predicted curves. Figure 43 gives the pressure- and velocity-coupled response values from Table 13 as a function of the percent linter content. The combination of these figures and table presents a picture of the driving response characteristics of the various propellants.

Careful and detailed examination of the data reveals several important conclusions concerning the effects of linter addition and also the effects of an AP size distribution change on the acoustic response of the propellant. The major condition upon which these conclusions are based is that a real variation in response characteristics does exist. This is

emphasized for two reasons. First, looking at the α versus area ratio data revealed very little difference between propellant data sets due to the amount of data scatter present. This is reflected in the error bands associated with the calculated response values printed in Table 13. The possibility exists that an error in interpretation could result from having an insufficient number of datum points for the data base. More data over a wider range of area ratios are needed to establish tighter confidence levels.* The second concern is based on the results in Figure 43 where B_s is seen to decrease with an increase in the percent of linters while Rv^i does the opposite. One might conclude that the computer is merely trading off one for the other, and the variations are caused in the analysis. Based on previous experience, the calculated variations appear to be real and do represent actual response changes resulting from the formulation variations. Where repeat tests were conducted, good comparisons resulted. With regard to the computer analysis, if the computer were trading off pressure-coupled driving versus velocity-coupled driving, a certain amount of random behavior should be apparent. However, a very consistent pattern is evident not only with the percent of linters but also with the size of linters. This is also true in particle damping characteristics which will be presented later. Therefore, the following conclusions are made with confidence that they are real effects.

Referring back to Table 12, a comparison of the AP size distribution shows that a major difference between NA-2L00-8 and NA-2L00-6M was the elimination of the 200 μ AP in NA-2L00-6M. Experience has shown that pressure-coupled response usually increases as the AP distribution shifts toward smaller particle sizes. With the elimination of the 200 μ AP, one might think that NA-2L00-6M type propellants would demonstrate a greater pressure-coupled response. However, the NA-2L00-8 series showed the largest values of B_s . The other major change in AP distribution was a 50% reduction of 2 μ AP from 30% to 14%. The conclusion is that the small AP has the greatest controlling influence on B_s . The reduction in the percentage of 2 μ AP had more effect than changing the 200 μ particles to 90 μ particles. The velocity-coupling response showed the opposite effect, suggesting that it may be more responsive to changes in the large AP particles. There are, however, several factors involved in the relation between AP size and response characteristics. Changes in size distributions are generally complex, several sizes being changed at the same time; and the results cause complex interactions which are not easily interpreted. Further study involving precisely controlled changes are necessary to provide usable information concerning general relations between formulation changes and acoustic response.**

 *The program was designed to provide preliminary data of a novel additive to show future potential rather than providing a comprehensive detailed assessment.

**Work in this area is currently being conducted by Hercules/ABL under AFRPL Contract No. FO4611-76-C-0006.

Definite conclusions can be reached with regard to the influence of linter variation because linter content and size were changed systematically in each baseline formulation. Increasing the percentage of linters has the effect of decreasing the pressure-coupled response. A significant reduction in this response is seen in the 3% linters propellants. There is no apparent relation to linters size. On the other hand, increasing the percent of linters increases the velocity-coupling response. The 200 μ linters cause a greater change than the 90 μ linters. The prime conclusion is that the size and quantity of linters can be used to tailor both pressure- and velocity-coupled response characteristics. This is a very desirable quality in a propellant additive.

4. Burn Rate

Measurements were also made to determine the effect of linter variation on burn rate. The burn rate measurements were taken from the VATB data at 1000 Hz. Only very poor quality measurements were possible from the end burning disk data at 2200 and 4000 Hz because of the small pressure variations experienced. Therefore, no frequency-dependence measurements were possible. Table 14 shows the burn rates from the various propellants. Also calculated is the percent increase in burn rate over the baseline for the linter-containing propellants. These values are plotted in Figure 44 as a function of the percent of linters. The percent increase in burn rate for a given linter percent and size was consistent for both baseline formulations. This made it feasible to plot the percent increase as a function of linter content irrespective of baseline formulation. Figure 44b shows that burn rate changes of up to 25% can be acquired with linter variation. It also indicates that the 200 μ linter has the greater effect.

5. Particle Damping Evaluation

The major objective of the acoustic analysis task was to evaluate the acoustic damping characteristics of graphite linters. All the data taken at frequencies of 1000, 2200, and 4000 Hz were analyzed, and Table 14 lists the measured values of α_{pd} at each frequency for each of the propellants evaluated. Several methods of correlating the particle damping characteristics were examined. Quantities pertinent to these correlations are also listed. They include the value of $\omega = 2 \pi f$, a theoretical particle size necessary to produce the measured damping, an optimum particle size which would produce maximum damping at the calculated frequency, and a measure of damping efficiency. Figure 45 shows the values of α_{pd} from Table 14 plotted as a function of frequency. Particularly noticeable in this figure is the fact that different damping values are indicated for the two linter sizes for the same concentration. A consistent trend is seen indicating that the 200 μ linters cause a greater damping than the 90 μ linters. This difference becomes greater at the higher frequencies, not only in magnitude but also in percentage difference.

In Figure 46, α_{pd} is plotted as a function of the percent linter concentration with frequency as a parameter. The difference in damping is perhaps more evident in this figure. The increase in damping as a function of concentration is in good agreement with theory which indicates that α_{pd} is proportional to weight percent, C_m , of the additive:

$$\alpha_{pd} = \frac{C_m}{(1+C_m)} \frac{\omega}{2} \frac{\omega\tau}{[1+(\omega\tau)^2]} \quad (6)$$

Evaluation of the two linter sizes shows that no significant difference due to particle size is evident at 1000 Hz. However, as frequency increases, the damping characteristics of the two sizes change considerably. To study possible reasons for this change, the theoretical particle sizes necessary to produce the observed damping were calculated. For values of $(\omega\tau)^2 \gg 1$, which is generally the case with the linters data, Equation 6 can be reduced to

$$\alpha_{pd} = \frac{C_m}{2(1+C_m)\tau} \quad (7)$$

or

$$\tau = \frac{2(1+C_m)}{C_m \alpha_{pd}} \quad (8)$$

From the value of τ calculated in Equation 8, a theoretical particle diameter can be calculated from

$$D = \sqrt{\frac{18 \mu \tau}{\rho}} \quad (9)$$

These values of D corresponding to the particle damping measured for the various propellants are listed in Table 15. The average diameter of the linters is 6 μ . As can be seen, most calculated diameters are on the order of 14-20 μ , indicating some degree of random orientation with respect to the acoustic flow. The fact that the 200 μ linters provide a greater damping suggests that this linter size is more closely oriented with the flow, thus presenting a smaller overall particle size to the acoustic flow.

Analysis of drag forces (Equation 10) on the particles indicates that at Reynold Numbers on the order of 1 to 10, which are average T-burner values, the drag is most heavily influenced by surface area. The coefficient of drag, C_D , on cylinders and spheres is nearly equal over this range.

$$F_D = C_D \rho \frac{U}{2} A \quad (10)$$

Thus, the larger particle size equivalent to a rod turning sideways in the flow would experience a larger net drag force than a spherical particle having the same diameter as the rod (Figure 47a). With the larger drag force a larger particle would be forced to move more in phase with oscillating flow than a small particle. Particle damping is a function of the phase relation of gas-particle motion, reaching a maximum at a 180° out-of-phase motion. A large particle traveling more in phase with the gas would produce the least damping effect. The longer linter length would tend to aid in orientation, minimizing drag.

The change in the difference in damping between the two particle sizes as a function of frequency is related to the total residence time of the particle in the burner chamber and the burning characteristics of the linters. Particle damping is also a function of the acoustic velocity which is greatest in the center of the burner and zero at the ends. Therefore, the greatest particle interaction occurs as the particles approach the center of the chamber. The lack of difference in the particle sizes as calculated from the data at 1000 Hz suggests that the particles are possibly consumed in a relatively short travel down the burner and before they enter the region of most active damping as suggested in Figure 47. As the frequency is increased and burner length shortened, the particles reside in the burner for longer relative travel distances and spend more time in the central portion of the burner before they burn up. Any differences in damping characteristics of the two particle sizes therefore become more evident as they react to greater acoustic velocities. This is demonstrated by the data in the fact that the greater the frequency, the greater the observed difference in α_{pd} .

Another examination of the data involved examining particle damping efficiency. This quantity was calculated as the ratio of actual damping to theoretically maximum damping. Table 4 lists the percent efficiency for each propellant. From these values a weighted average efficiency for each particle size at each frequency was calculated. The average was weighted based on the quality of data used to calculate the particle damping. For example, the NA-2L00-6M data at 4000 Hz show a 19% efficiency for $90\ \mu$ linters as compared with 58 and 47% efficiencies for mixes NA2L90-8 and NA-2L90-5(3)M. Since the NA-2L00-6M data appear to be significantly out of line, it was weighted arbitrarily at 50% confidence. The weighted average efficiencies were then plotted as a function of frequency and shown in Figure 48. The point of this figure is that a consistently higher efficiency is seen for the $200\ \mu$ linters than for the $90\ \mu$ linters, agreeing with previous results. The shape of the curve having a minimum at around 2500 Hz may be more indicative of hardware anomalies than of particle efficiency changes. Extrapolation beyond the range of test frequencies is therefore not advised. A comparison with other particulate additives was made using the Hercules baseline Sidewinder propellant with ZrC and Al_2O_3 additives. Figure 49 shows these data graphically. At the 3% concentration level, little or no difference between the graphite and ZrC with graphite flake is noted. No Al_2O_3 data were available. At the 1% concentration level, damping by the graphite linter is significantly greater than

that by ZrC with graphite flake and about the same as the damping by Al_2O_3 with flake. These data indicate that graphite linters are at least as good a damping additive as either ZrC or Al_2O_3 at 1000 Hz. It is interesting to note that the greatest difference in damping characteristics between 90 and 200 μ linters was observed at high frequency. It is conceivable to believe that similar differences may be seen between graphite linters and ZrC or Al_2O_3 at high frequencies. An important question as to the relative effectiveness of linters versus inert type additives is unanswered at this time due to a lack of comparative data at the higher frequencies.

Several important items have been learned about graphite linters with respect to their damping characteristics through this brief study. It was found that damping response comparable to that obtained with other typical smokeless propellant additives can be obtained with graphite linters. Particle damping characteristics of the linters are not affected by formulation changes such as those between mixes NA-2L00-8 and NA-2L00-6M which did result in significant driving response changes. A significant observation was the difference between the damping characteristics of the 200 and 90 μ linter lengths. It is evident that the 200 μ particles provide more effective damping at frequencies above 2000 Hz than the 90 μ linters.

General data quality is good, and consistency in analysis results suggests that observed variations in acoustic behavior are real and represent actual propellant response characteristics.

Several important facts were learned concerning the role of linters in propellant acoustic behavior:

- (a) Variation of linter concentration has an effect on both pressure- and velocity-coupled driving. The result of increasing linter concentration is to lower the pressure-coupled response and increase the velocity-coupled response.
- (b) Size variation had no appreciable effect on pressure-coupled driving but did influence the velocity-coupled response.
- (c) Burn rate studies indicate that a 3% linter concentration can increase the burn rate as much as 25% over a baseline containing no linters. The effect of size was apparent in that 200 μ linters had the greatest effect on burn rate.
- (d) The particle damping characteristics of graphite linters showed some variation with size. At 1000 Hz, no significant difference between the

two linter sizes was noted. However, as frequency increased, the damping efficiency of the 200 μ linters surpassed the 90 μ efficiency, resulting in a difference of about 115 sec^{-1} at 4000 Hz.

- (e) In comparison with other acoustic damping additives, such as ZrC and Al_2O_3 , the linters performed equally as well at the 3% concentration level. Linters actually provided more damping than the other additives at the 1% concentration level.

These damping characteristics, coupled with the ability to influence driving response and burn rate and the fact that linters are consumed, leaving little or no solid particle smoke residue, present a very desirable picture of graphite linters for use as an acoustic suppressant additive in smokeless propellants.

D. Task III - Demonstration of Processing Improvements

The goal of this task was to demonstrate that linters can be used to improve uncured propellant processability. That is, given a composition containing a UFAP fine solids fraction, the end-of-mix viscometric properties can be improved by replacing the UFAP with 2 μ AP and the addition of linters. The basic premise is that linters will augment the burning rate such that the loss of rate due to the increase in fine AP size (0.7 μ to 2 μ) is offset and the processing difficulties which arise from UFAP are eliminated.

The concept is illustrated in Table 16 by the compositions NA-.7L00-8 and NA-2L200-8A(3). The UFAP-containing composition, taken from Table 4, has a consistency index, m , of 10.9 Kp compared with a value of m equal to 7.1 Kp in the analog composition containing 2 μ fine AP and 3% linters (in addition, the analog composition contains 20 μ AP as an intermediate size rather than the 6 μ AP intermediate size of the UFAP composition).

Just as important as the decrease in m is the increase in n' , the flow behavior index, from 0.26 to 0.36. This increase is desirable because the slurry is less pseudoplastic (shear rate dependent) as n' increases toward unity. The lower the value of n' , the more difficulty one encounters in a mold-filling operation.

Considering the burn rates of the two compositions, Table 6 shows a value of 0.50 in./sec at 1000 psia for the UFAP composition (pressure exponent, n , is 0.52) and 0.59 in./sec for the 2 μ analog composition

(pressure exponent is 0.59). The rate was increased rather than maintained constant. However, it is a simple matter to lower the rate by increasing the overall AP particle size. The value of n can be reduced in a like manner. The fact that the burn rate was increased in the analog composition demonstrates the point to be made in this task.

The second pair of compositions in Table 16, NA-.7L00-7 and NA-2L200-7A(3), showed only partial success. That is, processability was significantly improved but when 0.7 μ AP was replaced by 2 μ AP and graphite linters, the burn rate decreased 10%. It is the author's opinion that a small adjustment in solids would raise the burn rate of the analog composition to equal that of the 0.7 μ fine AP composition while still maintaining improved processability. However, the scope of this task precluded any further work.

The third pair of compositions, NA-.7L00-4 and NA-2L150-4A(2), showed improved processability for the analog composition, but the burn rate was significantly reduced. To raise the analog burn rate would require extensive modifications to the solids distribution. These changes would deviate from the original intent of this task.

In addition, two one-pound mixes were attempted and scrapped because of poor castability. This was not unexpected since this task involves compositions at the extreme upper end of the processable regime.

A final point to be made from the results of Table 16 is the significant reinforcement in mechanical properties in most of the linter-containing compositions. Of particular importance is the increased tensile strength at -65°F for the first two compositions in the table (NA-7L00-8 and NA-2L200-8A(3)) without a loss in strain. Also, comparison of the 165°F properties for the same two mixes shows those of the linter-containing composition to be far superior.

Based on the results of this completed task, the conclusion drawn is that graphite linters can be used to overcome some of the undesirable aspects of UFAP. Namely, UFAP can be eliminated by replacement with a larger size AP plus linters. Two major advantages to this approach are (1) better processability upon removal of UFAP, and (2) elimination of the UFAP dispersion problem. The approach is limited only by linter orientation. That is, the total solids distribution must be such that linters are not preferentially oriented in the cured propellant. As shown in other areas of this program, preferential orientation of linters can be overcome in many compositions.

SECTION V

RECOMMENDATIONS

In light of the observations and conclusions made during this study, it is believed that some very important knowledge can be gained from further study of graphite linters as to their application in smokeless propellants. Several effects of linter size and concentration were observed, and theories as to why this behavior occurred have been made. Verification should involve investigation of linter behavior in the following areas: (1) burning characteristics, (2) flow orientation, (3) size effects and distribution of sizes, and (4) effects of changing test conditions over wider ranges of pressure and frequency. Further, comparison data for other additives such as Al_2O_3 and ZrC are also needed.

Studies involved in these areas are essential to evaluate fully the possibilities of using graphite linters as an effective acoustic suppressant.

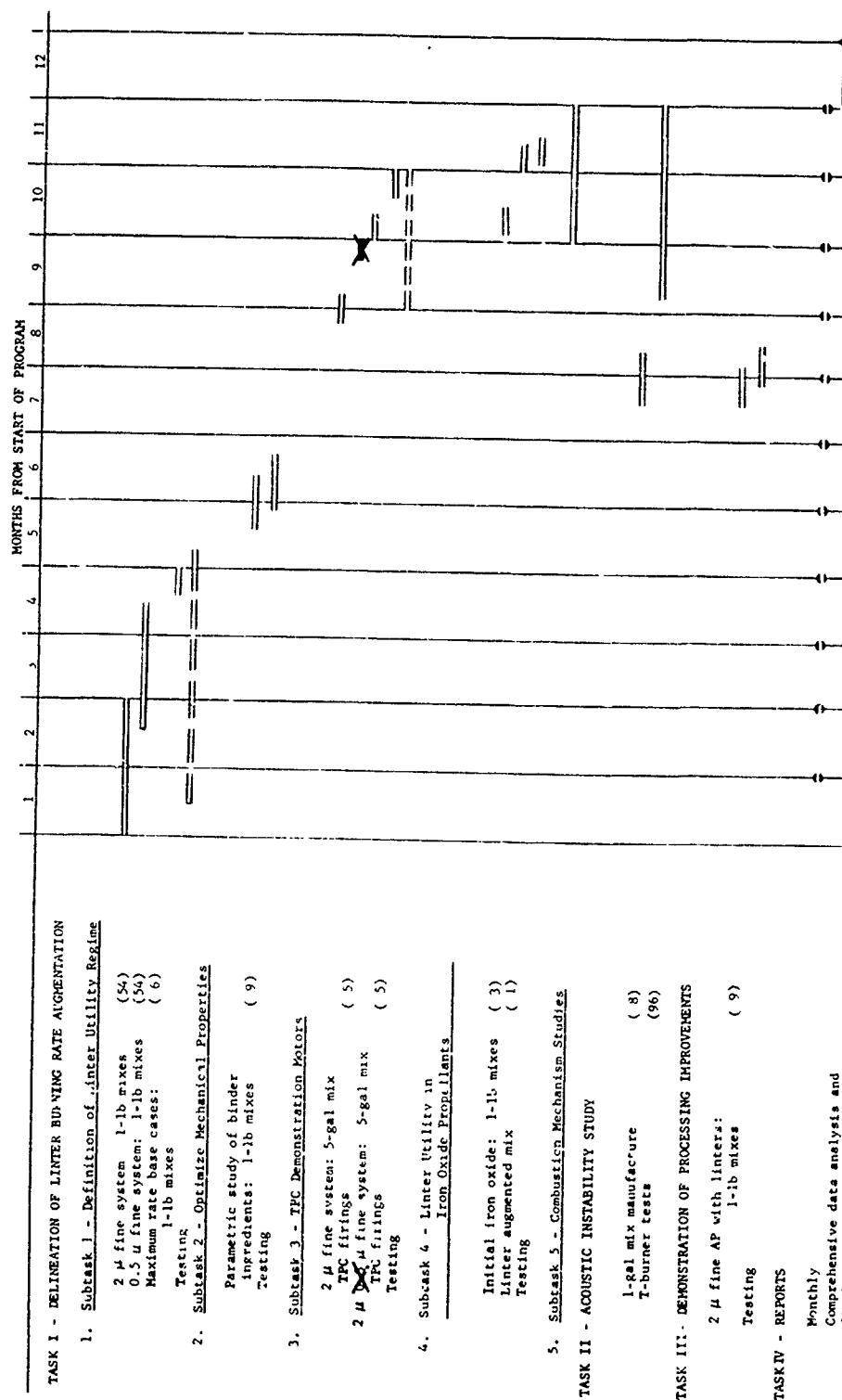


Figure 1. Program Milestone Chart

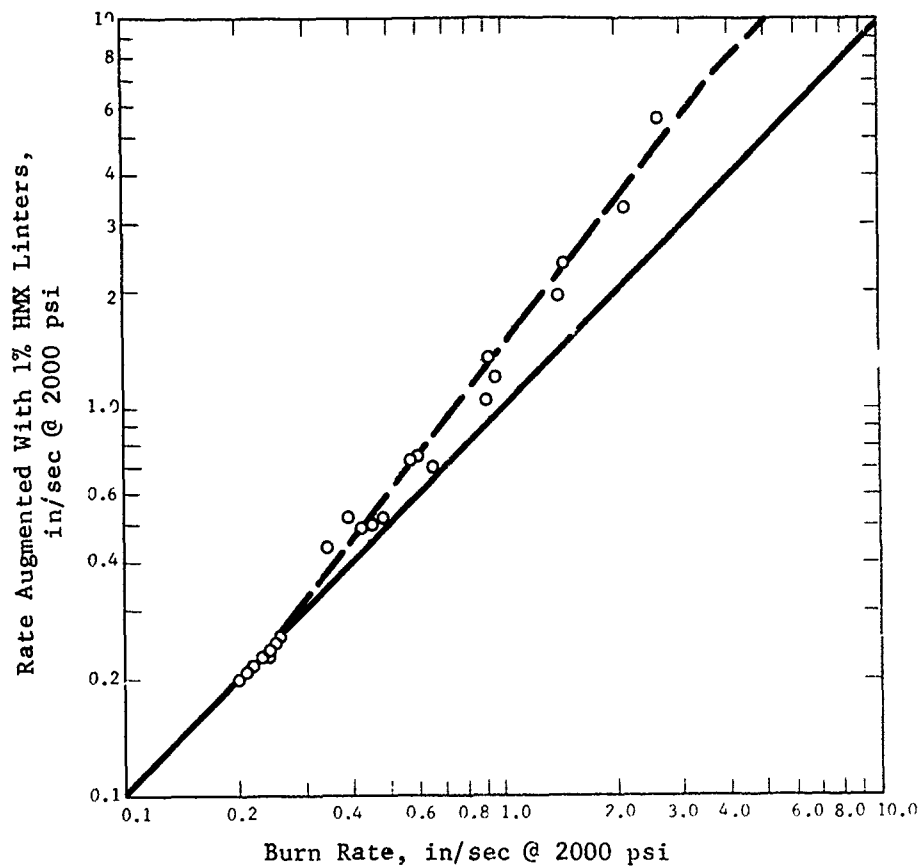


Figure 2. Influence of 400 μ Linters on Burning Rate at 2000 psia; for Double-Base and Composite Propellants - Lower Rate Range

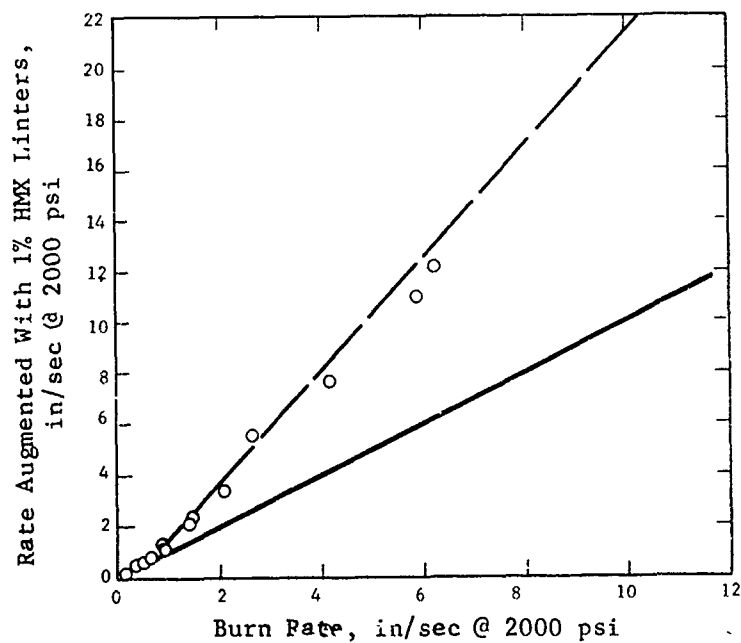


Figure 3. Influence of 400 μ Linters on Burning Rate at 2000 psia; for Double-Base and Composite Propellants - Higher Rate Range

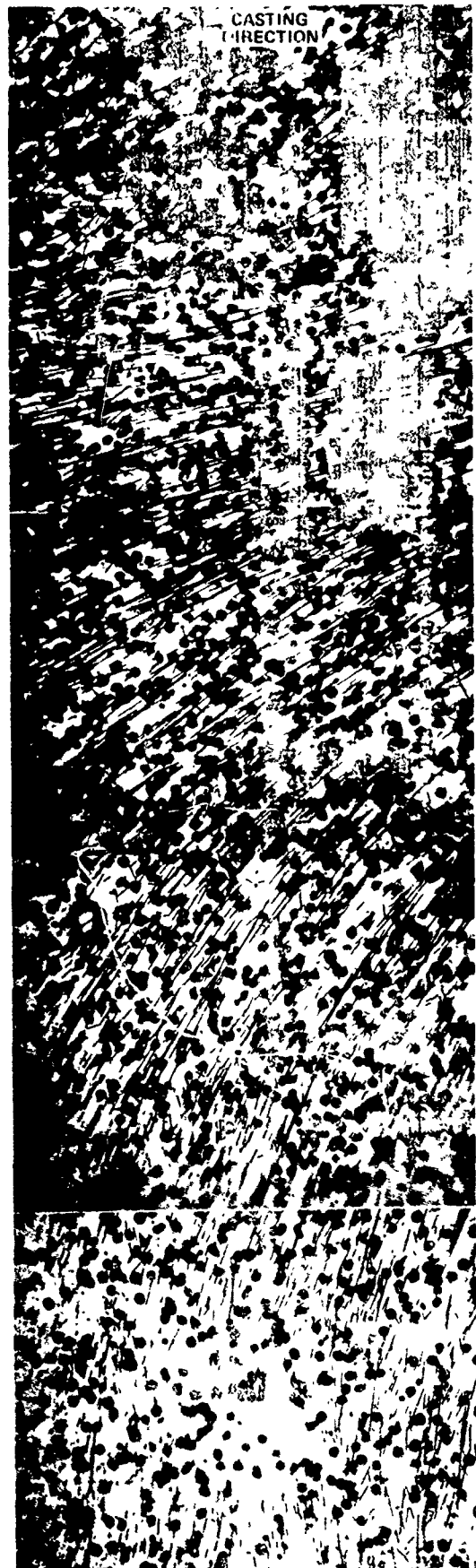


Figure 4. Typical Orientation Pattern for 400 μ Linters and 50 μ Coarse Solids

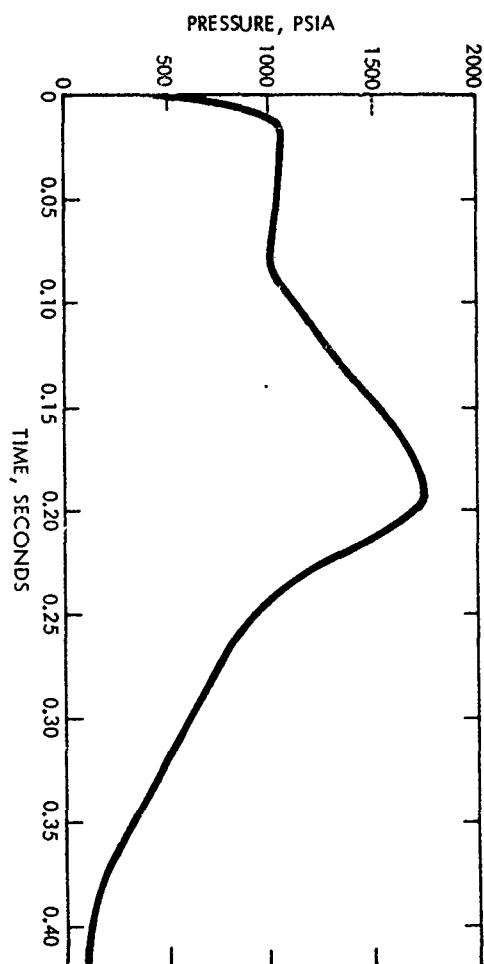


Figure 5. Typical Pressure-Time Trace for Center-Perforated Composite TPC Using 50 μ Coarse Solids and 400 μ Linters

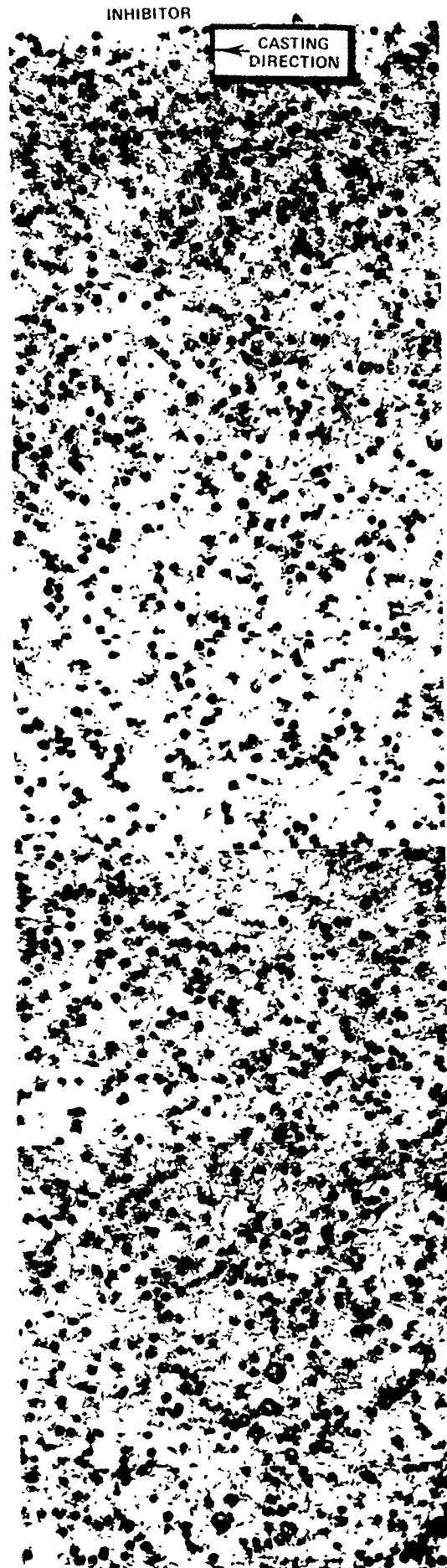


Figure 6. Typical Random Distribution of 3% 50 μ m Coarse Solids (Mag. 32X)

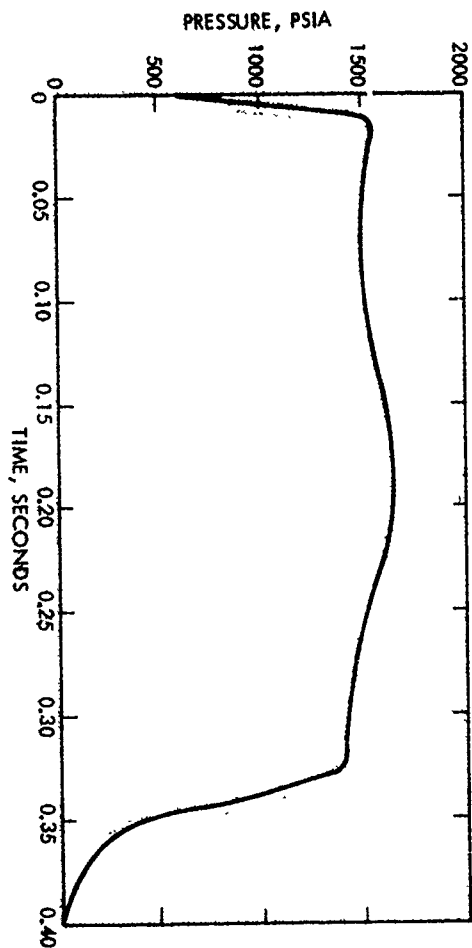


Figure 7. Typical Pressure-Time Trace for Center-Perforated Composite TPC Using 50 μ m Coarse Solids with 50 μ m Inhibitors of 3% Concentration

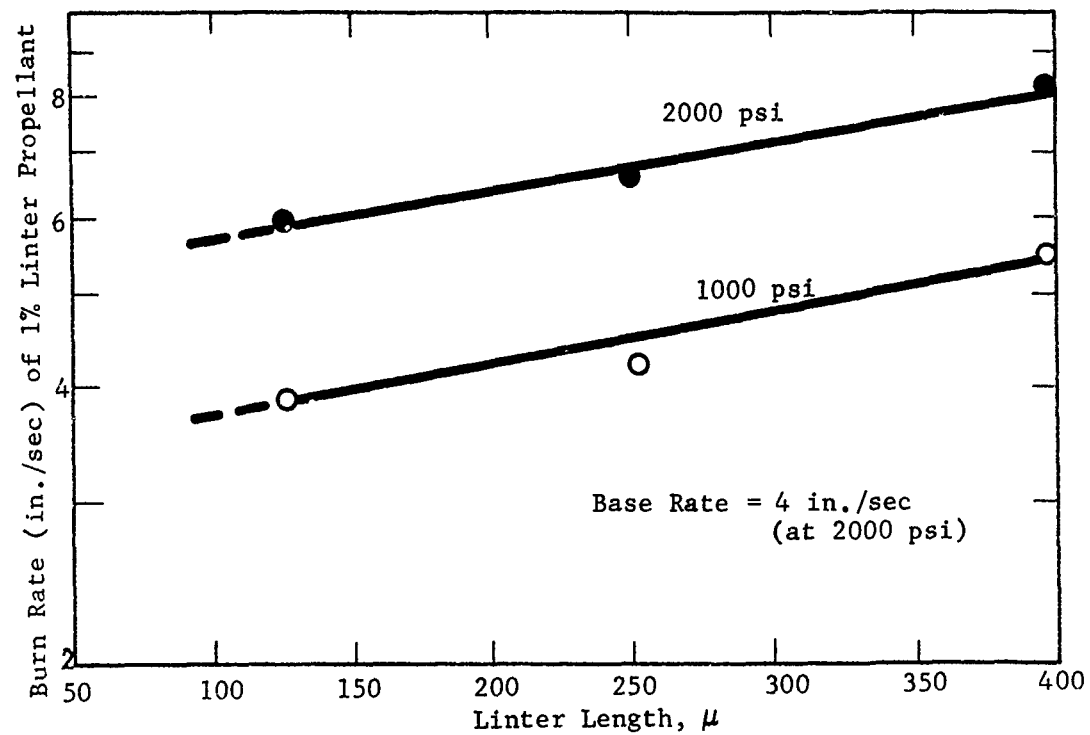


Figure 8. Influence of Linter Length on Burning Rate

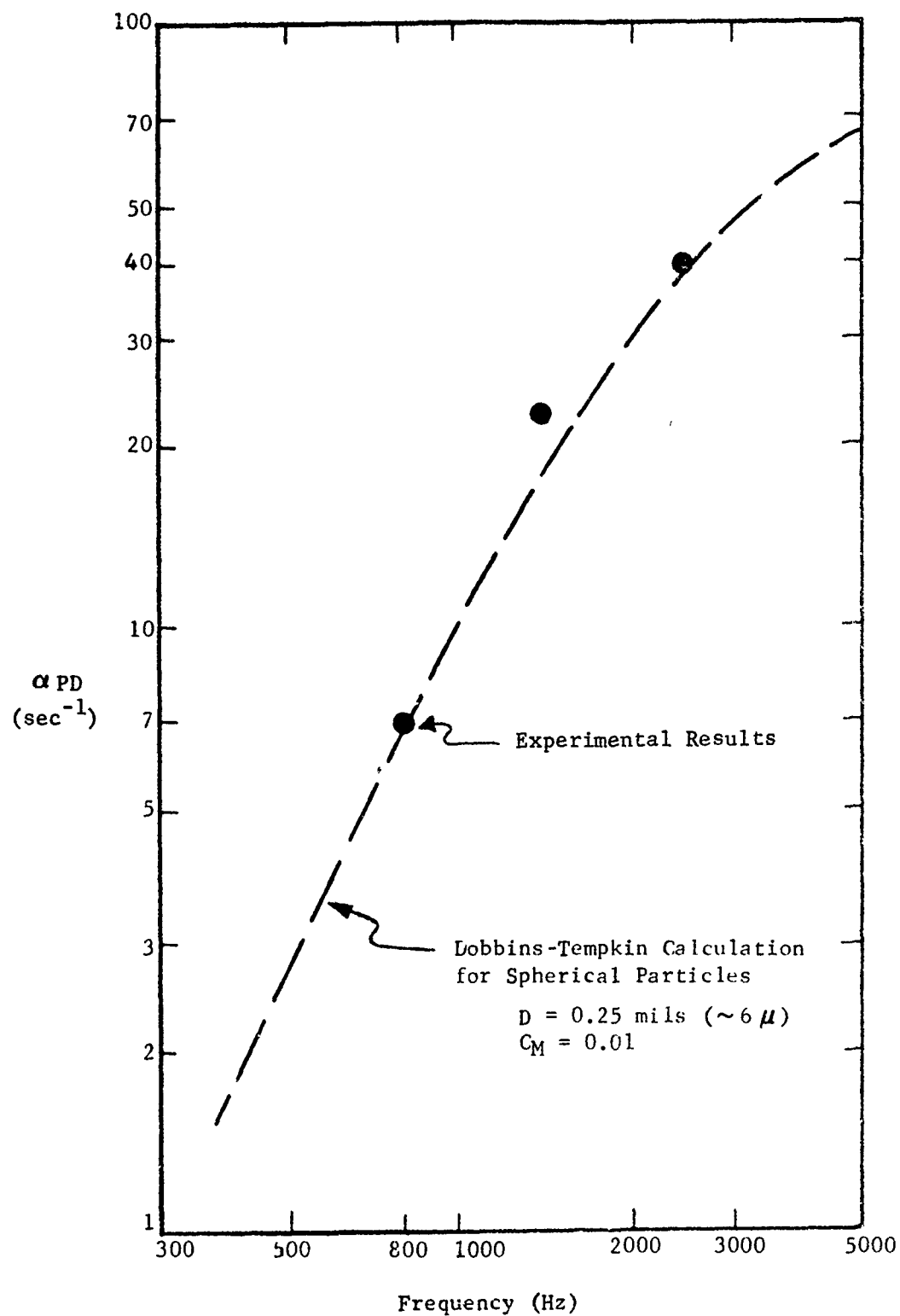


Figure 9. Effect of Frequency on Particulate Damping for Graphite Linters

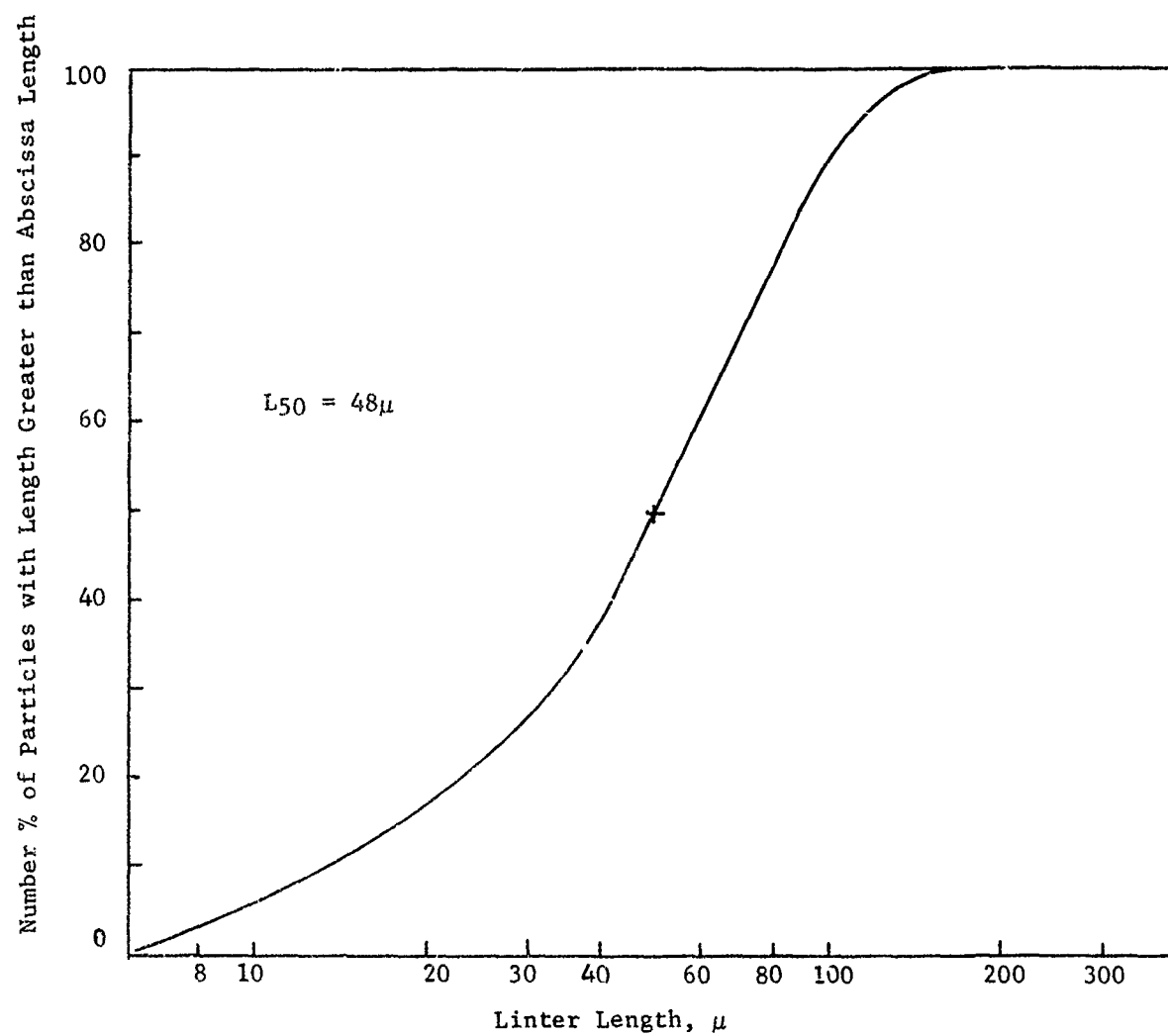


Figure 10. Linter Length Distribution for Nominal 50 μ Linters

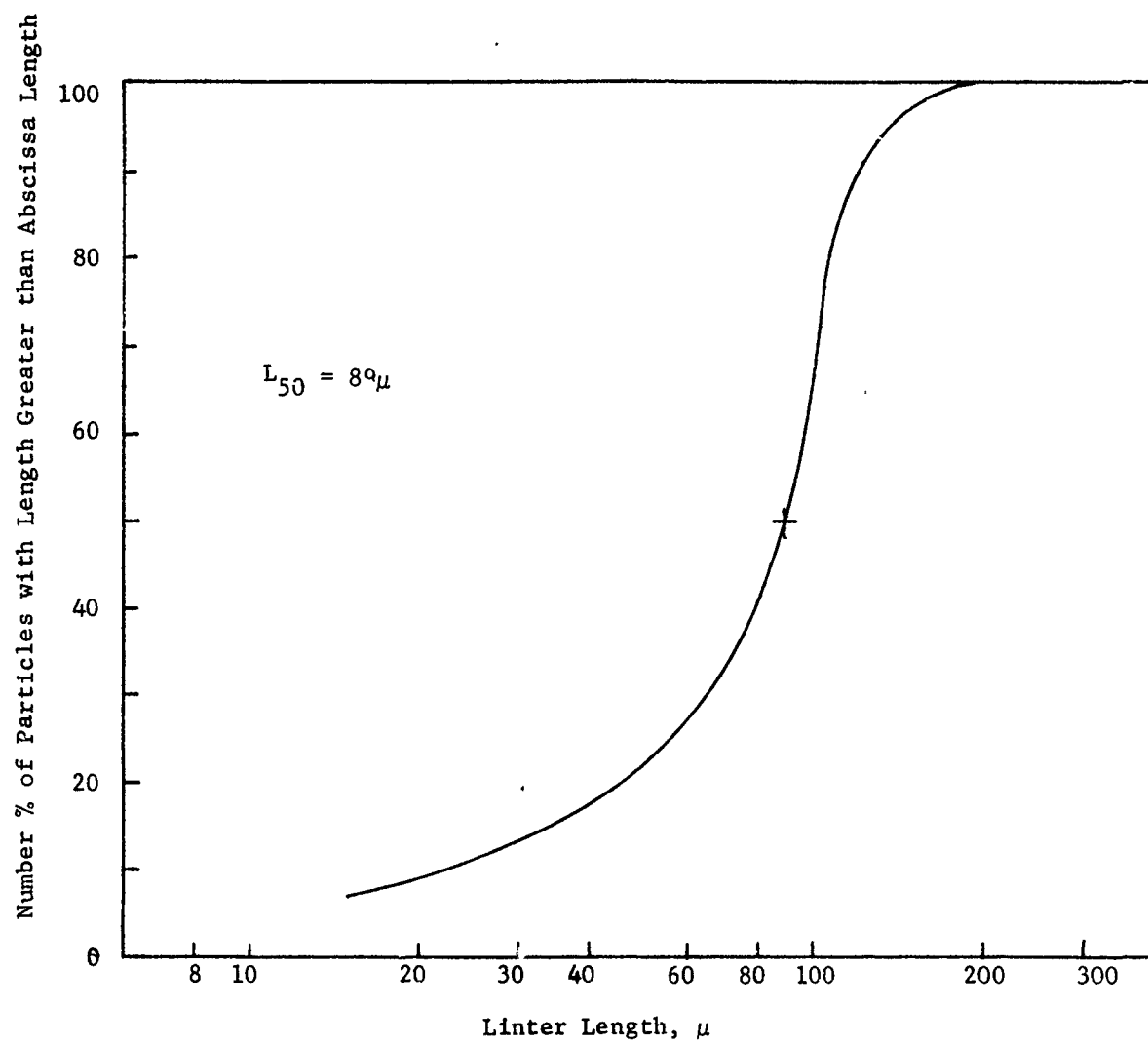


Figure 11. Linter Length Distribution for Nominal 90 μ Linters

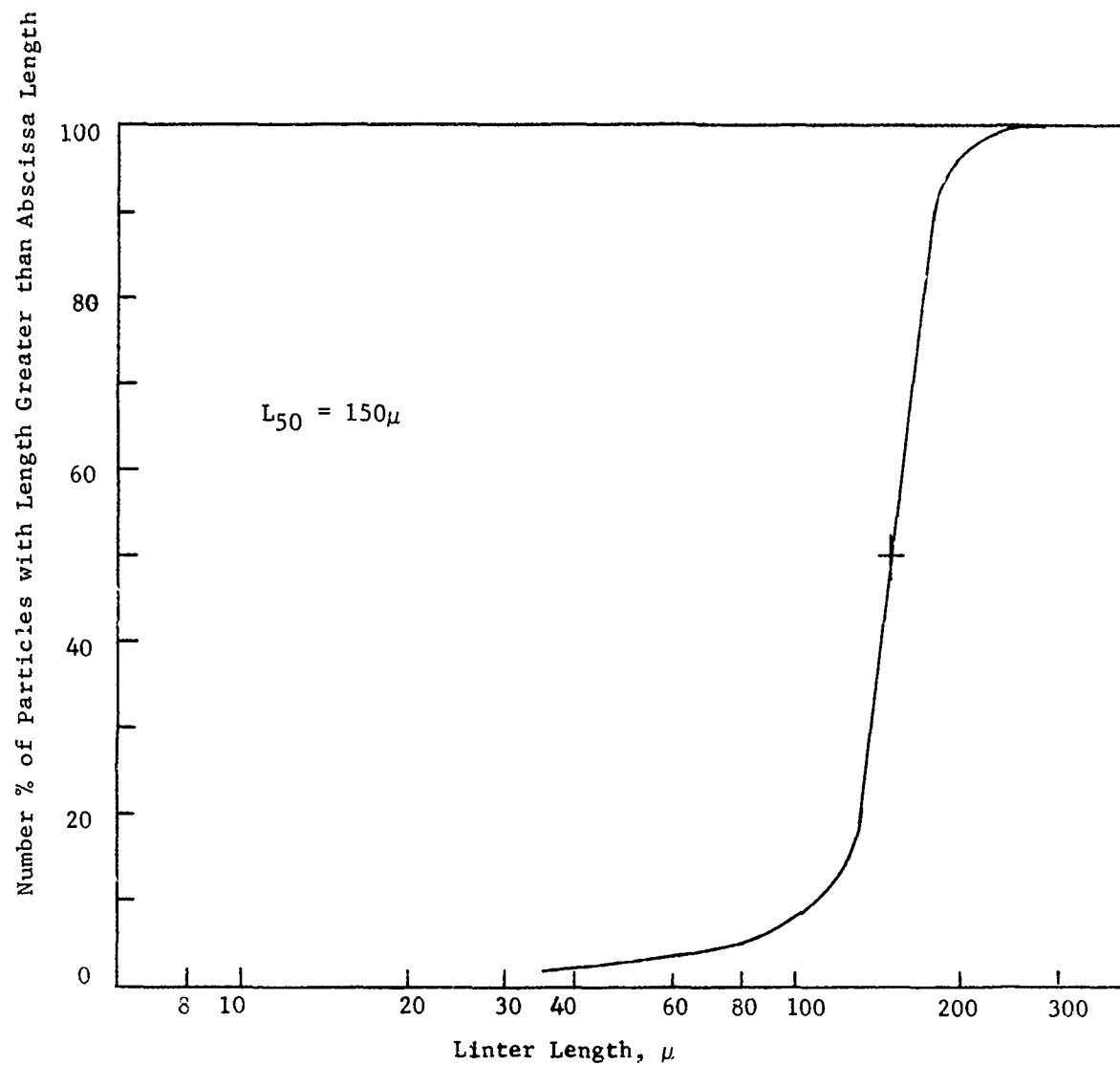


Figure 12. Linter Length Distribution for Nominal 150 μ Linters

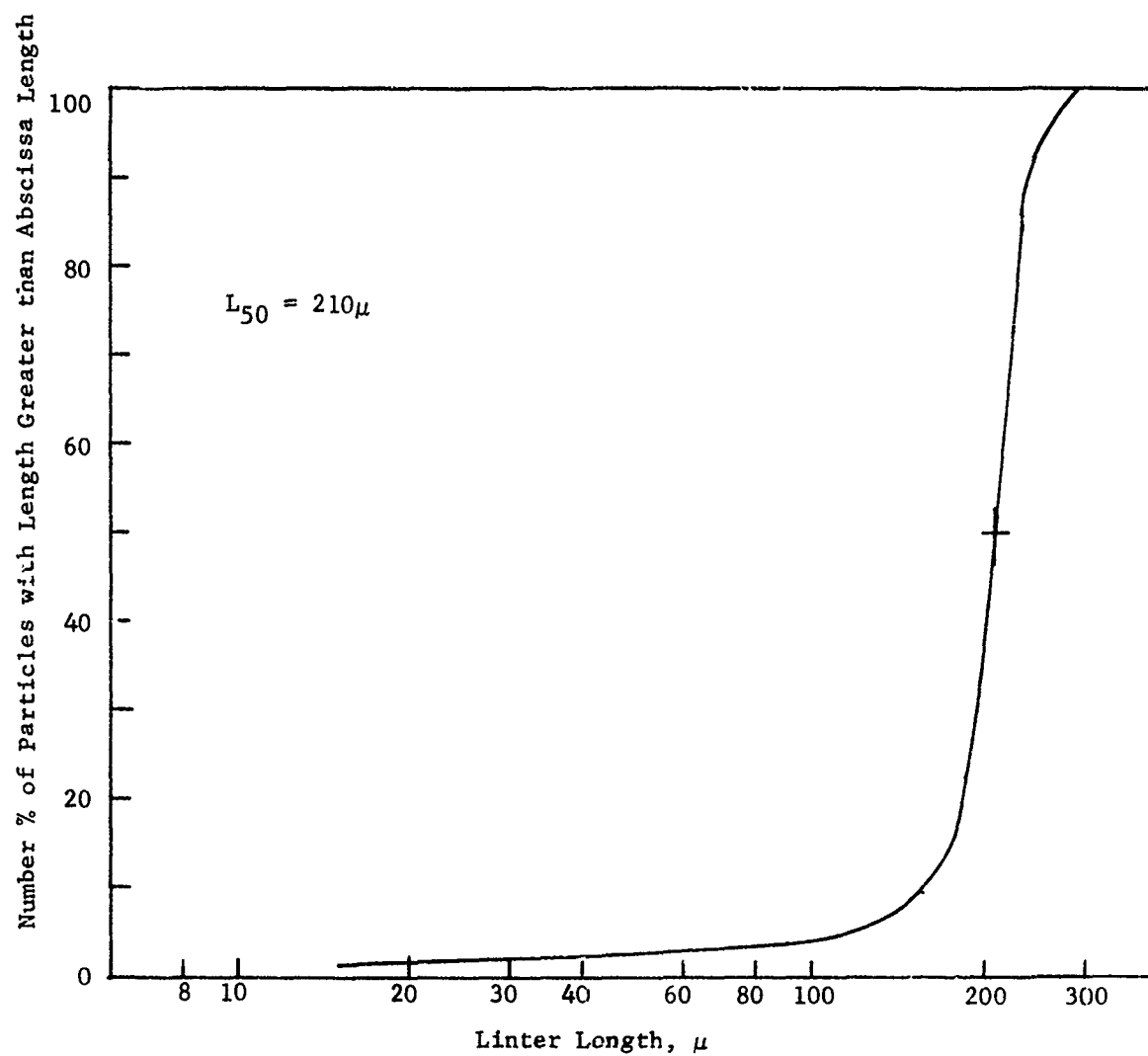
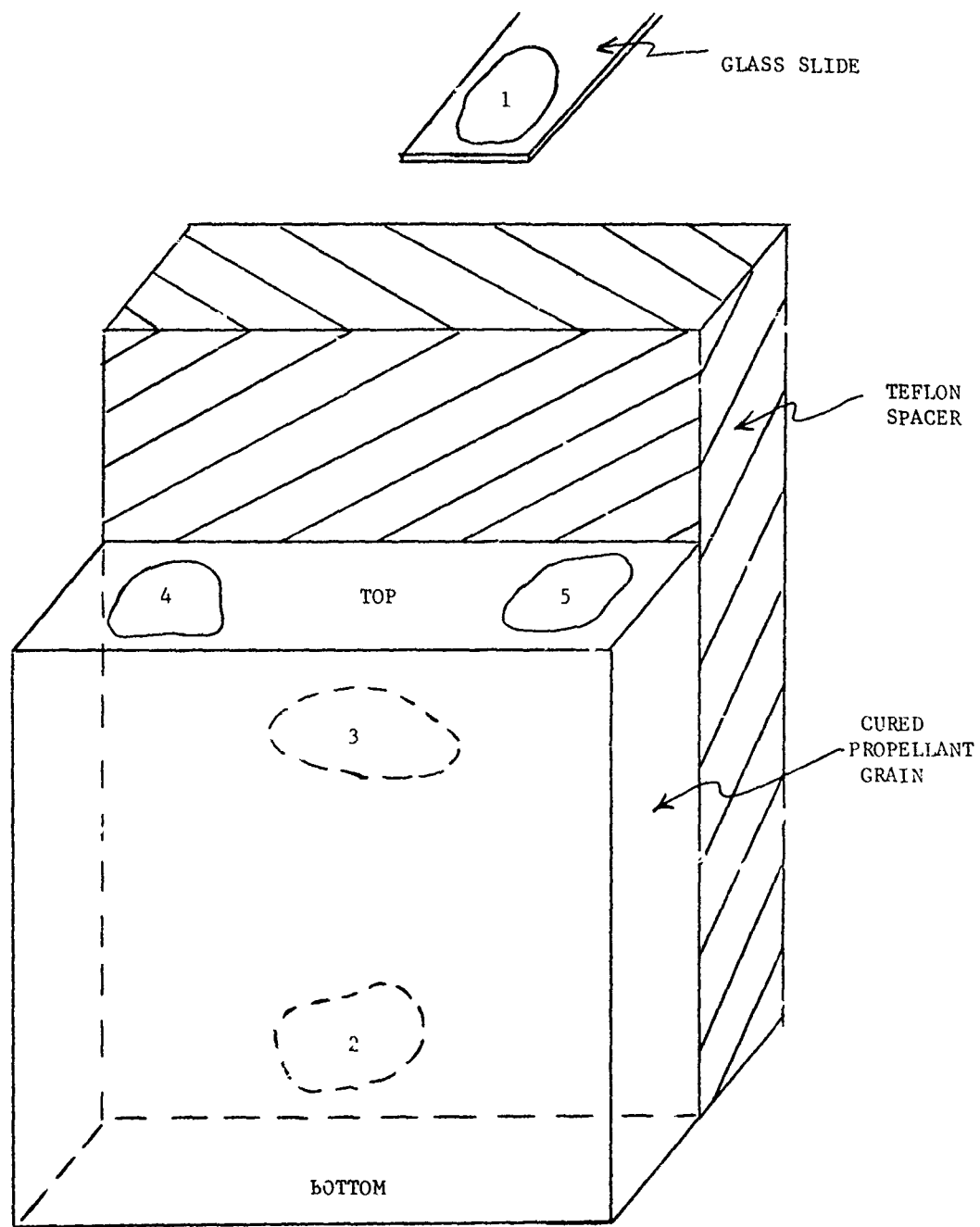
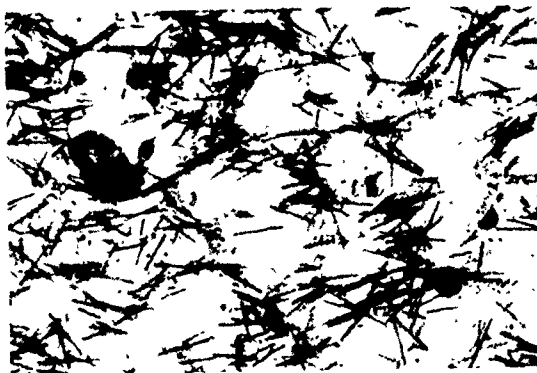


Figure 13. Linter Length Distribution for Nominal 200 μ Linters

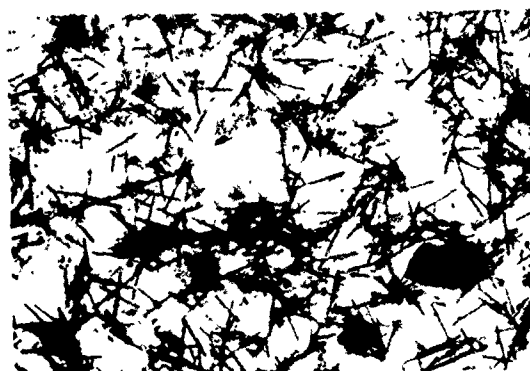


1, ..., 5 SLICES FOR PHOTOMICROGRAPHS

Figure 14. Diagram Showing Location of Slices for Microscopic Examination



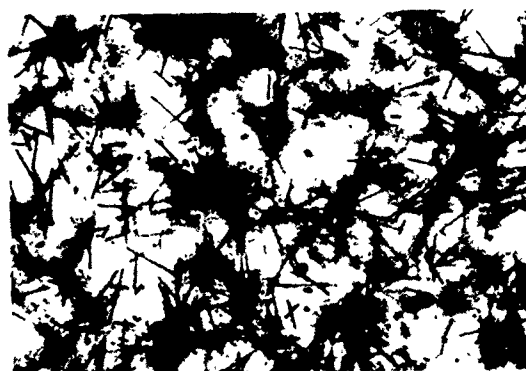
(a) Sample No. 1*



(b) Sample No. 2



(c) Sample No. 3



(d) Sample No. 4



(e) Sample No. 5

*Refer to Figure 14 for Sample Location in Propellant Grain

G 3410

Figure 15. Photographs Showing Random Linter Orientation in Propellant 2L150-9
(50X Magnification)



(a) Sample No. 1*



(b) Sample No. 2



(c) Sample No. 3



(d) Sample No. 4



(e) Sample No. 5

*Refer to Figure 14 for Sample Location in Propellant Grain

G-1111

Figure 16. Photographs Showing Preferential Linter Orientation in Propellant 2L150-1 (50X Magnification)

2 μ Fine AP Fraction
Total AP d₃₂ ~4.9 μ

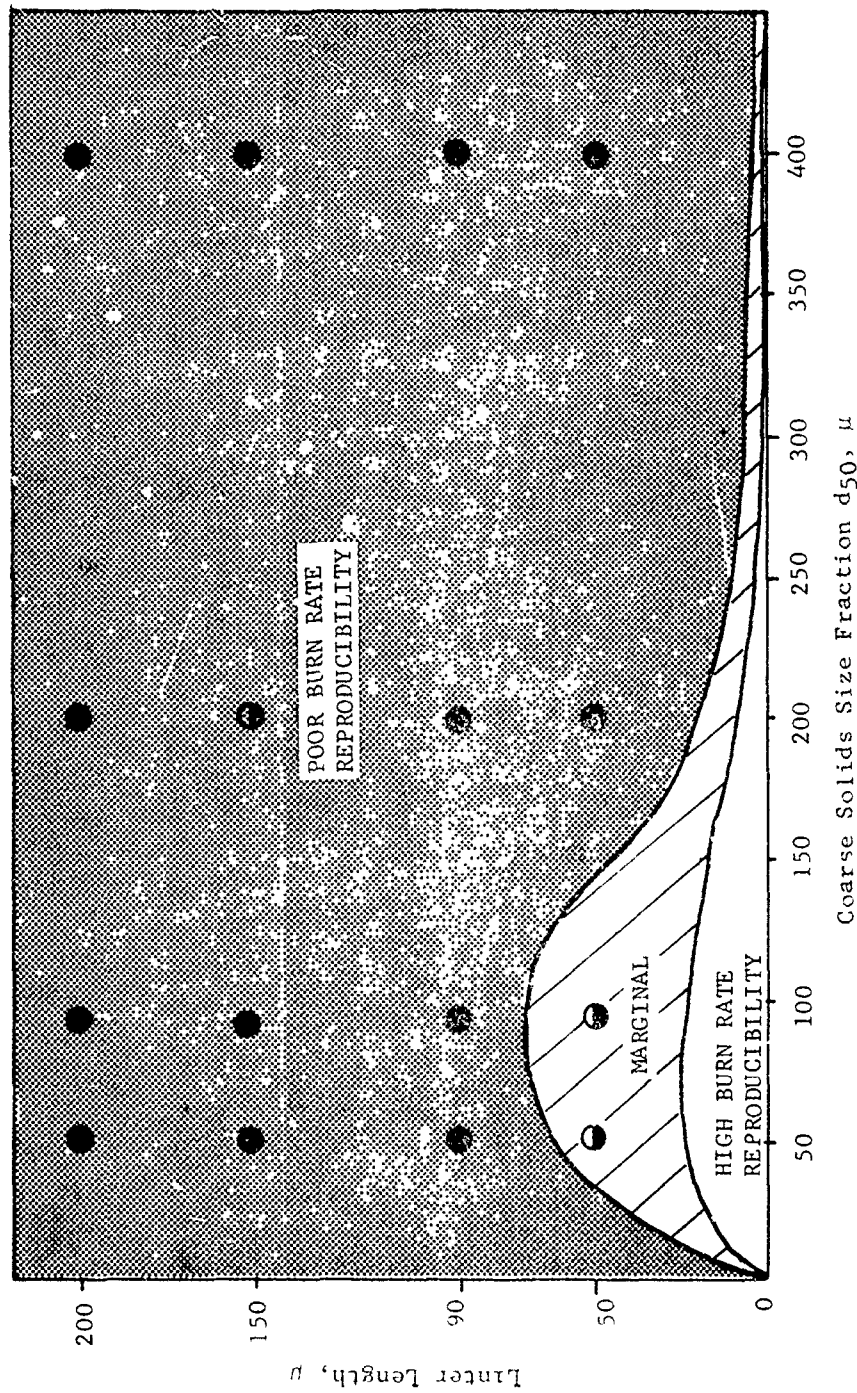


Figure 17. Linter Utility Regimes for Fixed Fine Oxidizer Size (2 μ) and Total Oxidizer Surface Mean Diameter (4.9 μ)

2 μ Fine AP Fraction
Total AP $d_{32} \approx 5.6 \mu$

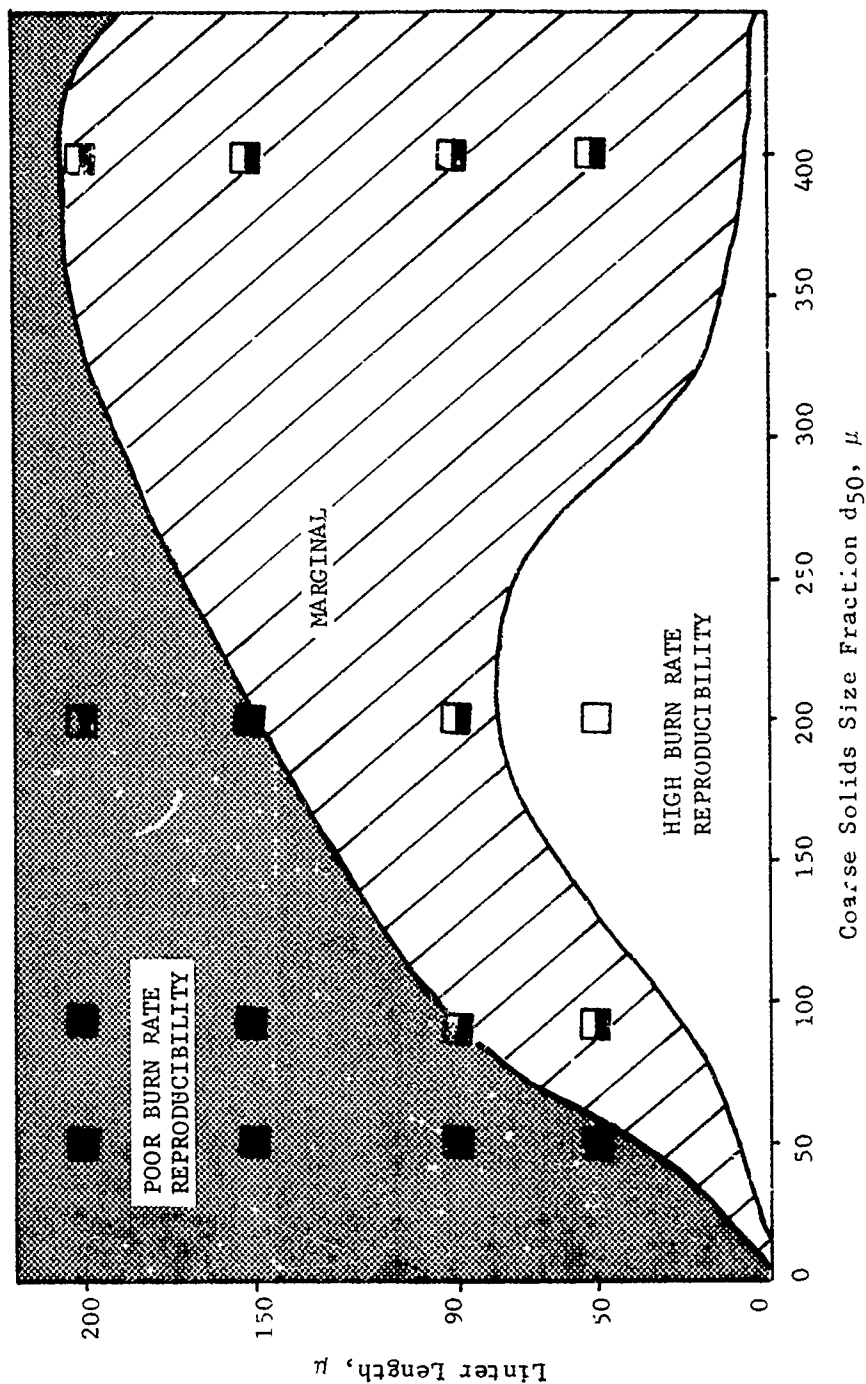


Figure 18 Quality Regimes for Fixed Fine Oxidizer Size (2 μ) and Total Oxidizer Surface Mean Diameter (5.6 μ)

2 μ Fine AP Fraction
Total AP $d_{32} \approx 8.0 \mu$

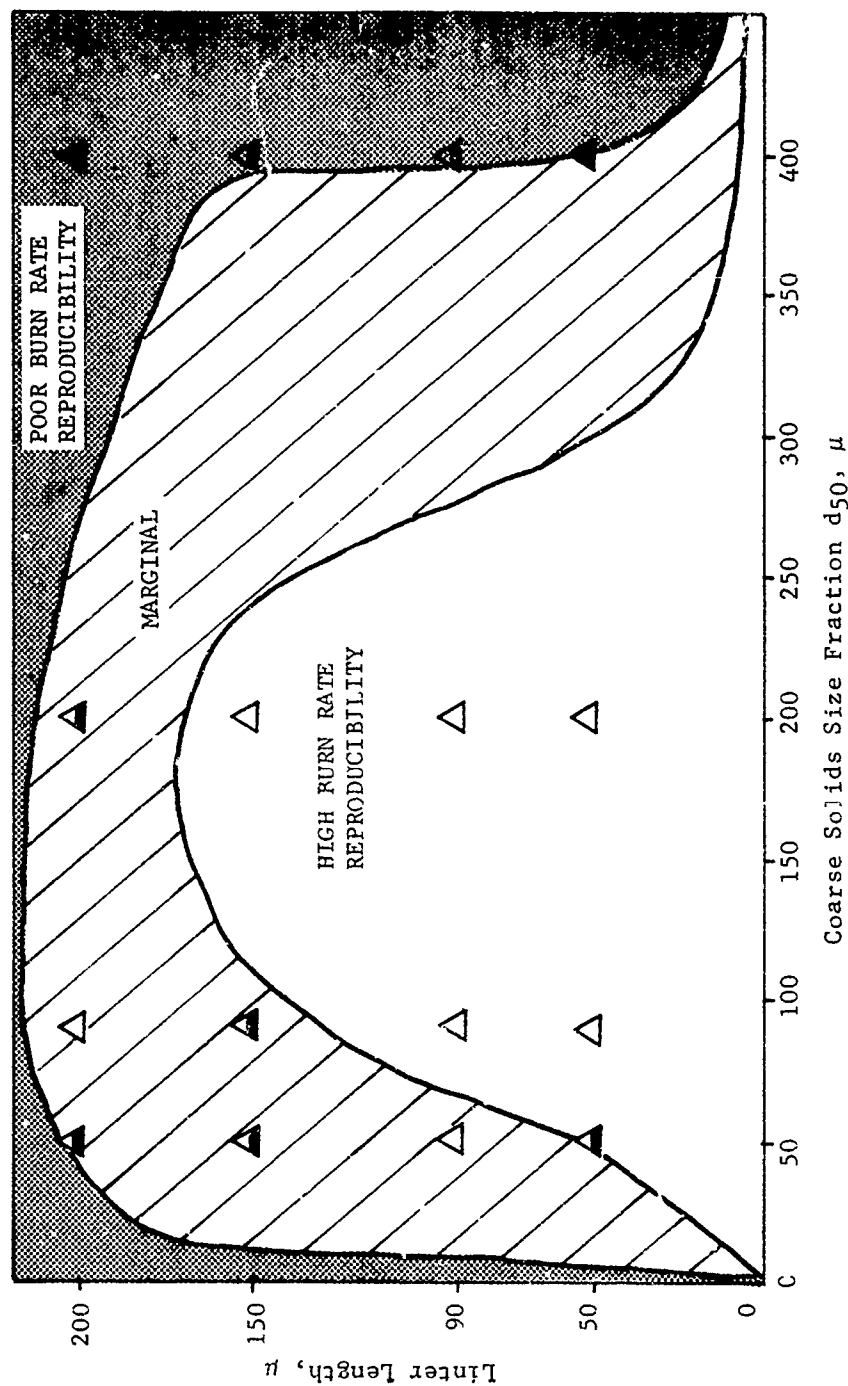


Figure 19. Linter Utility Regimes for Fixed Fine Oxidizer Size (2 μ) and Total Oxidizer Surface Mean Diameter (8.0 μ)

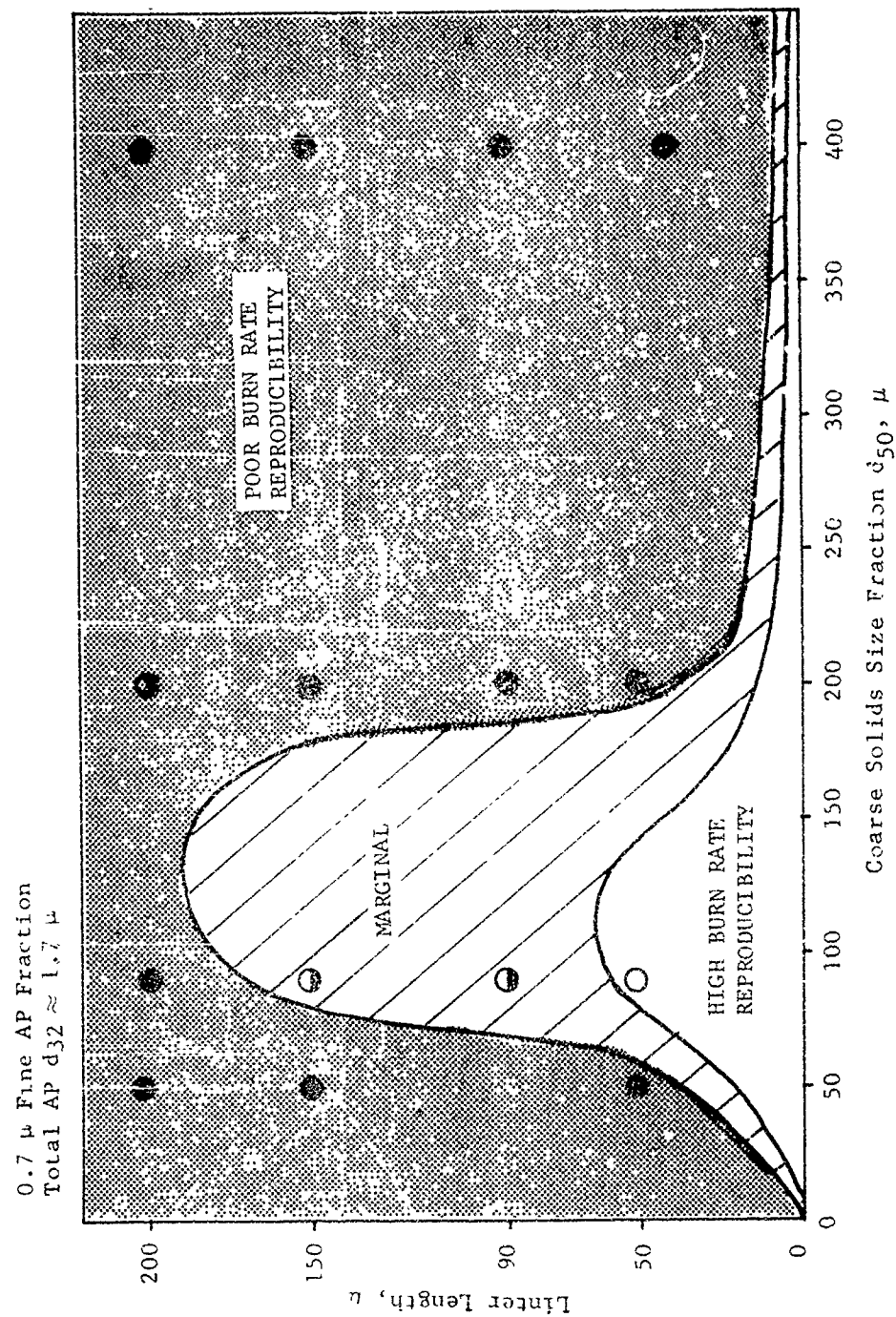


Figure 20. Linter Utility Regimes for Fixed Fine Oxidizer Size (0.7 μ) and Total Oxidizer Surface Mean Diameter (1.7 μ)

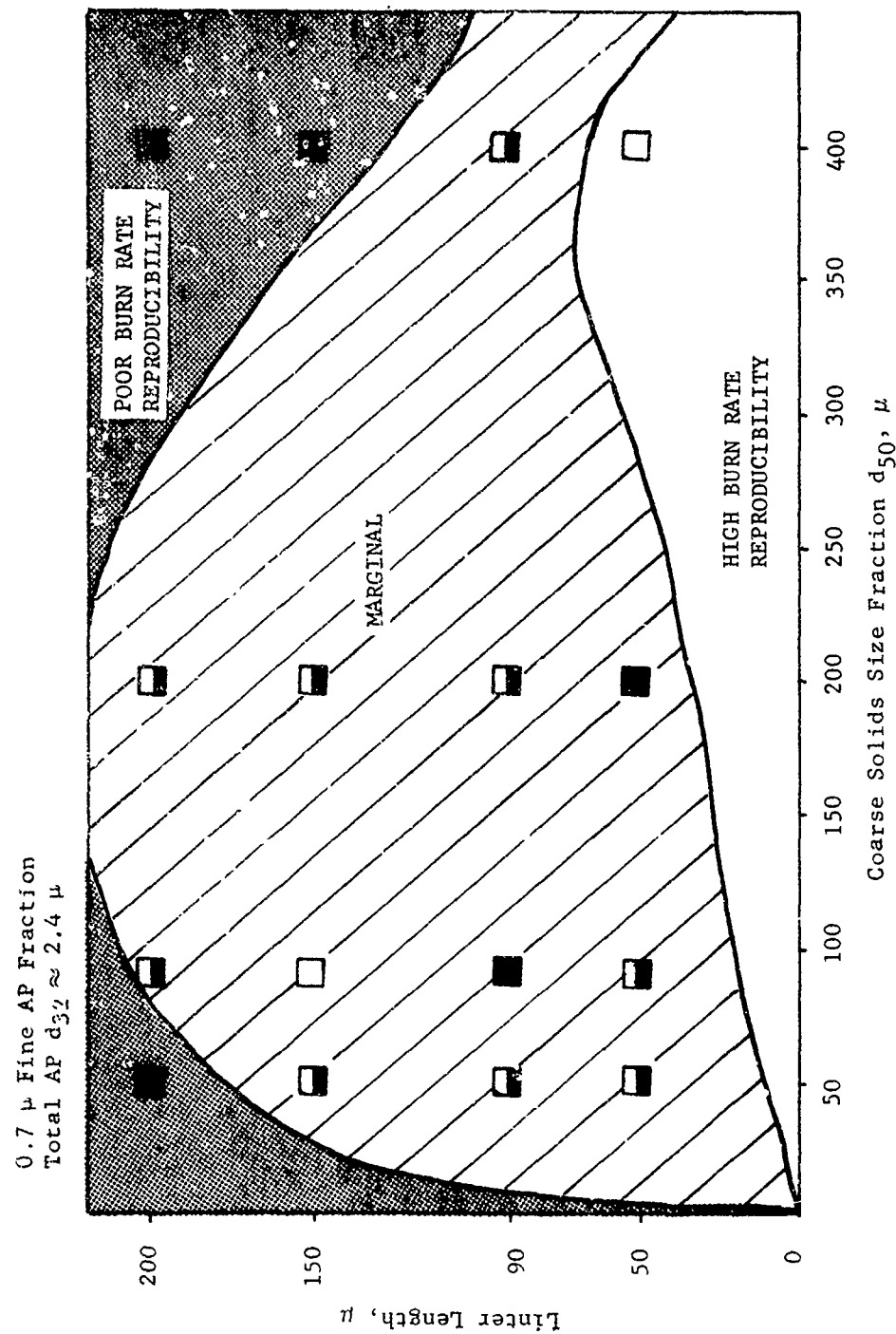


Figure 21. Linter Utility Regimes for Fixed Fine Oxidizer Size (0.7 μ) and Total Oxidizer Surface Mean Diameter (2.4 μ)

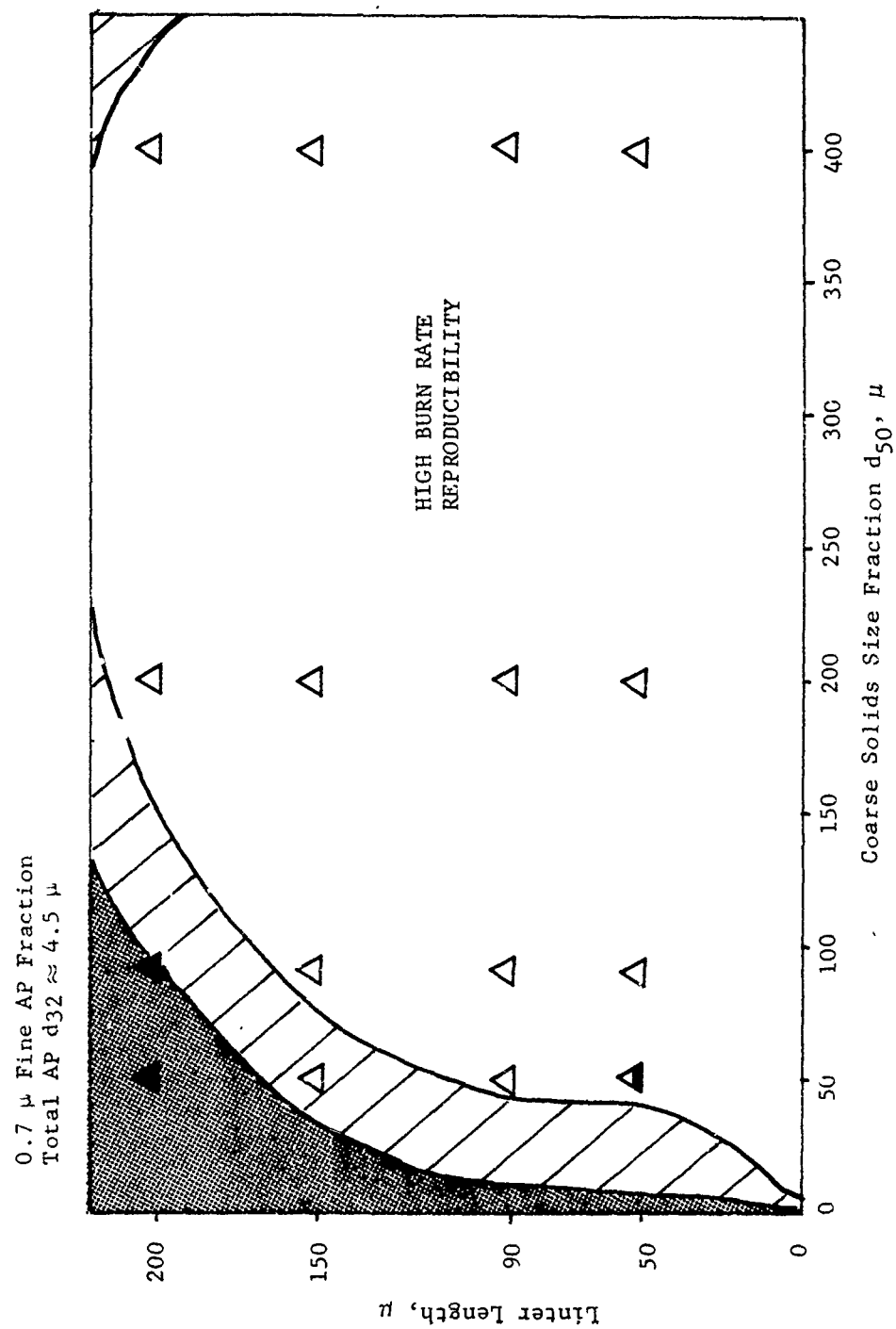


Figure 22. Linter Utility Regimes for Fixed Fine Oxidizer Size (0.7 μ) and Total Oxidizer Surface Mean Diameter (4.5 μ)

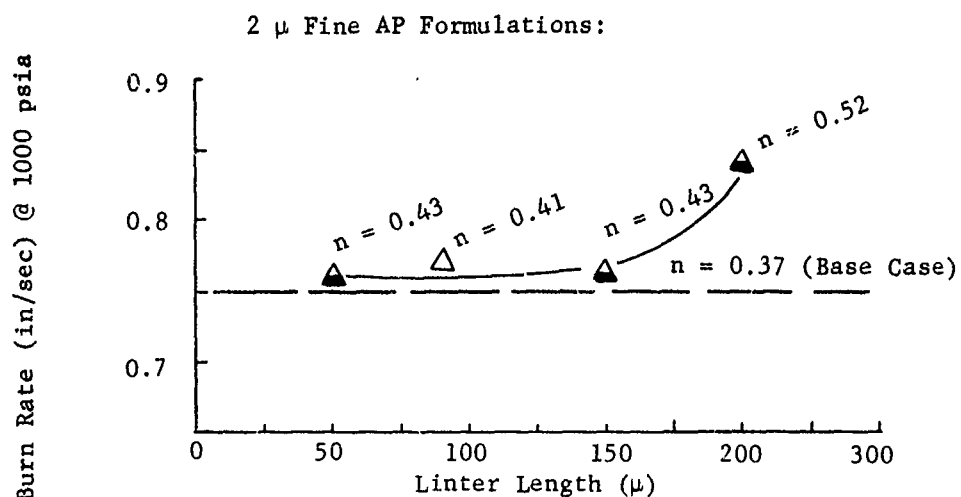


Figure 23. Rate Versus Linter Length for Composition NA-2Lxx-3 (Highest Augmented Rate with Most Reliable Random Linter Orientation is NA-2L90-3) at 1% Linter Concentration

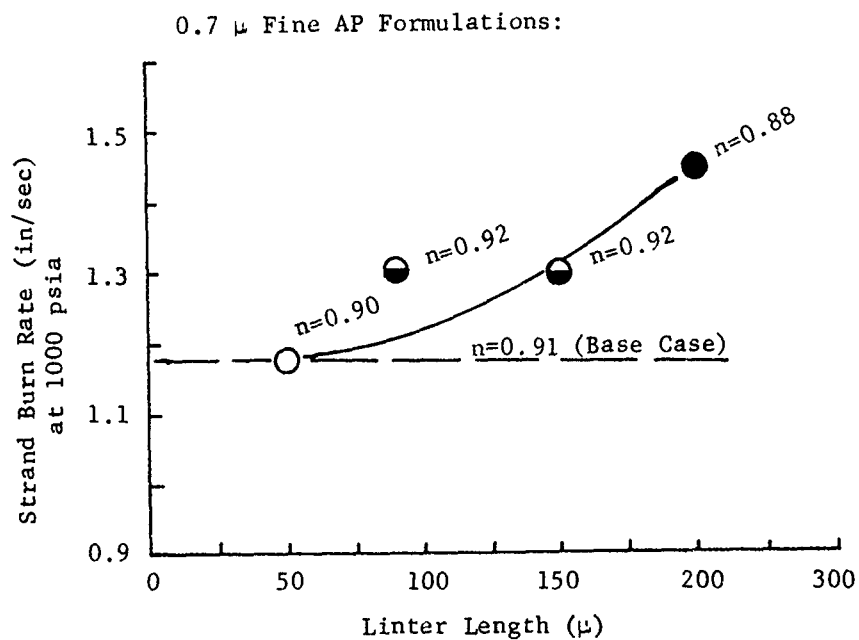


Figure 24. Rate Versus Linter Length for NA-.7xx-4 at 1% Linter Concentration

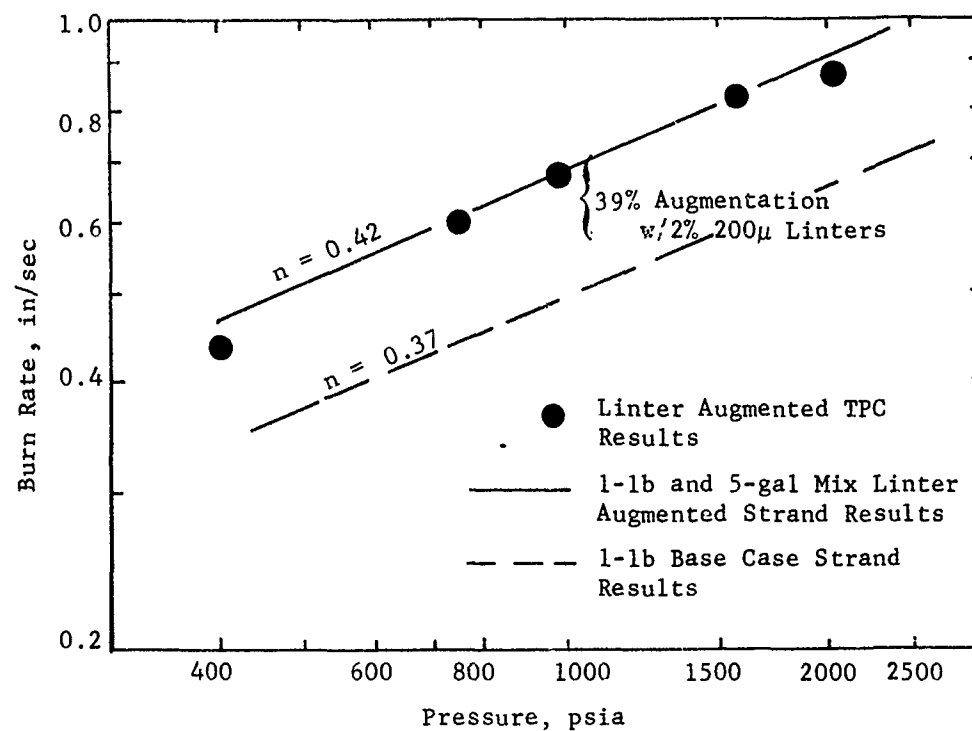


Figure 25. Burn Rate Results (Strands and TPC's) for Demonstration Motor Propellant and the Corresponding Base Case Propellant

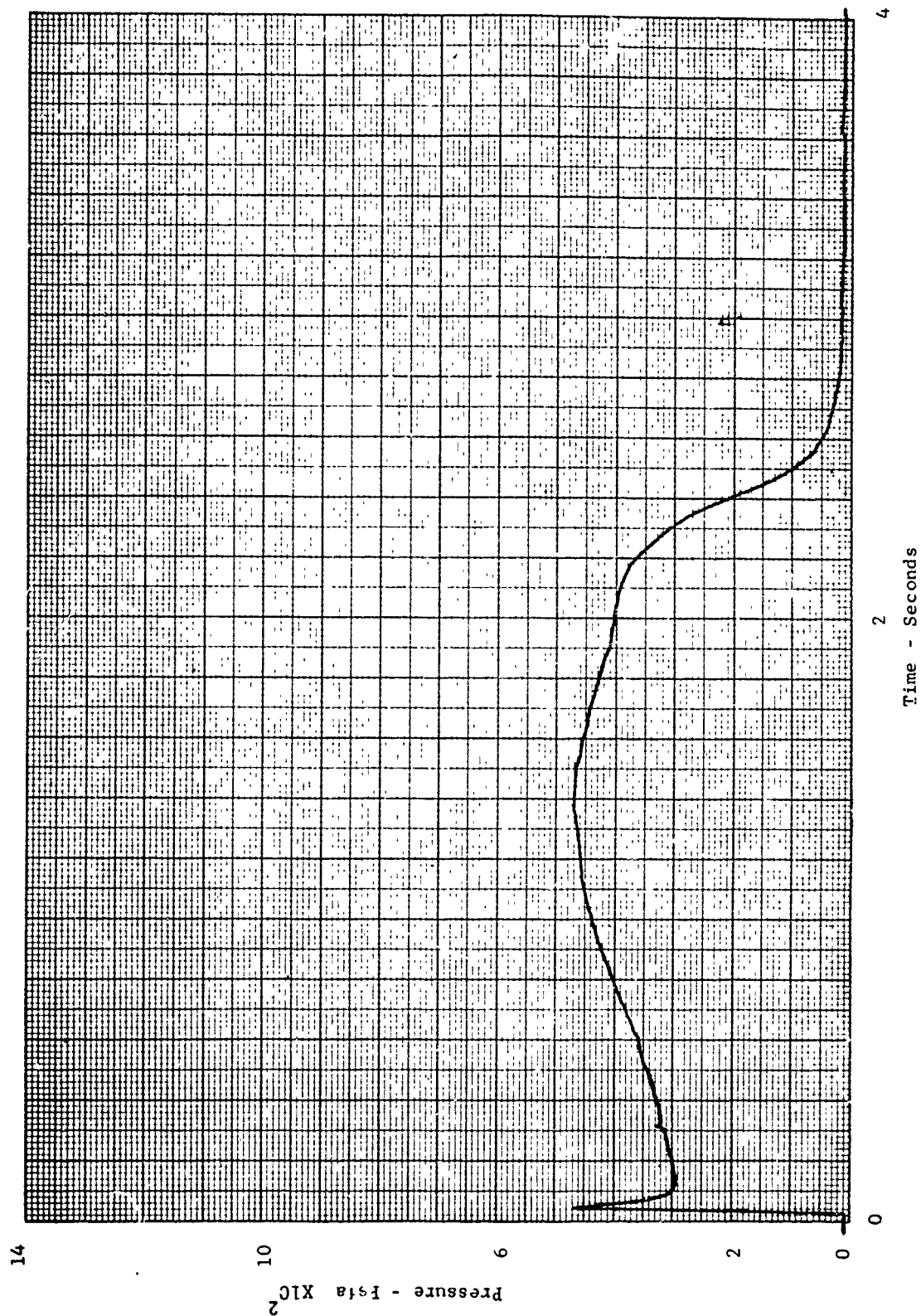


Figure 26. Pressure-Time Trace for TPC Demonstration Motor (Nominal 400 psia)

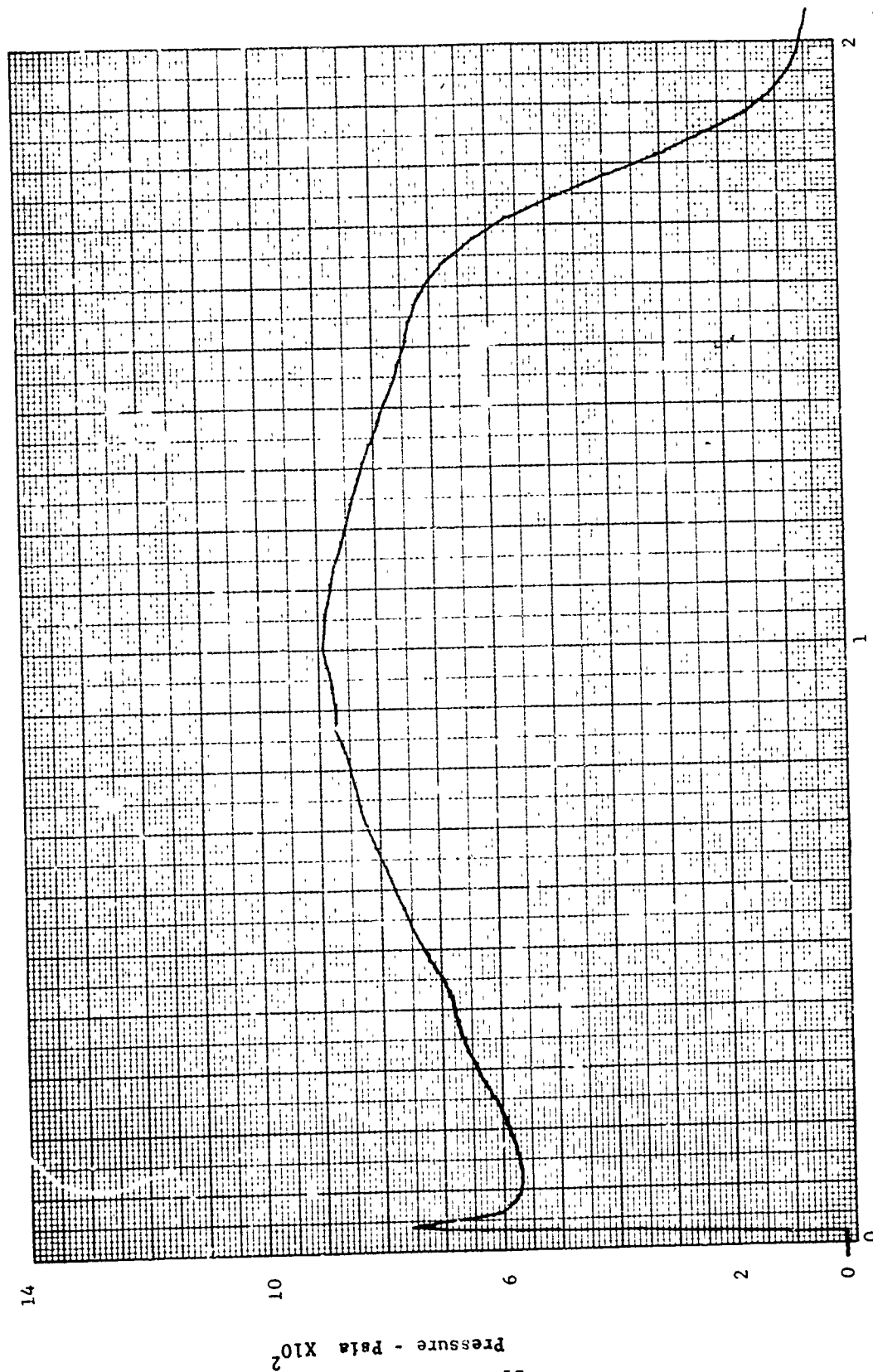


Figure 27 Pressure-Time Trace for TPC Demonstration Motor (Nominal 750 psia)

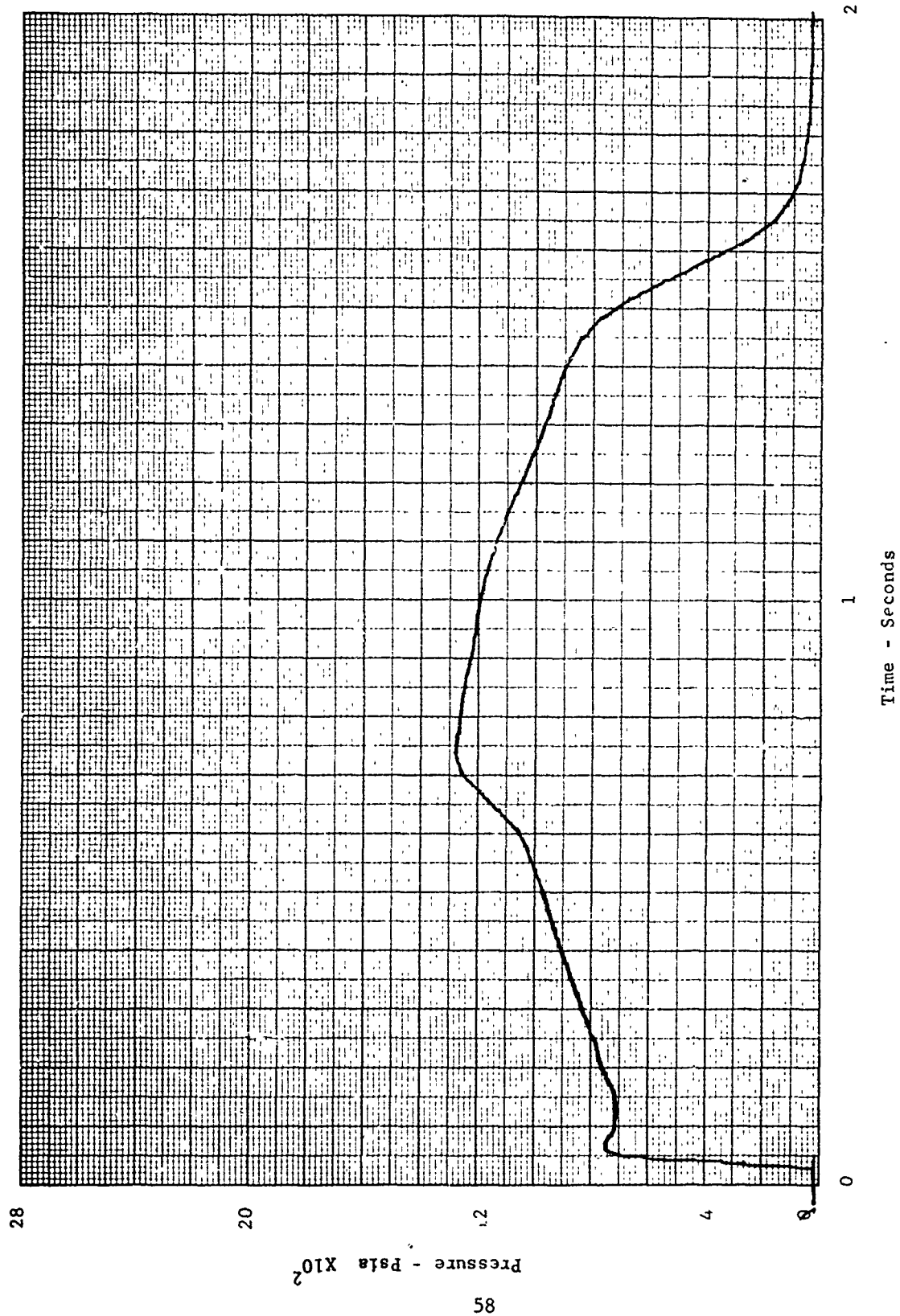


Figure 28. Pressure-Time Trace for TPC Demonstration Motor (Nominal 1000 psia)

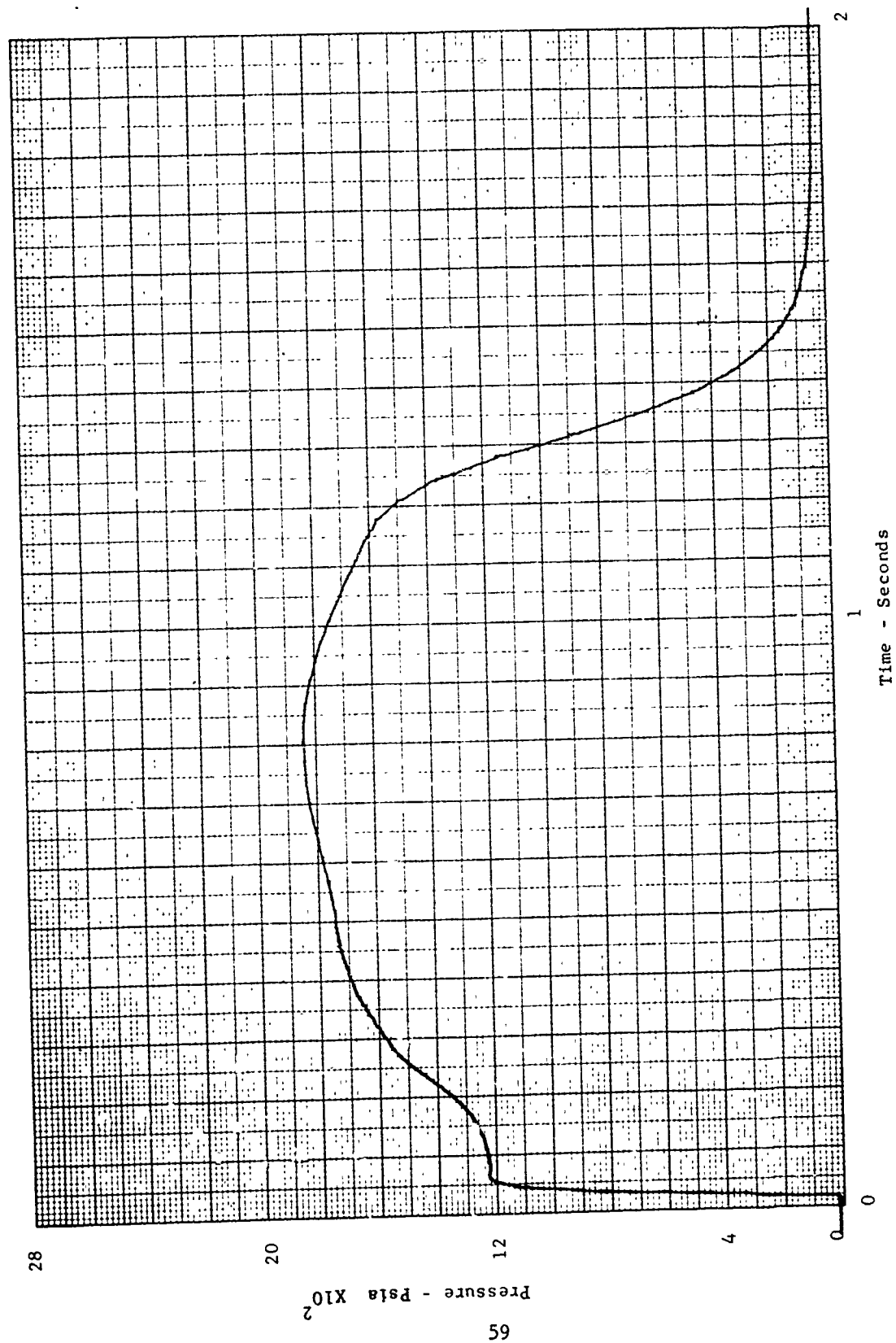


Figure 29. Pressure-Time Trace for TPC Demonstration Motor (Nominal 1600 psia)

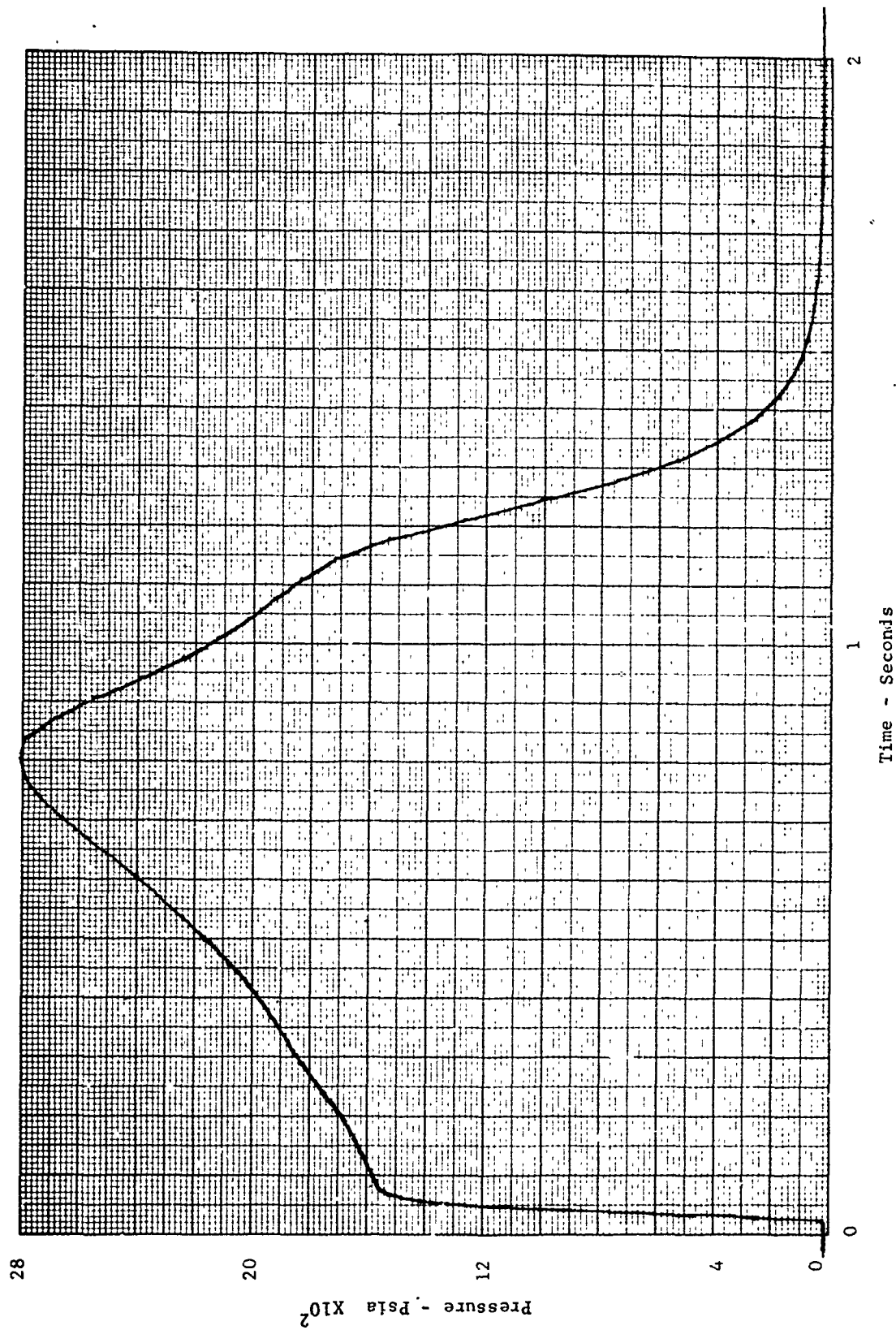


Figure 30. Pressure-Time Trace for TPC Demonstration Motor (Nominal 2100 psia)



INHIBITOR



Figure 31. Typical Orientation Pattern in Vertical Web Cross-Section of TPC Motor for 200 μ Linters (Rated MARGINAL) in Composition NA-2L200-6(2) (Mag. 50X)

Q-3543

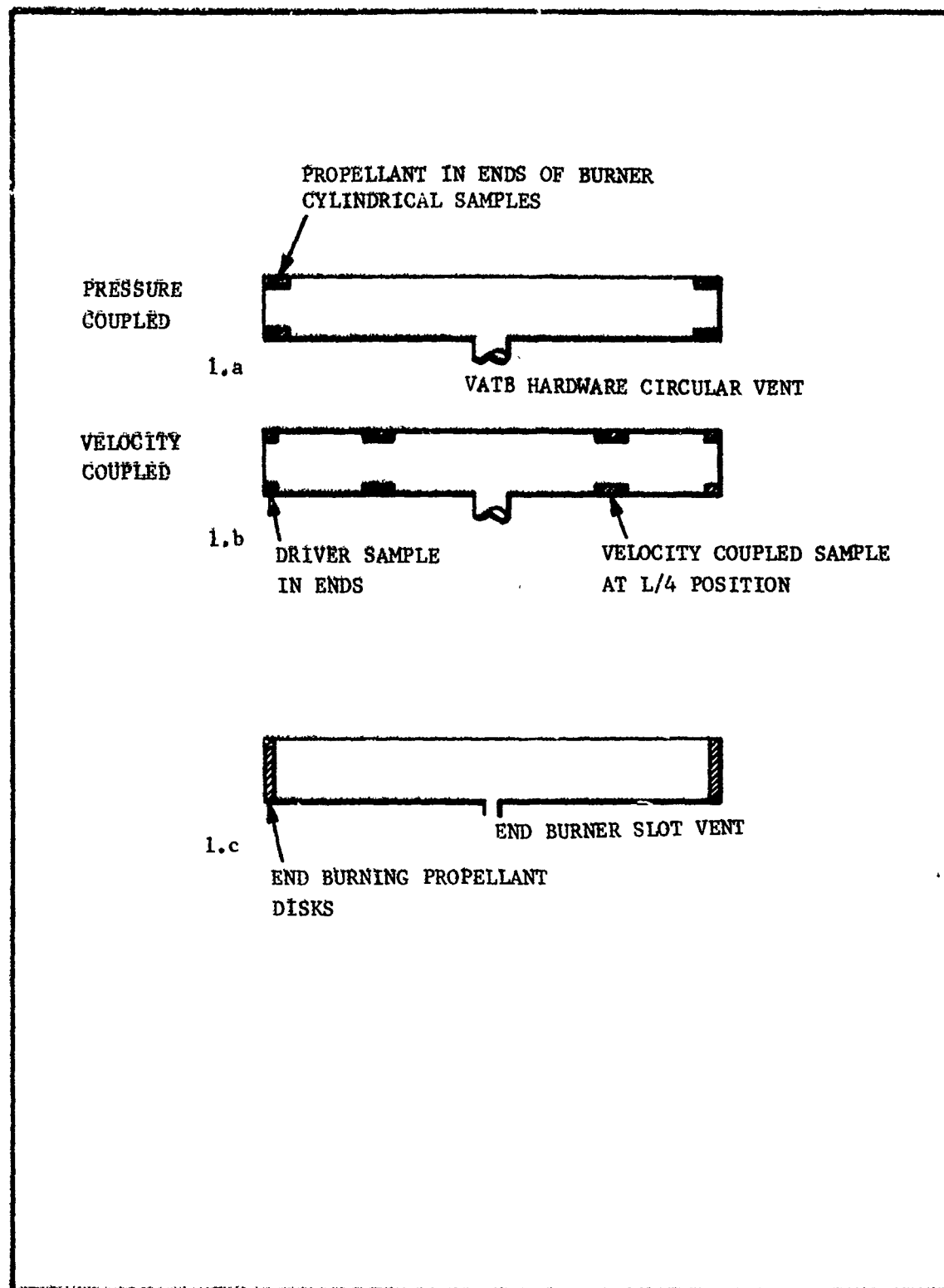


Figure 32. T-Burner Hardware Test Configurations for VATB and End Burner Testing

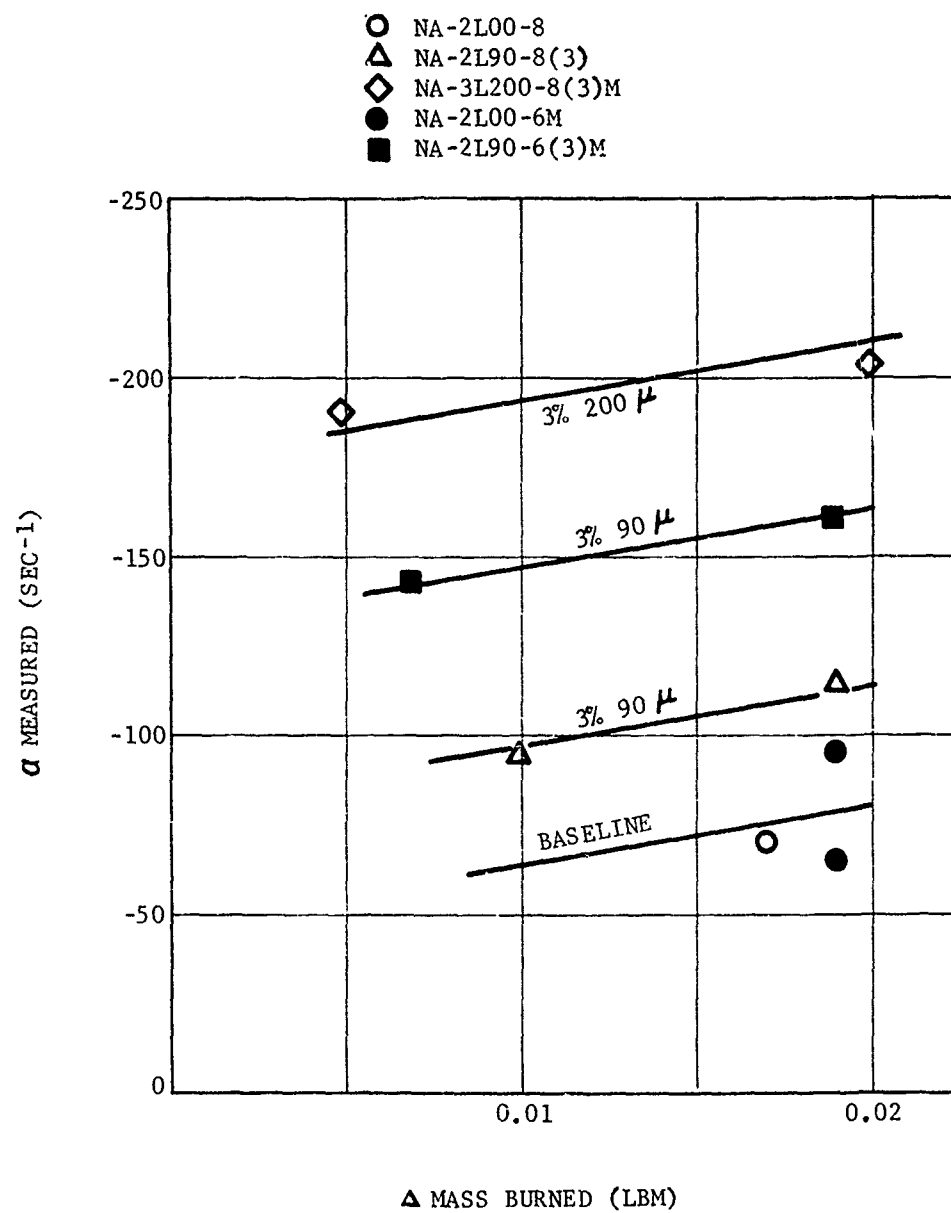


Figure 33. Relation of Pulse Decay Measurements to Total Mass Burned.
 Data Taken at 4000 Hz in End Burner Hardware

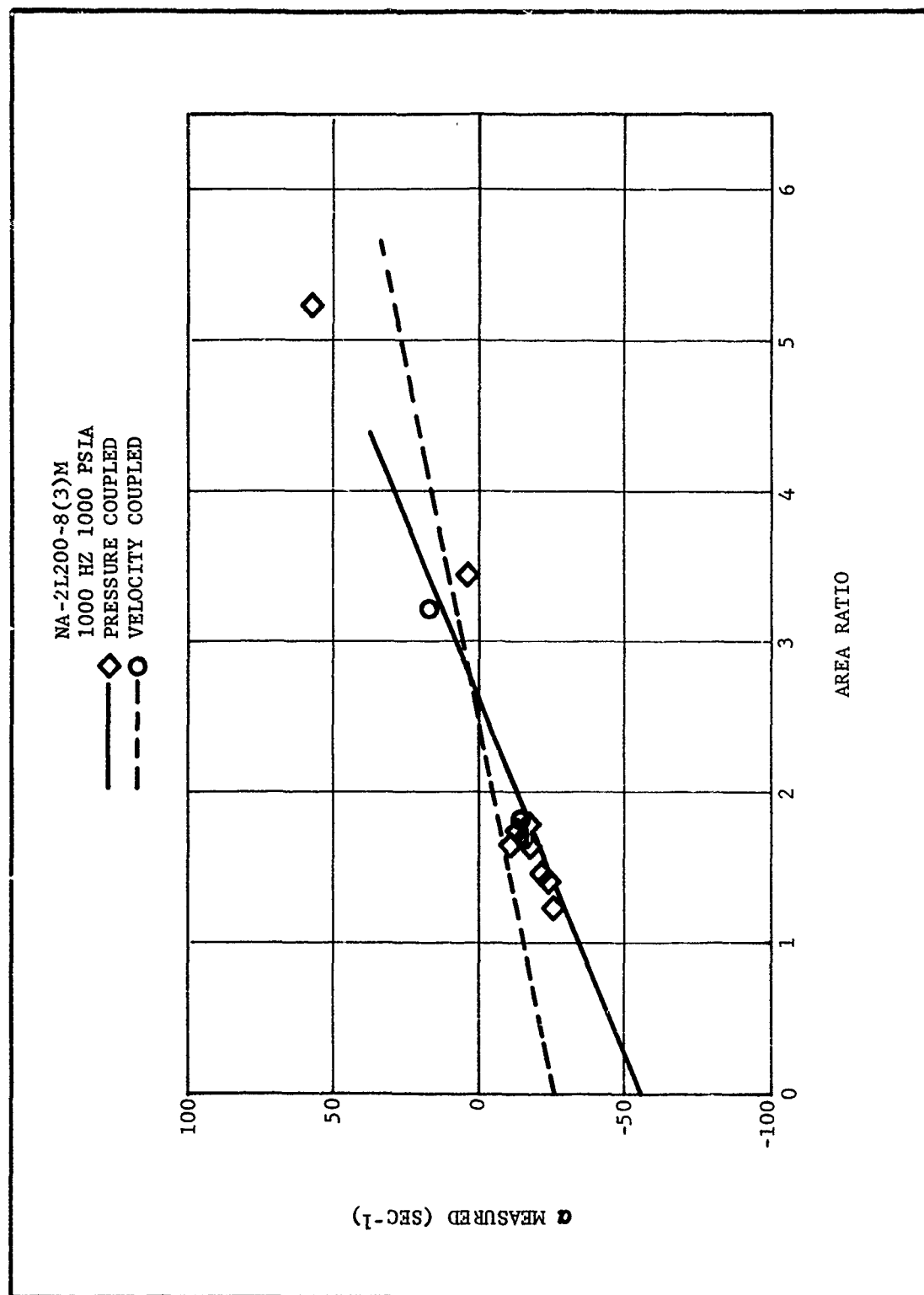


Figure 34. Uncorrected α as a Function of Area Ratio for Mix
NA-2L200-8(3)M

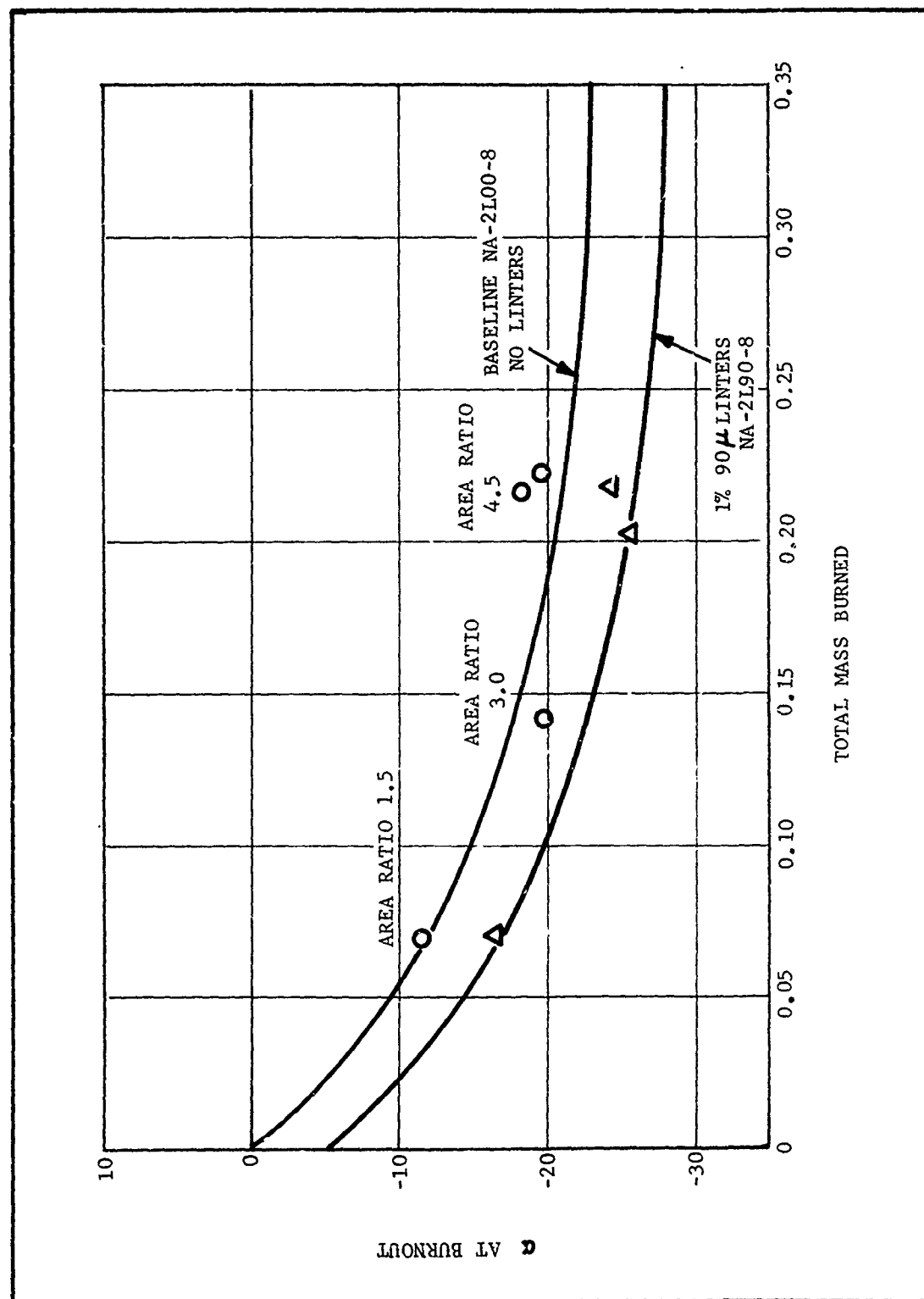


Figure 35. Burnout Decay Measurements Showing Increased Losses as a Function of Mass Burned

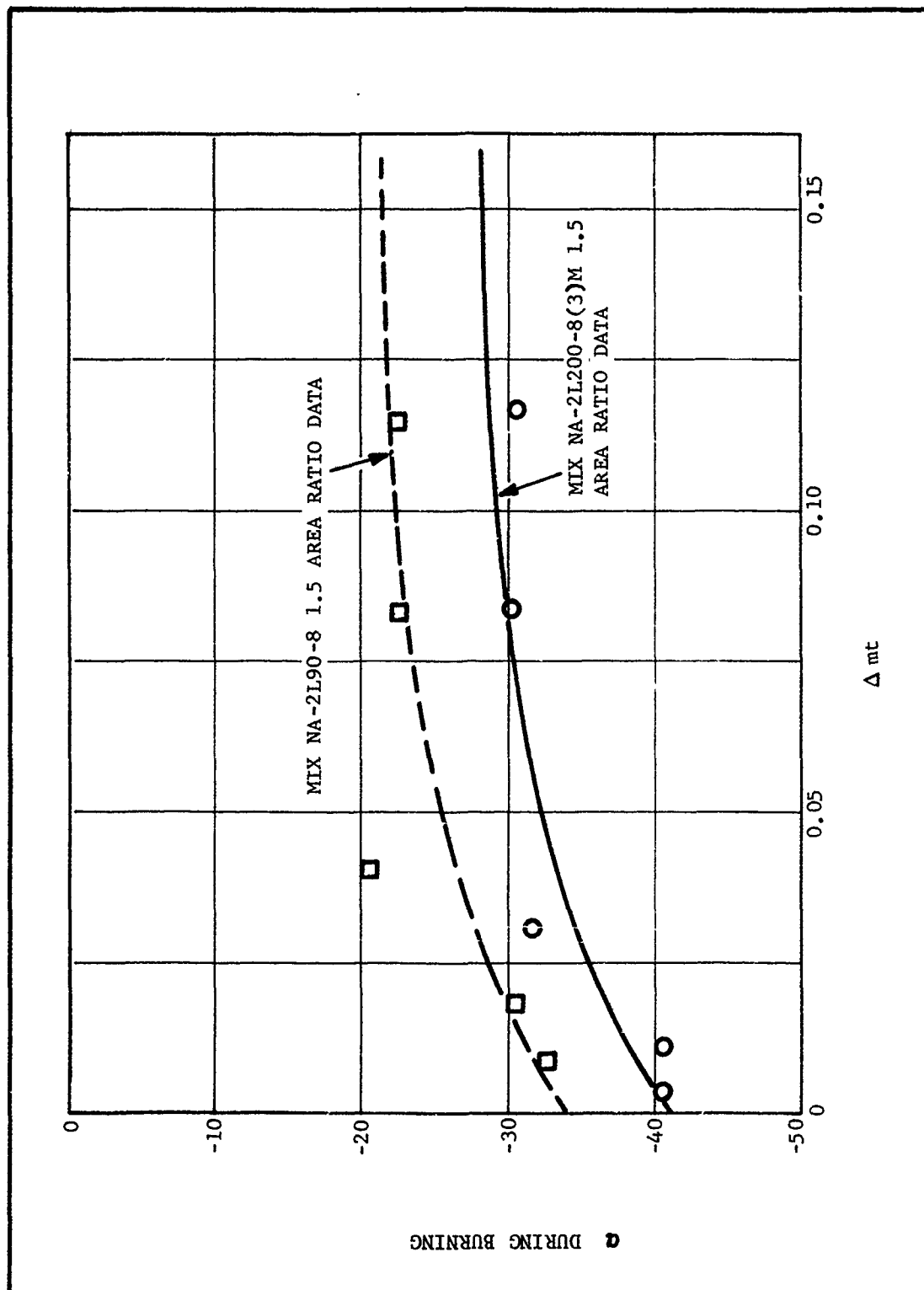


Figure 36. Loss Variation During Burning for 1.5 Area Ratio Samples. Data from Two Tests Each from Mixes NA-2L90-8(3) and NA-2L200-8(3)M

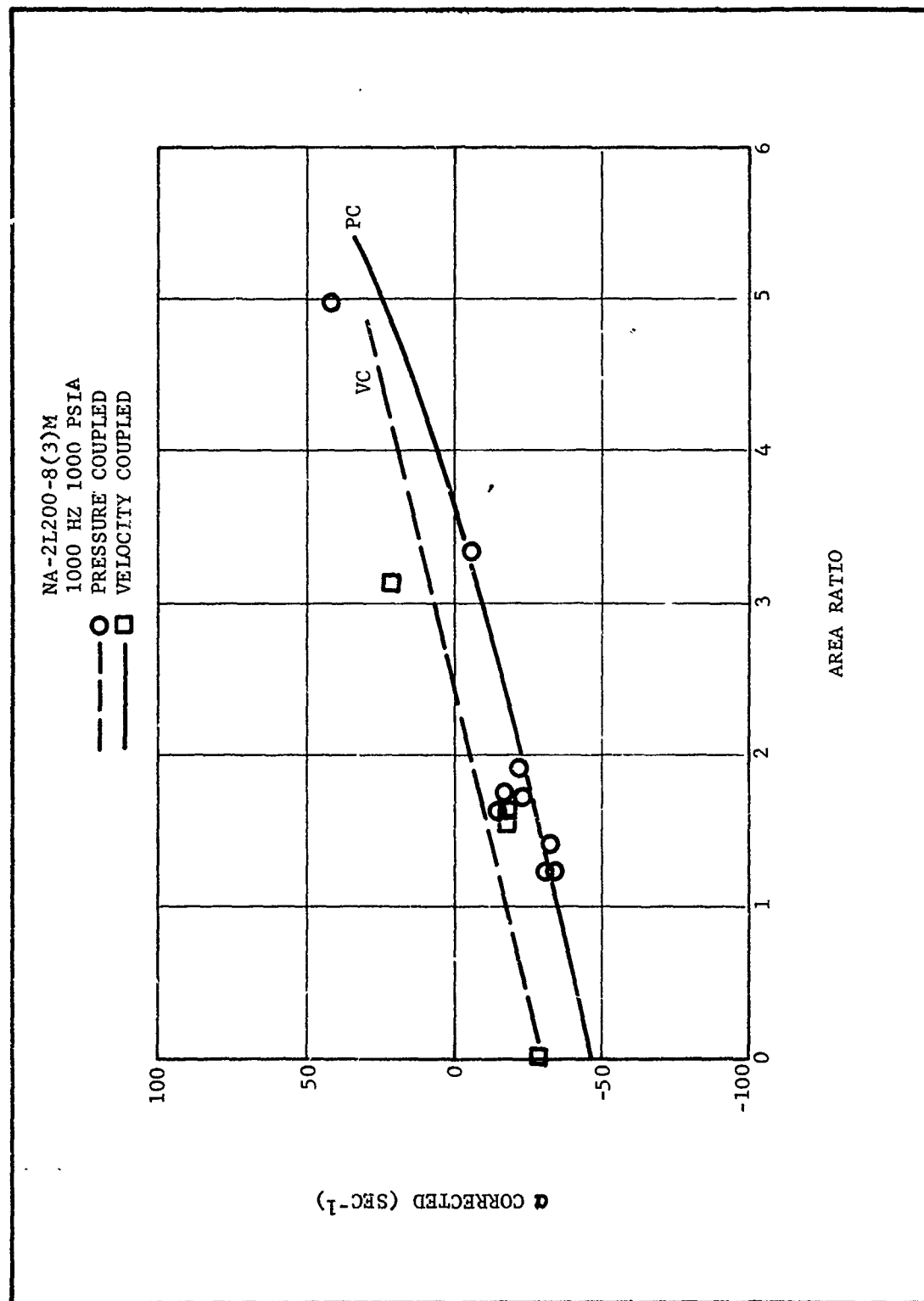


Figure 37. Final Adjusted α Versus Area Ratio Data NA-2L200-8(3)M
1000Hz, 1000 psia

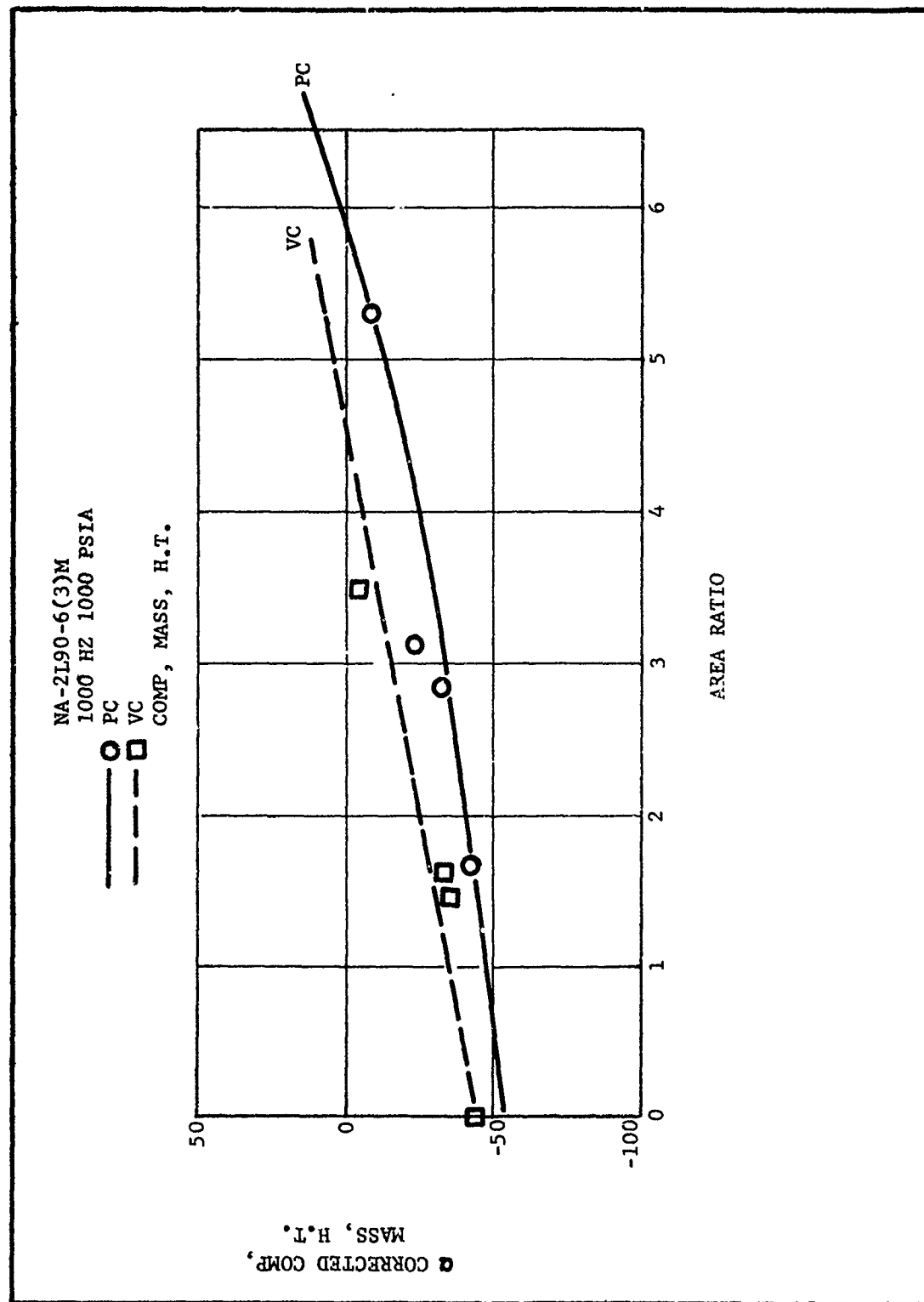


Figure 38. Final Adjusted α Versus Area Ratio Data NA-2L90-6(3)M
1000 Hz, 1000 psia

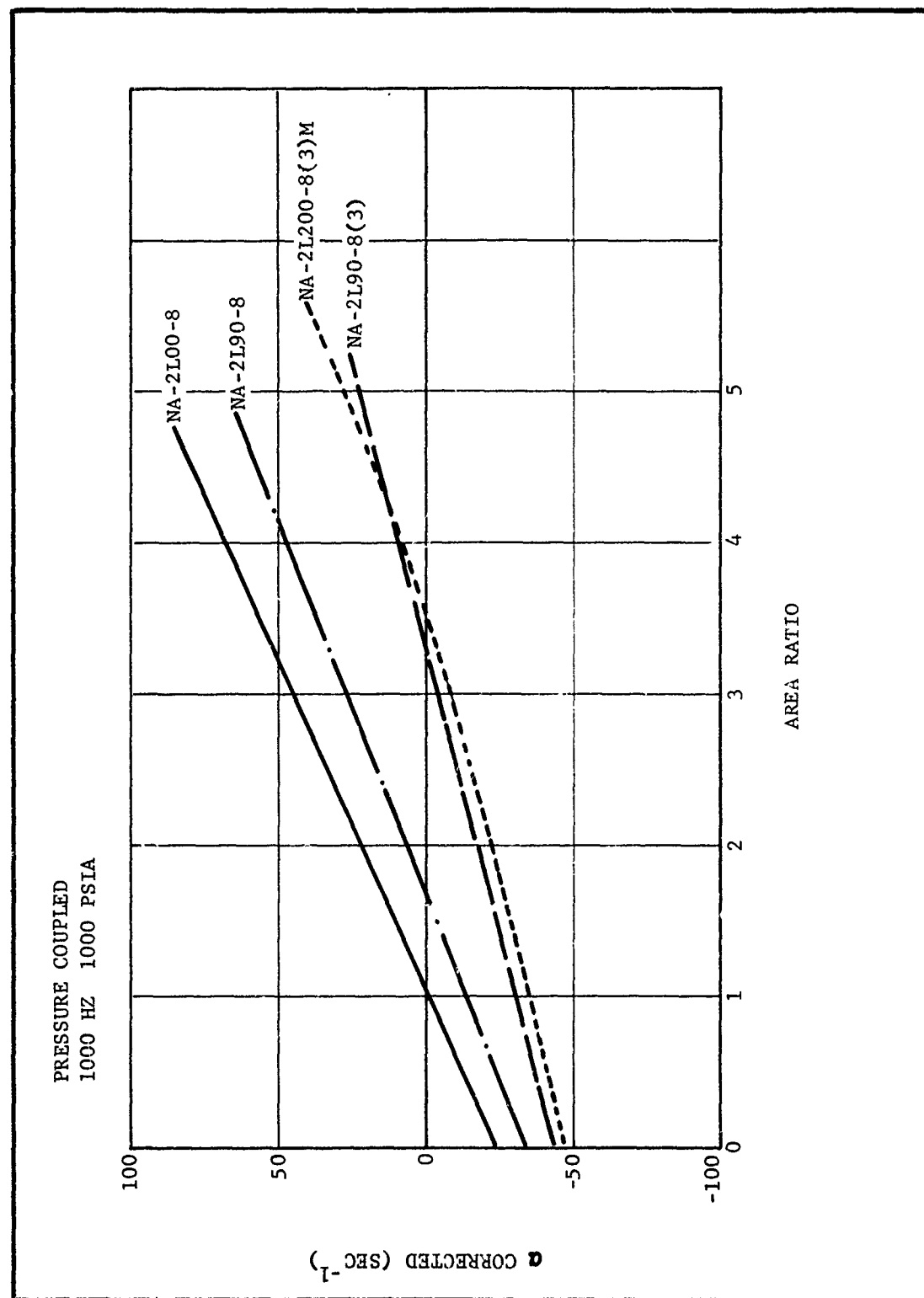


Figure 39. Computer Calculated Curves for Pressure Coupled NA-2L00-8
 Baseline Propellant Test Data

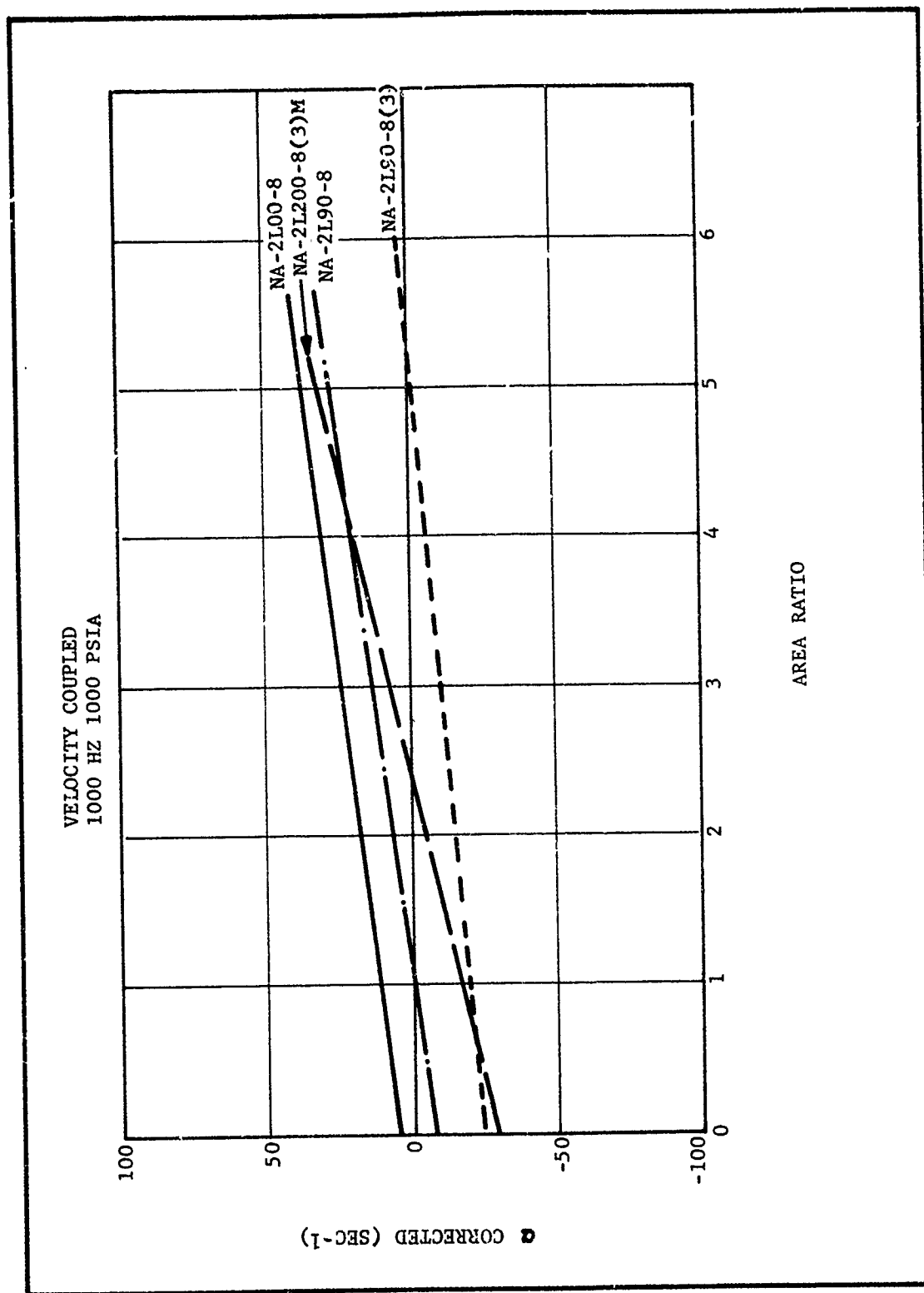


Figure 40. Computer Calculated Curves for Velocity Coupled NA-2L00-8
Baseline Propellant Test Data

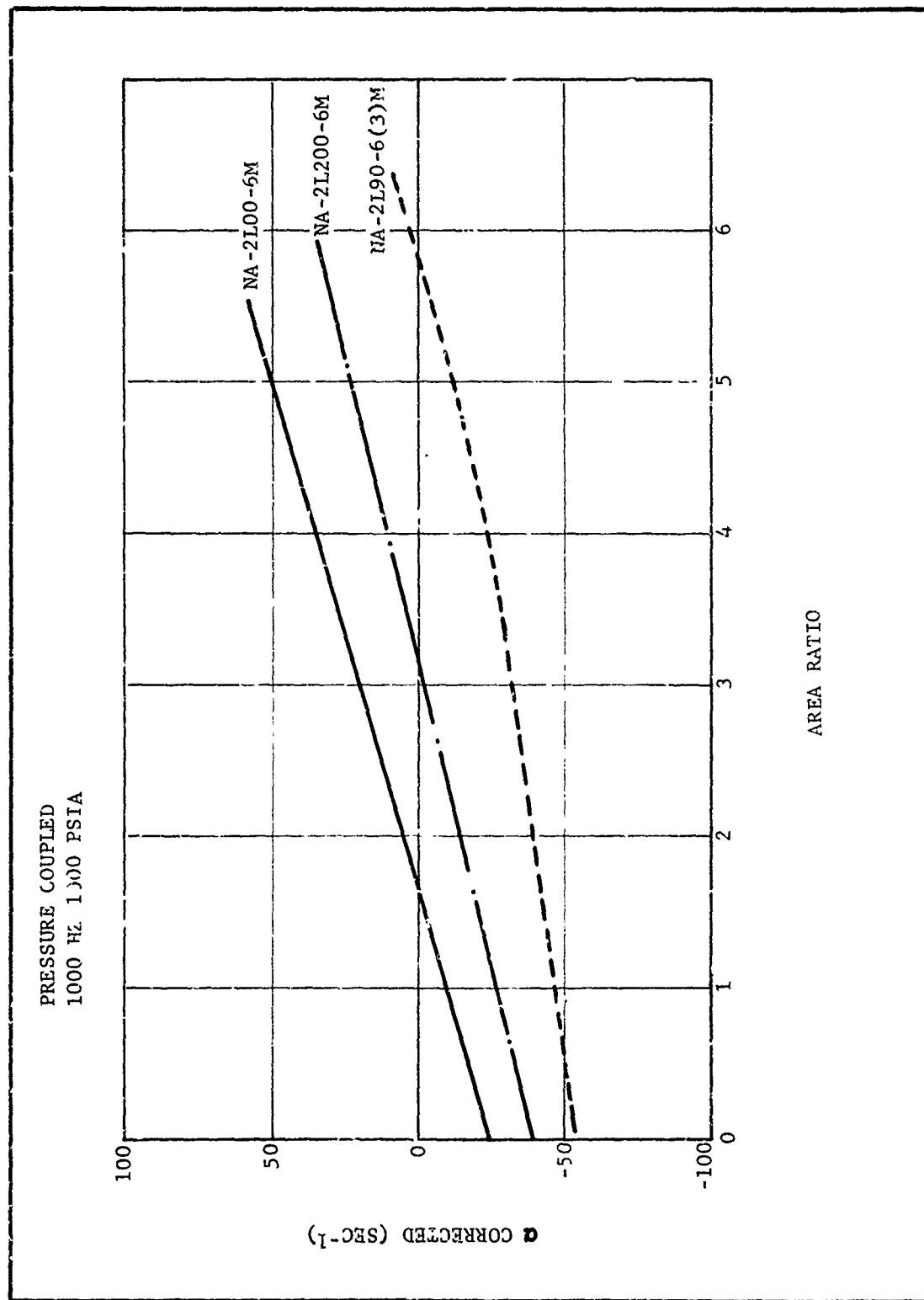


Figure 41. Computer Calculated Curves for Pressure Coupled NA-2L00-6M
Baseline Propellant Test Data

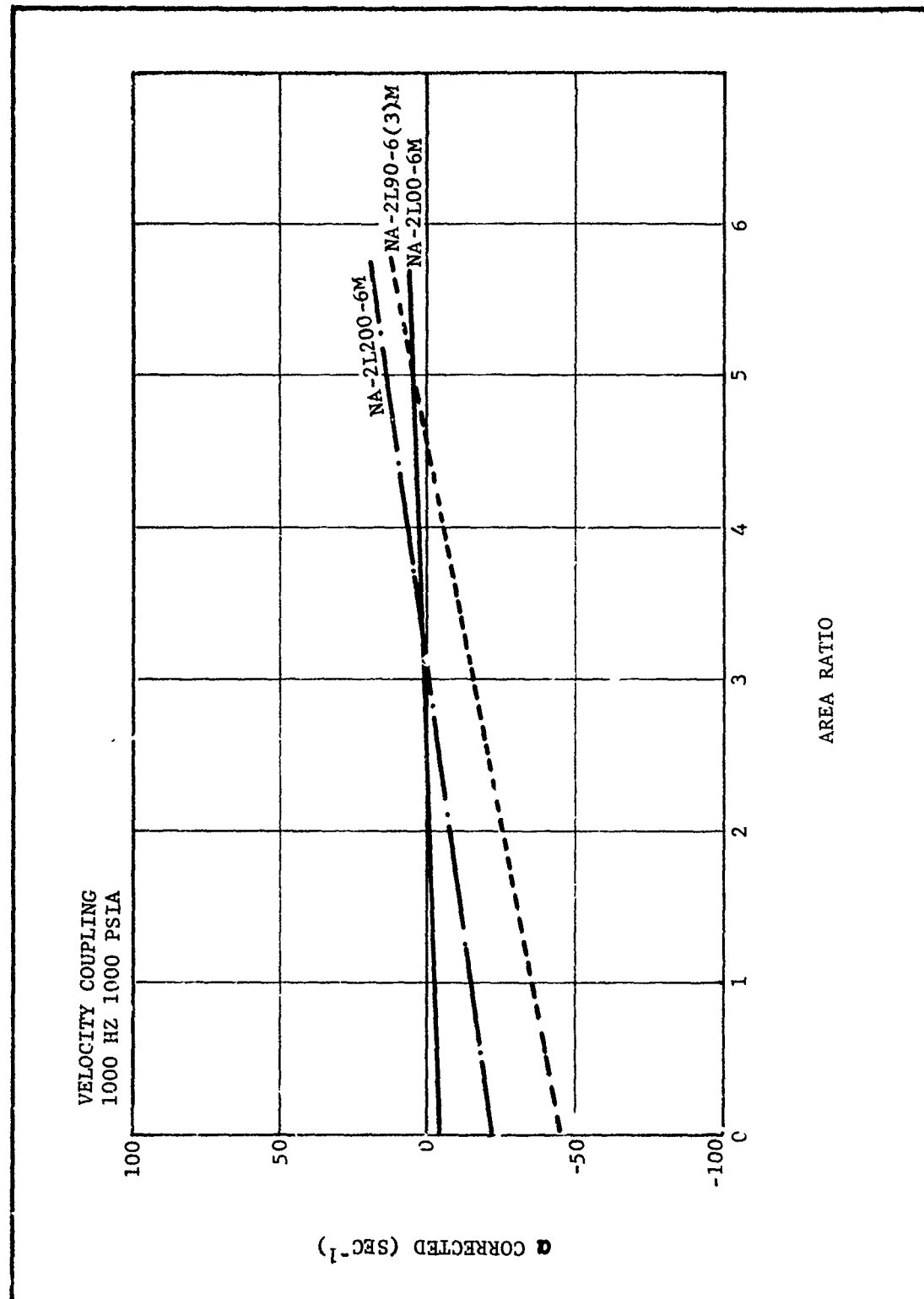


Figure 42. Computer Calculated Curves for Velocity Coupled NA-2L00-6M
Baseline Propellant Test Data

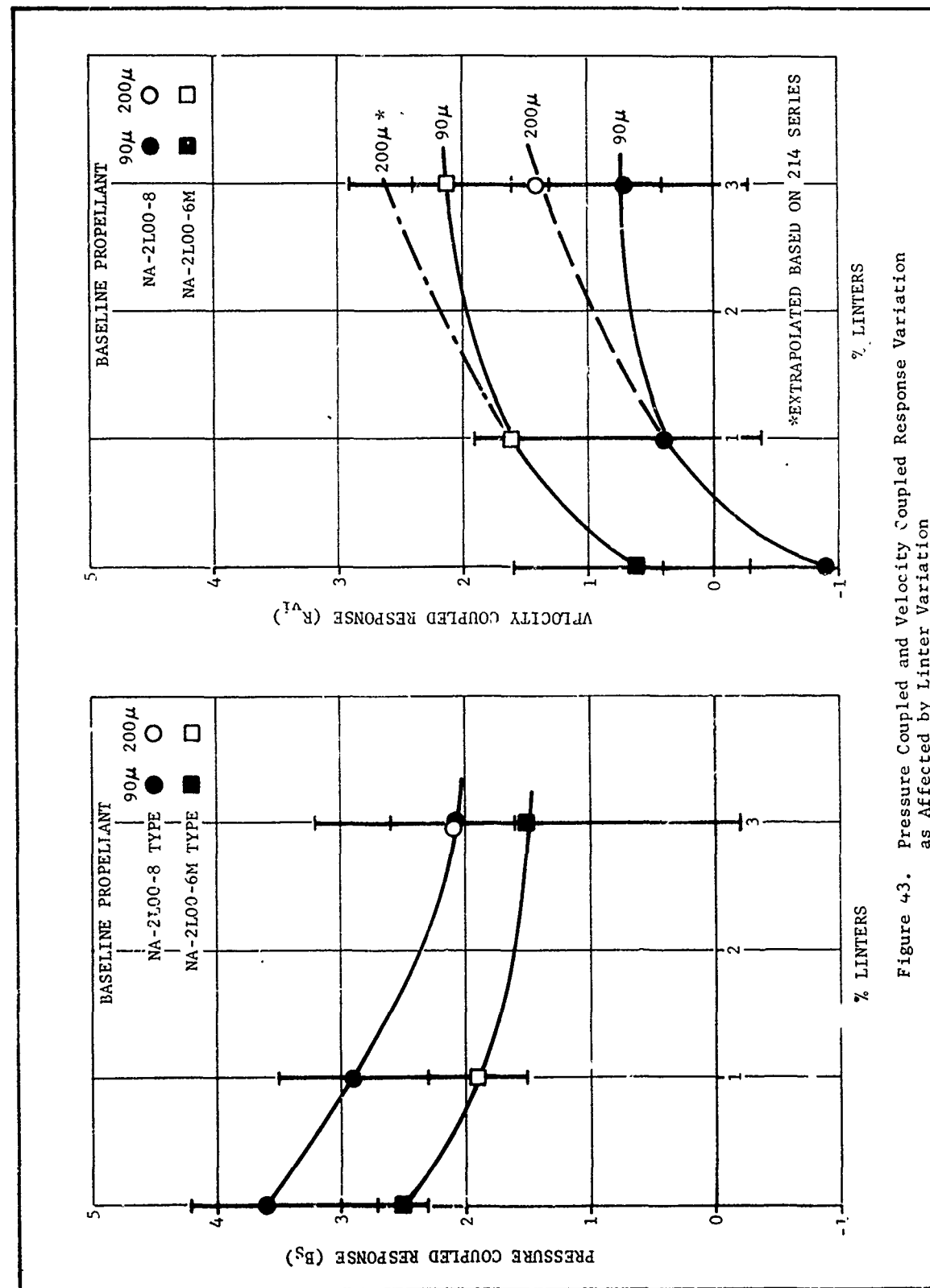


Figure 43. Pressure Coupled and Velocity Coupled Response Variation as Affected by Linter Variation

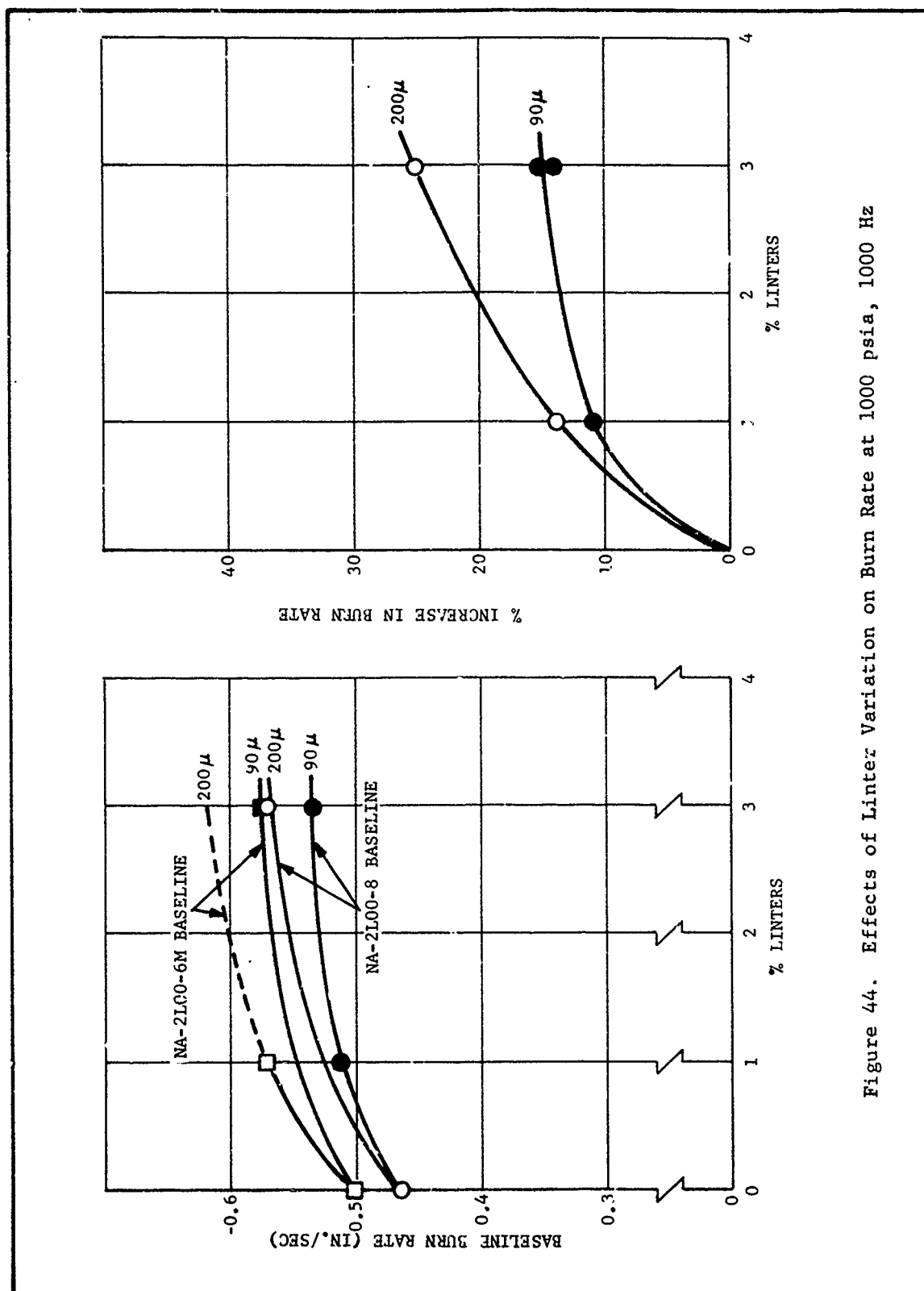


Figure 44. Effects of Linter Variation on Burn Rate at 1000 psia, 1000 Hz

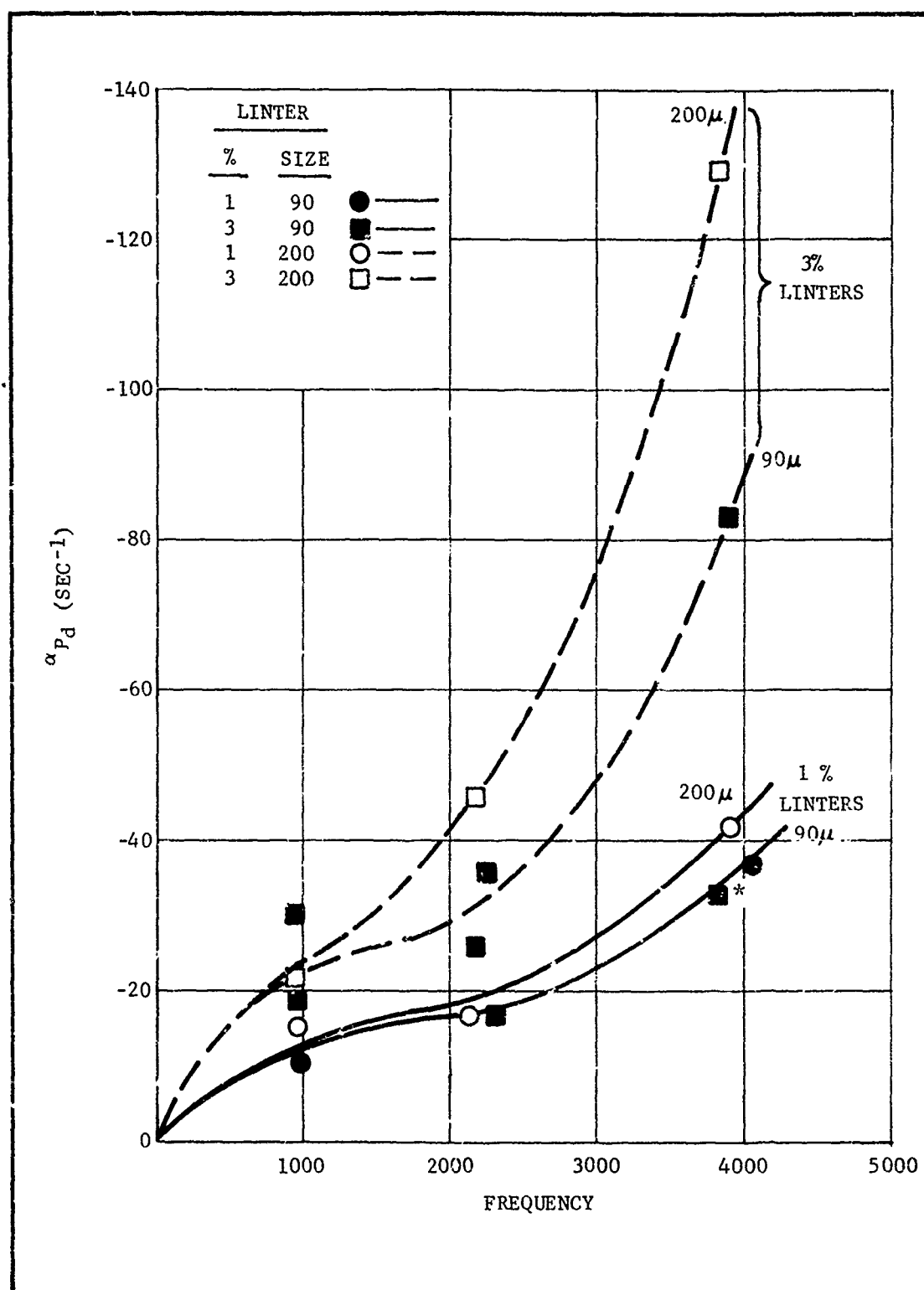


Figure 45. Particle Damping as a Function of Frequency Showing Linter Variation Effects

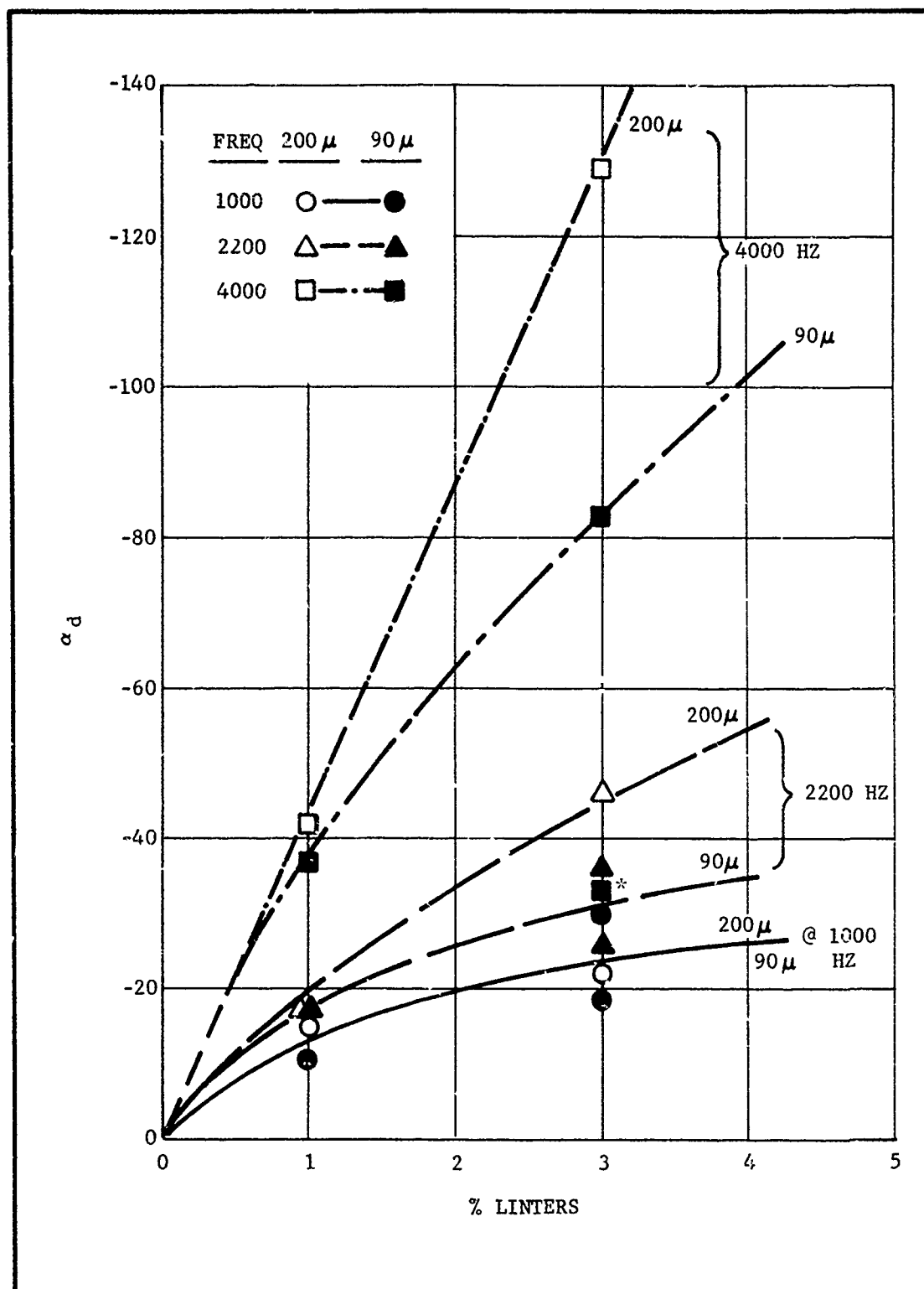


Figure 46. Effects of Linter Variation on Particle Damping

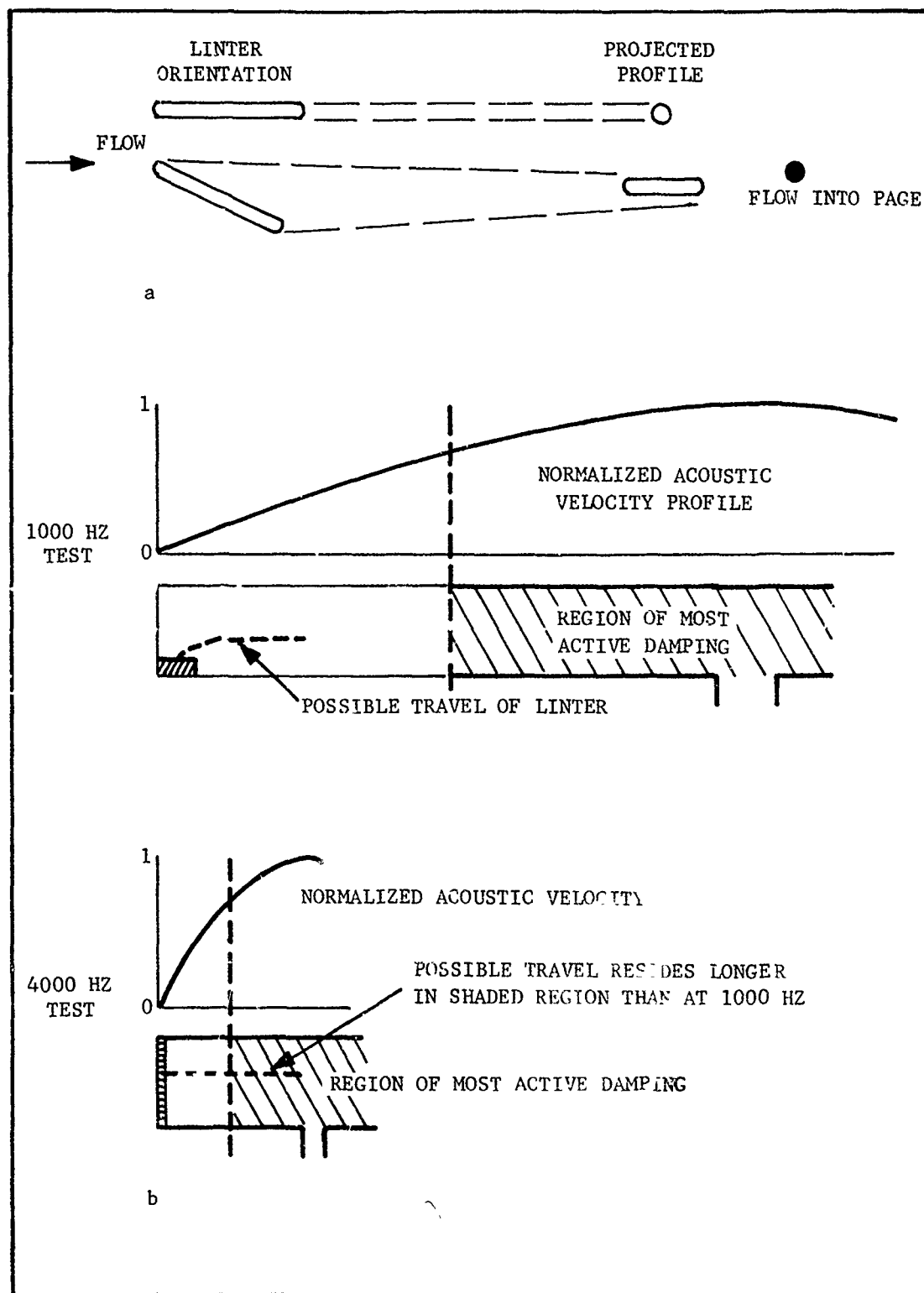


Figure 47. Flow Profile and Travel Distance in Burner Chambers of Different Lengths Showing Relation to Acoustic Velocity Mode Shape

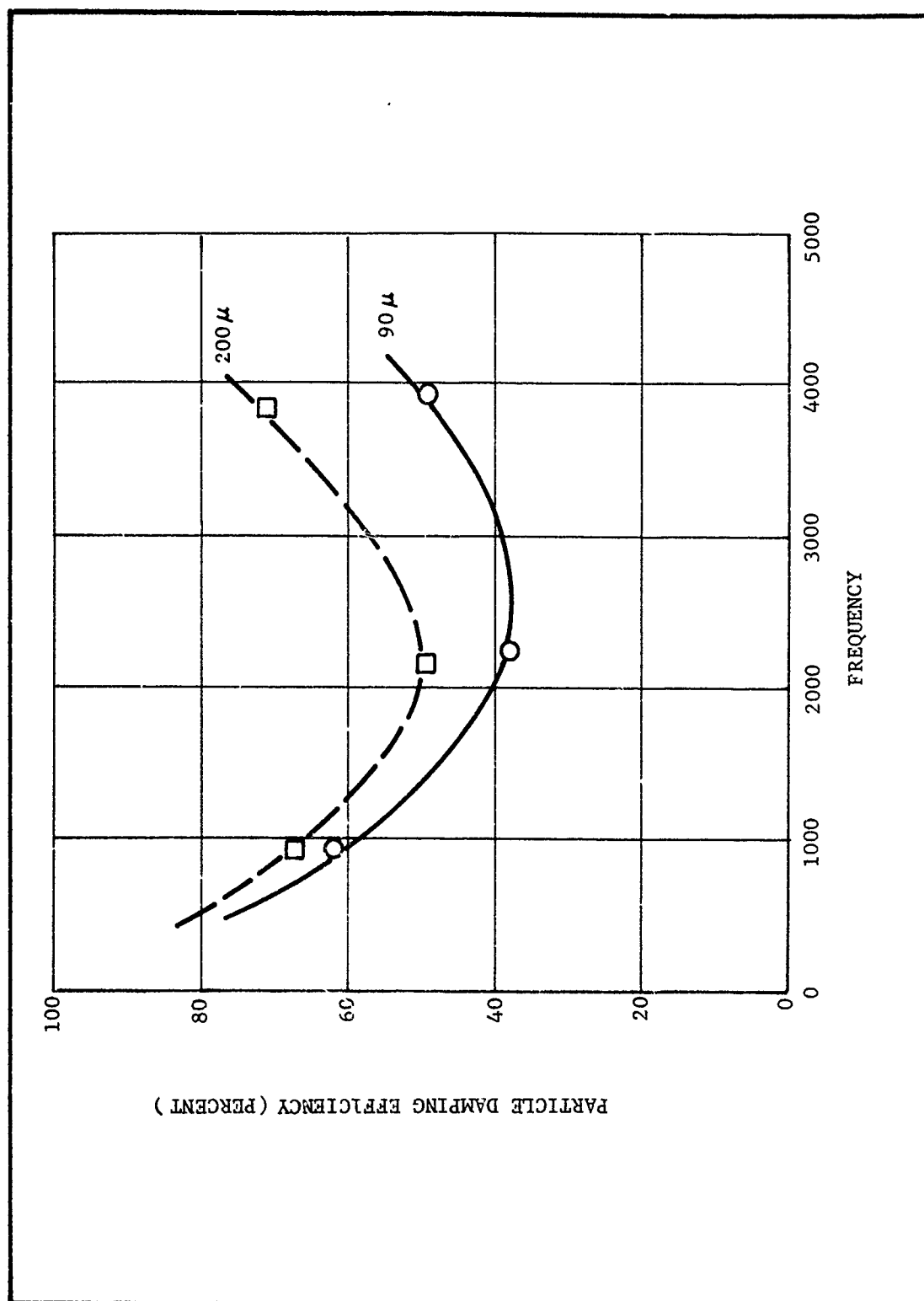


Figure 48. Particle Damping Efficiency for 90 and 200 μ Linter Lengths

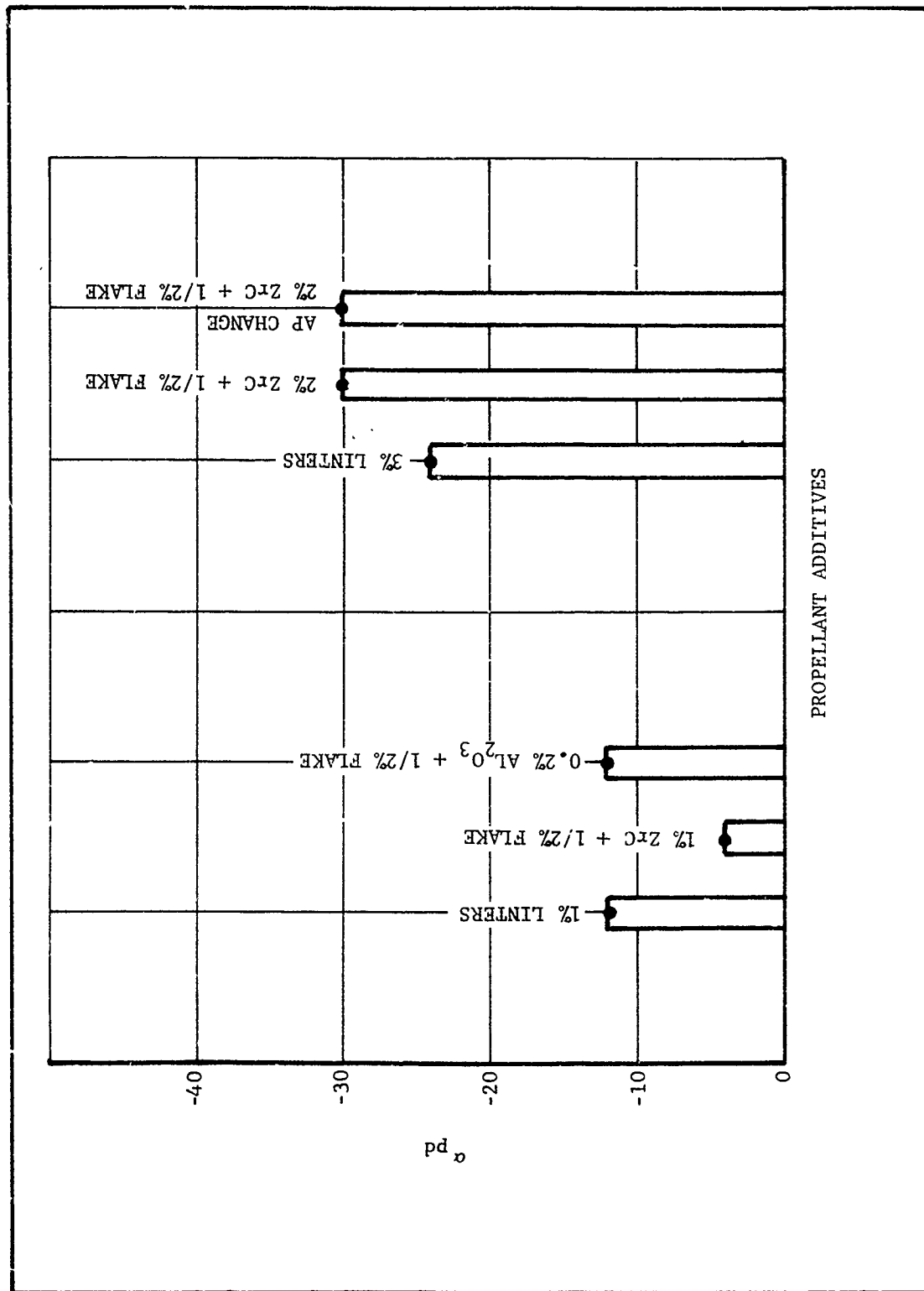


Figure 49. Comparison of Damping Characteristics of Linters, ZrC and Al_2O_3 at 1000 Hz, 1000 psia

TABLE 1. AMMONIUM PERCHLORATE PROPERTIES

Nominal AP Size (μ)	Lot Number	*Surface Mean Dia. d_{32} (μ)	*Volume Mean Dia. d_{43} (μ)
0.7	NA357-4	0.64	2.08
2	NAJ130-75-2-2	2.03	2.47
6	NAJ135-75-2-3	4.98	8.03
20	NAA352677-01	8.50	22.4
50	NAABL-131	24.1	46.7
90	NA90-15	34.0	77.8
200	NAABL-135	61.2	199
400	NAABL-129	429	446

$$* d_{32} = \frac{\sum n_i d_i^3}{\sum n_i d_i^2} = \frac{\sum S_i d_i}{\sum S_i}$$

$$d_{43} = \frac{\sum n_i d_i^4}{\sum n_i d_i^3} = \frac{\sum V_i d_i}{\sum V_i}$$

$$\bar{d}_{rate} = \left(\frac{\sum n_i d_i^3}{\sum n_i d_i^3 d_i^{-1/3}} \right)^3 = \left(\frac{\sum V_i}{\sum V_i d_i^{-1/3}} \right)^3$$

where: n_i = number of particles in i^{th} size fraction

d_i = diameter of i^{th} size fraction

S_i = particle surface area of i^{th} size

V_i = particle volume of i^{th} size

TABLE 2. BINDER COMPOSITION

<u>Ingredient</u>	<u>Wt. %</u>
R45M (HTPB Prepolymer)	65.98
IPDI (Isocyanate)	5.19
IDP (Plasticizer)	26.00
AO2246 (Antioxidant)	1.02
Polygard (Peroxide Decomposer)	1.02
0.1% DBTDA in IDP (Cure Catalyst)	0.79

Uniaxial Mechanical Properties at $\dot{\epsilon} = 0.76$ in/in-min

82

TABLE 4. COMPOSITIONS AND RESULTS FOR 1-PT MIXES CONTAINING 0.7M FINE AF FRACTION

Propellant Designation	Grain Dimensions				Average AF Size				Viscosity (cP)				Strength Data (psi/sec)				Tensile Mechanical Properties at $\dot{\epsilon} = 0.24$ in/in-min						Orientation			
	4000	2000	800	500	400	300	200	100	500	1000	2000	n/E	E _t (ksi)	E _c (ksi)	E _u (ksi)	E _h (ksi)	E _h (ksi)	E _h (ksi)	E _h (ksi)							
MA-71200-1	-	-	27	32	27	1.0	18.4	1.23	3.81	30/17	33/21	45/30	.77/14.62	1.42/100	1.42/100	2.55/100	.84/004	320	96	46/46	679	122	31/33	10,190	824	16/18
MA-71200-2	-	-	61	26.8	18.2	1.0	25.2	2.42	6.14	13/41	15/61	19/30	67/12	1.91/142	1.91/142	2.55/100	.84/004	425	95	50/50	532	124	31/34	8,374	610	13/23
MA-71200-3	-	-	58	-	20	8	33.2	4.55	12.1	23/38	24/34	24/34	59/10	1.37/102	1.37/102	2.55/100	.84/004	425	95	50/50	532	124	31/34	8,374	610	13/23
MA-71200-4	-	-	27	32	27	1.0	28.1	1.74	4.06	19/17	20/24	23/33	Missed Reading	64/0	64/0	64/0	.81/004	422	113	34/34	756	136	31/32	8,433	675	16/19
MA-71200-5	-	-	41	-	26.8	18.2	1.0	40.0	2.46	6.97	10/47	11/77	13/37	38/12	48/12	48/12	.91/004	422	113	34/34	756	136	31/32	8,433	675	16/19
MA-71200-6	-	-	58	-	20	8	1.0	53.8	4.68	15.3	19/37	19/37	13/37	38/12	48/12	48/12	.91/004	422	113	34/34	756	136	31/32	8,433	675	16/19
MA-71200-7	-	-	32	27	32	1.0	36.3	1.75	4.44	27/22	31/22	38/23	.78/10.97	1.42/100	1.42/100	2.55/100	.84/004	422	113	34/34	756	136	31/32	8,433	675	16/19
MA-71200-8	-	-	33	8	-	26.8	18.2	1.0	86.5	2.50	8.19	9/87	10/21	16/31	31/31	54/11	.87/002	431	85	31/33	677	114	29/32	9,725	672	12/14
MA-71200-9	-	-	64	-	12	10	1.0	149	4.51	25.2	7/37	7/37	7/37	7/37	7/37	7/37	.74/009	516	95	30/33	365	75	30/37	4,707	424	18/25
MA-71200-10	-	-	32	27	32	1.0	116	1.76	4.73	30/34	31/20	41/17	.91/10.12	1.37/10.12	1.37/10.12	2.55/100	.84/004	555	72	23/27	893	97	20/24	810	436	9/10
MA-71200-11	-	-	34	20	-	9	21	1.0	234	2.46	13.5	12/31	14/31	17/47	17/47	17/47	.50/011	555	72	23/27	893	97	20/24	810	436	9/10
MA-71200-12	-	-	12	-	-	12	1.0	333	4.47	44.8	10/21	13/35	13/35	33/17	42/12	42/12	.39/022	637	78	22/26	907	105	22/28	10,190	308	8/12
MA-71200-13	-	-	26	30	30	1.0	17.6	1.59	3.46	43/087	Off Scale	Off Scale	Off Scale	Off Scale	Off Scale	Off Scale	.39/022	637	78	22/26	907	105	22/28	10,190	308	8/12
MA-71200-14	-	-	41	24	18.2	1.0	25.2	2.42	6.14	18/61	19/30	21/16	.68/10.32	1.03/10.32	1.03/10.32	2.55/100	.84/004	403	135	25/29	869	169	29/30	10,340	807	13/17
MA-71200-15	-	-	65	12	9	1.0	36.6	4.49	13.4	Off Scale	Off Scale	Off Scale	Off Scale	Off Scale	Off Scale	Off Scale	.92/002	659	114	27/27	1,183	149	27/27	11,700	554	14/20
MA-71200-16	-	-	32	27	27	1.0	28.1	1.74	4.09	31/20	39/15	Off Scale	.56/10.92	89/10.92	89/10.92	2.55/100	.84/004	377	93	39/40	629	111	29/31	9,735	690	13/16
MA-71200-17	-	-	61	-	26.8	18.2	1.0	40.0	2.46	6.97	12/97	12/97	12/97	61/13	61/13	61/13	.67/030	570	103	30/30	886	123	24/24	-	-	-
MA-71200-18	-	-	41	13	9	1.0	59.3	4.75	14.4	22/21	30/19	36/19	.82/10.92	1.46/10.92	1.46/10.92	2.55/100	.84/004	508	100	27/28	886	127	24/27	12,830	715	10/13
MA-71200-19	-	-	32	27	1.0	86.5	2.50	8.19	11/29	12/34	13/31	7/33	.87/10.22	1.85/10.22	1.85/10.22	2.55/100	.84/004	453	101	25/28	738	119	26/28	11,040	557	10/13
MA-71200-20	-	-	12	10	1.0	149	4.51	25.2	4.8/4.8	6/41	35	8/1	.56/10.92	40/10.92	40/10.92	2.55/100	.84/004	644	81	20/22	978	104	19/22	13,840	509	7/9
MA-71200-21	-	-	32	27	1.0	234	2.46	13.5	10/31	11/67	12/31	24/24	.27/10.92	32/10.92	32/10.92	2.55/100	.84/004	639	79	23/26	894	94	23/27	9,091	374	9/13
MA-71200-22	-	-	12	-	-	12	1.0	333	4.47	44.8	10/21	13/35	13/35	32/12	42/12	42/12	.39/022	637	79	23/26	894	94	23/27	9,091	374	9/13
MA-71200-23	-	-	27	32	27	1.0	18.4	1.23	3.81	33/23	37/27	36/24	.76/10.12	1.39/10.12	1.39/10.12	2.77/100	.83/002	-	-	-	-	-	-	-	-	-
MA-71200-24	-	-	41	26.8	18.2	1.0	25.2	2.42	6.14	19/31	29/41	18/18	Off Scale	1.15/10.32	1.15/10.32	2.55/100	.83/002	473	118	36/36	912	135	32/35	11,170	832	13/16
MA-71200-25	-	-	58	-	20	8	1.0	33.2	4.55	12.1	33/32	35/43	38/41	.61/10.72	.61/10.72	.61/10.72	.92/002	662	137	28/28	817	159	25/25	9,828	690	13/18
MA-71200-26	-	-	27	32	27	1.0	28.1	1.74	4.09	29/23	43/27	44/24	.48/10.32	1.30/10.32	1.30/10.32	2.55/100	.83/002	-	-	-	-	-	-	-	-	-
MA-71200-27	-	-	41	-	26.8	18.2	1.0	40.0	2.46	6.97	13/31	19/31	19/31	.61/10.12	.61/10.12	.61/10.12	.92/002	528	114	31/31	725	119	33/34	-	-	-
MA-71200-28	-	-	57	-	21	8	1.0	53.8	4.68	14.4	22/45	21/36	18/39	.49/10.32	.49/10.32	.49/10.32	.53/019	544	129	30/33	774	147	27/31	8,372	645	16/21
MA-71200-29	-	-	32	27	1.0	86.5	2.50	8.19	8/97	10/17	11/22	36/20	.48/10.22	.91/10.22	.91/10.22	2.55/100	.83/002	248	46	44/50	500	69	31/40	8,375	627	13/16
MA-71200-30	-	-	33	8	-	26.8	18.2	1.0	149	4.51	25.2	15/10	13/31	13/31	13/31	13/31	.33/10.92	654	98	21/21	800	116	24/26	8,812	526	12/15
MA-71200-31	-	-	64	-	12	10	1.0	149	4.51	25.2	29/23	28/20	24/24	.39/10.92	.39/10.92	.39/10.92	.39/028	654	98	21/21	800	116	24/26	8,812	526	12/15
MA-71200-32	-	-	6	-	30	30	1.0	114	1.76	4.25	13/17	15/19	16/17	27/13	27/13	27/13	.53/010	581	81	24/28	897	99	22/27	9,810	472	9/11
MA-71200-33	-	-	9	21	-	9	21	1.0	234	2.46	13.5	13/17	15/19	16/17	27/13	27/13	.38/10.92	581	81	24/28	897	99	22/27	9,810	472	9/11
MA-71200-34	-	-	12	-	-	12	1.0	333	4.47	44.8	9/21	13/33	9/17	13/35	13/35	13/35	.30/022	499	65	23/28	738	78	23/30	9,304	379	9/15
MA-71200-35	-	-	32	27	1.0	18.4	1.23	3.81	40/21	54/25	Off Scale	Off Scale	.77/10.62	1.46/10.62	1.46/10.62	2.55/100	.83/002	457	57	15/15	666	129	31/31	18,770	823	7/8
MA-71200-36	-	-	41	26.8	18.2	1.0	25.2	2.42	6.14	22/23	22/23	22/23	72/10	1.22/10.62	1.22/10.62	2.55/100	.83/002	683	130	24/28	948	169	27/27	12,450	936	12/12
MA-71200-37	-	-	65	12	9	1.0	36.6	4.49	13.4	Off Scale	Off Scale	Off Scale	Off Scale	83/10.62	83/10.62	2.77/10.62	.88/003	-	-	-	-	-	-	-	-	-
MA-71200-38	-	-	27	32	27	1.0	28.1	1.74	4.09	21/20	23/20	36/24	.63/10.32	1.44/10.32	1.44/10.32	2.55/100	.83/002	439	142	22/22	939	151	27/25	12,200	713	13/16
MA-71200-39	-	-	64	-	12	9	1.0	59.3	4.75	14.4	20/19	22/17	28/15	.46/10.92	.46/10.92	.46/10.92	.90/005	439	142	22/22	939	151	27/25	12,200	713	13/16
MA-71200-40	-	-	32	27	1.0	86.5	2.50	8.19	13/01	16/57	17/24	32/19	32/19	32/19	32/19	32/19	.93/002	439	142	22/22	939	151	27/25	12,200	713	13/16
MA-71200-41	-	-	33	8	-	26.8	18.2	1.0	149	4.51	25.2	13/01	16/57	17/24	32/19	32/19	.93/002	439	142	22/22	939	151	27/25	12,200	7	

TABLE 5. BURN RATE RESULTS FOR COMPOSITION NA-2L90-3

Mix Designation:	NA-2L00-3	NA-2L90-3	NA-2L90-3(3)**
	<u>Base Case</u>	<u>1% Linters (90μ)</u>	<u>3% Linters (90μ)*</u>
<u>Ballistic Results</u>			
Strand Burn Rate (in/sec) @ 1000 psia	0.75	0.77	0.82
Slope, n	0.37	0.41	0.45
<u>Linter Orientation</u>			
% Disparity	Good	Good	Good
Photomicrographs	-	Good	Good
<u>Composition, Wt. %</u>			
Binder	14	13	13
50 μ AP	58	58	56.65
20 μ AP	15	15	14.65
2 μ AP	13	13	12.70
90 μ Linters	-	1	3
Theoretical Specific Impulse (lb-f-sec/lb)	245.8	245.3	238.9

*Linters are added at expense of AP for concentrations greater than 1%.

**Linter concentrations greater than 1% are given in parentheses ().

TABLE 6. BURN RATE RESULTS FOR COMPOSITION NA-.7L90-4

Mix Designation:	NA-.7L00-4	NA-.7L90-4	NA-.7L90-4(3)**
	<u>Base Case</u>	<u>1% Linters (90μ)</u>	<u>3% Linters (90μ)*</u>
<u>Ballistic Results</u>			
Strand Burn Rate (in/sec) @ 1000 psia	1.18	1.30	1.37
Slope, n	0.91	0.92	0.95
<u>Linter Orientation</u>			
% Disparity	Marginal	Good	Good
Photomicrographs	-	Marginal	Marginal
<u>Composition, Wt. %</u>			
Binder	14	13	13
90 μ AP	27	27	26.37
6 μ AP	32	32	31.26
0.7 μ AP	27	27	26.37
90 μ Linters	-	1	3

*Linters are added at expense of AP for concentrations greater than 1%.

**Linter concentrations greater than 1% are given in ().

TABLE 7. TAILORING UFAP COMPOSITION TO OBTAIN LOW PRESSURE EXPONENT

Mix Designation:	<u>NA-2L90-3</u>	<u>NA-.7L90-13*</u>	<u>NA-.7L150-13</u>	<u>NA-.7L200-13</u>
<u>Ballistic Results</u>				
Strand Burn Rate (in/sec) @ 1000 psia	0.77	0.86	.89	.93
Slope, n	0.41	0.51	.56	.58
<u>Linter Orientation</u>				
% Disparity	Good	Marginal	Good	Good
Photomicrographs	Good	Good	Good	Good
<u>Composition, Wt. %</u>				
Binder	13	13	13	13
50 μ AP	58	58	58	58
20 μ AP	15	-	-	-
6 μ AP	-	15	15	15
2 μ AP	13	-	-	-
0.7 μ AP	-	13	13	13
Linters	1	1	1	1

* xx in NA - .7Lxx-13 indicates linter length used at the 1% level.

TABLE 8. RESULTS OF FIRST 5-GALLON MIX FOR COMPOSITION NA-2L90-3(3)M*

Composition, Wt. %

Binder	14.00
50 μ AP	55.66
20 μ AP	14.65
2 μ AP	12.69
90 μ Graphite Linters	3.00

Viscometric Results

Consistency Index, m Kp	18.3
Flow Behavior Index, n'	0.18

Ballistic Results

Strand Burn Rate, in/sec**	0.81
at 1000 psia	
Pressure Exponent	0.46
Rate Augmentation	$\approx 10\%$

Linter Orientation

% Disparity	Good
Photomicrographs	Good

Mechanical Properties

77°F	E ₀ , psi	629
0.74 min ⁻¹	σ_m , psi	124
	ϵ_m , %	29
-65°F	E ₀ , psi	8500
0.74 min ⁻¹	σ_m , psi	545
	ϵ_m , %	16
165°F	E ₀ , psi	510
0.74 min ⁻¹	σ_m , psi	113
	ϵ_m , %	28

*M indicates modification (reduced solids level).

**Motor molds filled improperly, no motors were fired.

TABLE 9. RESULTS OF SECOND 5-GALLON MIX FOR COMPOSITION NA-2L200-6(2)

Composition, Wt. %

Binder	15.00
90 μ AP	55.66
20 μ AP	13.18
2 μ AP	14.16
200 μ Linters	2.00

Viscometric Results

Consistency Index, m Kp	8.0
Flow Behavior Index, n'	0.31

Lintar Orientation

% Disparity
Photomicrographs

Marginal
Marginal

Mechanical Properties

77°F	{	E _o , psi	656
0.74 min ⁻¹		σ_m , psi	149
		ϵ_m , %	30
-65°F	{	E _o , psi	5580
0.74 min ⁻¹		σ_m , psi	597
		ϵ_m , %	25
165°F	{	E _o , psi	467
0.74 min ⁻¹		σ_m , psi	129
		ϵ_m , %	36

TABLE 10. LINTER UTILITY IN IRON OXIDE RESULTS

Mix Designation:	NA-.7L00-2M* (85% Solids)	NA-.7L00-2MI* (85% Solids)	NA-.7L150-2(3)MI (86% Solids)
<u>Composition</u>			
Binder	15.00	15.00	14.00
H60 Al	15.00	14.82	14.82
50 μ AP	25.30	25.00	24.27
6 μ AP	26.63	26.32	25.56
0.7 μ AP	18.07	17.86	17.35
Imperial Iron Oxide	-	1.00	1.00
150 μ Linters	-	-	3.00
<u>Viscometric Results</u>			
Consistency Index, m Kp	5.2	Missed	11.7
Flow Behavior Index, n'	0.28	Readings	0.13
<u>Ballistic Results</u>			
Strand Burn Rate, in/sec at 1000 psia	0.78	1.50	2.10
Pressure Exponent	0.70	0.58	0.72
<u>Linter Orientation</u>			
% Disparity	Good	Good	Marginal
Photomicrographs			Marginal

*M indicates modification; namely, aluminum fuel is added to the composition and solids level is reduced. I indicates iron oxide is present in composition.

TABLE 11. COMPOSITIONS FOR COMBUSTION MECHANISM STUDIES

Propellant Designation

NA-2L00-2

NA-2L00-2 w/0.5% Fe_2O_3

NA-2L00-2 w/1.0% Fe_2O_3

NA-2L00-3

NA-2L00-3 w/0.5% Fe_2O_3

NA-2L00-3 w/1.0% Fe_2O_3

NA-2L00-8

NA-.7L00-2

NA-.7L00-2 w/0.5% Fe_2O_3

NA-.7L00-2 w/1.0% Fe_2O_3

NA-2L1/4-2(.1)

For each composition, 200 μ and 1/4 inch graphite linters were manually placed between two 1/16-inch layers of propellant.

1/4-inch graphite linter were evenly dispersed at a concentration of 0.1%.

TABLE 12. PROPELLANT INGREDIENTS

Mix Designation	Linter		AP Distribution (%)			
	Size	Weight (%)	200 μ	90 μ	20 μ	2 μ
NA-2L00-8 10-BPC-214	---	0.0*	33.0	23.0		30.0
NA-2L90-8 10-BPC-215	90	1.0	33.0	23.0		30.0
NA-2L90-8(3) 10-BPC-216	90	3.0	32.2	22.5		29.3
NA-2L200-8M(3) 10-BPC-217	200	3.0	36.1	21.5		26.4
NA-2L00-6M 10-BPC-226	---	0.0*		57.0	14.0	14.0
NA-2L90-6(3) M 10-BPC-228	90	3.0		55.6	13.7	13.7
NA-2L200-6M 10-BPC-229	200	3.0		57.0	14.0	14.0

*Baseline formulations with no linters

TABLE 13. COMPUTER ANALYSIS RESULTS OF 1000 HZ DATA

Prop	B_s	R_{Vi}	α_{Pd}	Variance Explained
NA-2LOC-8	$3.6 \pm 0.6^*$	-0.9 ± 1.3	0	0.842
NA-2L90-8	2.9 ± 0.6	0.4 ± 1.5	10.5 ± 29	0.929
NA-2L90-8(3)	2.1 ± 0.5	0.7 ± 0.9	18.7 ± 11	0.901
NA-2L200-8(3)M	2.1 ± 0.5	1.4 ± 1.0	22.0 ± 10	0.927
NA-2L00-6M	2.5 ± 0.2	0.6 ± 0.9	0	0.954
NA-2L90-6(3)M	1.5 ± 0.4	2.1 ± 0.8	30.2 ± 18	0.938
NA-2L200-6M	1.9 ± 1.7	1.6 ± 2.2	15.3 ± 120	0.850

*Error bands represent a 95 percent confidence level

TABLE 14. BURN RATE CHANGES AS MEASURED FROM T-BURNER DATA
(Measured at 1000 psia, 1000 Hz)

Prop	Avg Burn Rate	Percent Increase Over Baseline	Linter Content
NA-2L00-8	0.46	Baseline	None
NA-2L90-8	0.51	11%	1% - 90 μ
NA-2L90-8(3)	0.53	15%	3% - 90 μ
NA-2L200-8(3)M	0.57	24%	3% - 200 μ
NA-2L00-6M	0.50	Baseline	None
NA-2L90-6(3)M	0.57	14%	3% - 90 μ
NA-2L200-6M	0.57	14%	1% - 200 μ

TABLE 15. PARTICLE DAMPING CHARACTERISTIC DATA

Prop	Measured Test Frequency	ω	α_{Pd} Measured	Dia (μ) at α_{Pd}	Dia (μ) at Maximum α_{Pd}	Damping Efficiency $\frac{\alpha_{Pd}}{\alpha_{Pd \text{ max}}}$
NA-2L00-8	2309	1.45E4	No particle additive			
	4188	2.63E4	No particle additive			
	987	0.62E4	No particle additive			
NA-2L90-8	997	0.63E4	-10.5	17.4	10.7	67%
	2324	1.46E4	-17.0	14.5	7.0	47%
	4074	2.56E4	-37.0	9.9	5.3	58%
NA-2L90-8(3)	979	0.62E4	-18.7	23.6	10.8	41%
	2275	1.43E4	-36.0	17.1	7.1	35%
	3841	2.41E4	-33.0	17.9	5.5	19%
NA-2L200-8(3)M	964	0.61E4	-22.0	21.5	10.9	50%
	2197	1.38E4	-46.0	15.2	7.3	46%
	3846	2.42E4	-129.0	9.1	5.5	73%
NA-2L00-6M	1010	0.63E4	No particle additive			
	2240	1.41E4	No particle additive			
	3829	2.41E4	No particle additive			
NA-2L90-6(3)M	965	0.61E4	-30.2	17.7	10.9	68%
	2198	1.38E4	-26.0	20.2	7.3	26%
	3902	2.45E4	-83.0	11.3	5.4	47%
NA-2L200-6M	983	0.62E4	-15.3	11.3	10.8	100%
	2147	1.35E4	-17.0	14.5	7.3	51%
	3914	2.46E4	-42.0	9.2	5.4	69%

TABLE 16. PROCESSING IMPROVEMENT RESULTS

Mix Designation	NA-.7L00-8 (14% Binder)	NA-2L200-3A*(3) (13% Binder)	NA-.7L00-7 (14% Binder)	NA-2L200-7A(3) (13% Binder)	NA-.7L00-4 (14% Binder)	NA-2L150-4A(2) (13% Binder)
<u>Viscometric Results</u>						
Consistency, m Kp	10.9	7.1	16.0	7.4	12.9	11.4
Flow Behavior Index, n'	0.26	0.36	0.25	0.38	0.14	0.43
<u>Ballistic Results</u>						
Strand Burn Rate, in/sec @ 1000 psia	0.50	0.59	1.22	1.10	1.39	1.02
Pressure Exponent	0.52	0.59	0.74	0.80	0.89	0.78
<u>Mechanical Properties</u>						
77°F						
0.74 min ⁻¹	E _o , psi σ _m , psi ε _m , %	396 45 30	457 107 33	1,038 140 26	577 128 33	1,910 221 17
-65°F						
0.74 min ⁻¹	E _o , psi σ _m , psi ε _m , %	6,130 428 16	10,340 647 16	11,130 706 11	12,150 728 11	20,410 796 8
165°F						
0.74 min ⁻¹	E _o , psi σ _m , psi ε _m , %	170 27 37	321 79 31	437 105 23	644 112 25	1,250 198 19
<u>Linters Orientation</u>						
Burn Rate Disparity		Poor**		Poor**		Marginal
Photomicrographs		Marginal		Marginal		Marginal

*A indicates analog where the base case 0.7μ AP fraction is replaced by 2μ AP and linters. In addition, the 6μ AP fraction of the base case is replaced by 20μ AP in the analog composition.

**2000 psia results gave poor rating.

(This page is intentionally left blank)

SECTION VI
APPENDIX I

NOMENCLATURE

a	Empirical constant in burn rate correlation
α	Acoustic response function
α_c	Corrected acoustic growth or decay
α_{pd}	Particle damping coefficient
α_o	Measured acoustic growth or decay
A	Particle surface area
B_s	Pressure-coupled driving function
C_D	Drag coefficient
C_m	Weight of acoustic stabilizing additive
c	Burn rate coefficient
\bar{d}_{rate}^*	Rate mean diameter
d_{32}^*	Surface mean diameter
d_{43}^*	Volume mean diameter
d_i	Diameter of i^{th} particle size fraction
D	Theoretical particle diameter for T-burner
ϵ_b	Strain at break
ϵ_m	Strain at maximum tensile strength
$\dot{\epsilon}$	Normal strain rate
E_o	Initial normal modulus
f	Frequency
F_D	Drag on particle
$\dot{\gamma}$	Shear rate
h	Rate of curvature change for α versus mass burned
ht	Curvature

*See Table 1 for defining expressions.

H	Total heat transfer change
J(Δ)	Parameter in burn rate correlation
k ₁ , k ₂	Empirical constants in burn rate correlation
Kp	Kilopoise
L	Total change in acoustic losses
m	Consistency index (apparent viscosity at 1 sec ⁻¹)
n	Burn rate exponent
n'	Flow behavior index
n _i	Number of particles in i th size fraction
η_{app}	Apparent Newtonian viscosity
ω	Angular frequency
r _b	Burn rate
Rv ⁱ	Velocity-coupled driving function
ρ	Density
σ_m	Maximum tensile strength
S _i	Particle surface area of i th size
t	Time α was measured
τ	Time
τ_s	Shear stress
V _i	Particle volume of i th size
% Disparity	[100(high rate-low rate)/high rate] constant pressure
AP	Ammonium perchlorate
Al	Aluminum
Al ₂ O ₃	Aluminum oxide
A02246	Antioxidant

DBTDA	Dibutyltin diacetate
Fe ₂ O ₃	Imperial iron oxide (transparent)
IDP	Isodecyl pelargonate plasticizer
IPDI	Isophorone diisocyanate
Polygard	Peroxide decomposer
R45M	Hydroxyl terminated polybutadiene
VATB	Variable area T-burner
ZrC	Zirconium carbide

APPENDIX II

BURN RATE CORRELATION

The strand burn rate results generated for the 2 μ fine AP series in the screening exercise indicate that the 50 μ linter-containing compositions have a rate the same as the base case (no linters). Attempts to correlate unaugmented burn rates using simple moments of the solids (AP) distributions produced anomalous behavior. Conventional moments such as d_{43} , d_{32} (or SSA), and \bar{d}_{rate} do not correlate the entire range of results.

The approach to developing a semi-empirical burn rate model was phenomenological. It is postulated that coarse AP particles have the potential to or conceal the influence of fine AP particles during propellant burning. That is, the flame structure is envisioned to overlap the cross-sectional area of the coarse AP particles whereby smaller AP particles are engulfed and nullified. The area of overlap contributes to adjustable parameters in a burn rate model which, in simplified form, is:

$$r_b = k_1 (\bar{d}_{rate})^{-1/3} - k_2 (C') \quad (A1)$$

where: r_b = burn rate
 \bar{d}_{rate} = theoretically derived average size
 k_1, k_2 = adjustable empirical constants
 C' = correction factor for flame overlap

$$= \sum_{i=0}^{\infty} w_i d_i^{-1/3} - \sum_{j=j(\Delta)}^{\infty} w_j d_j^a \quad (A2)$$

where: a = constant dependent on model for hidden areas
 $j(\Delta)$ = lower size limit representing smallest coarse crystal that will hide a diameter, d_i .

Solving for the effective correlating average particle size yields:

$$\left(\bar{d}_{rate_{eff}} \right)^{-1/3} = \left(\bar{d}_{rate} \right)^{-1/3} - \frac{k_2}{k_1} (C') \quad (A3)$$

where: $\bar{d}_{rate_{eff}}$ = effective or corrected correlating moment.

The model was applied to the 2μ fine AP series base rates (50μ linter-containing compositions) and the results are shown in Figure A1. The correlation is quite good for the entire set of results. The use of conventional moments did not produce the good fit shown in Figure A1. Figure A2 shows an attempted correlation using the single moment d_{43} as an example of not being able to fit all the data using a single conventional moment.

The conclusion drawn from this burn rate analysis is that oxidizer distribution width must be accounted for when a general burn rate correlation is attempted.

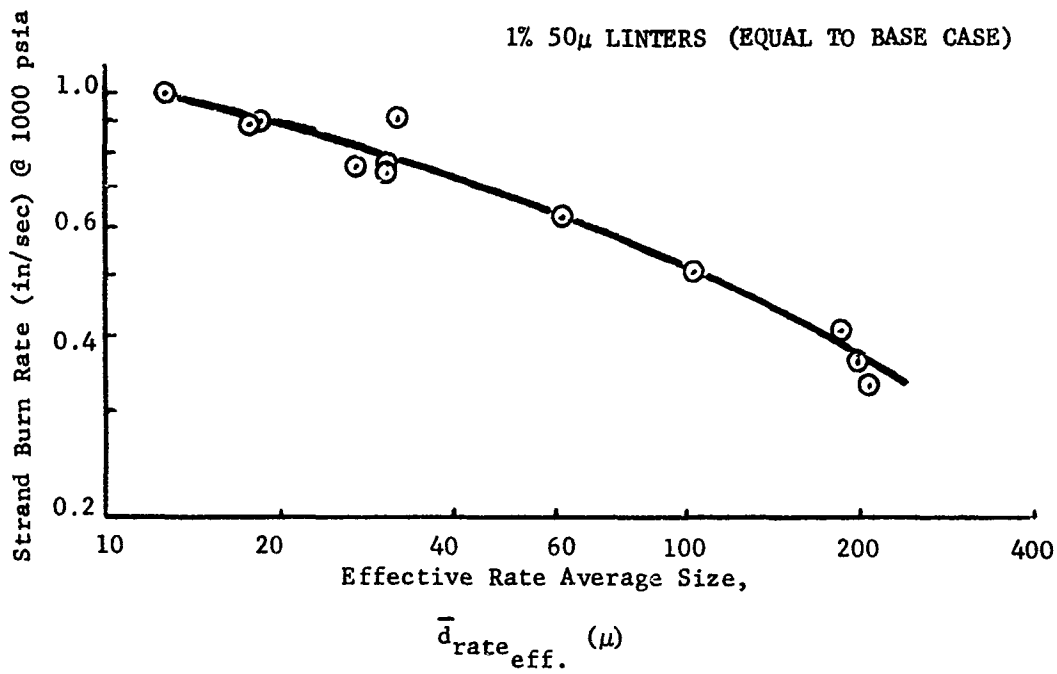


Figure A1. Test of Oxidizer Distribution Correlating Function

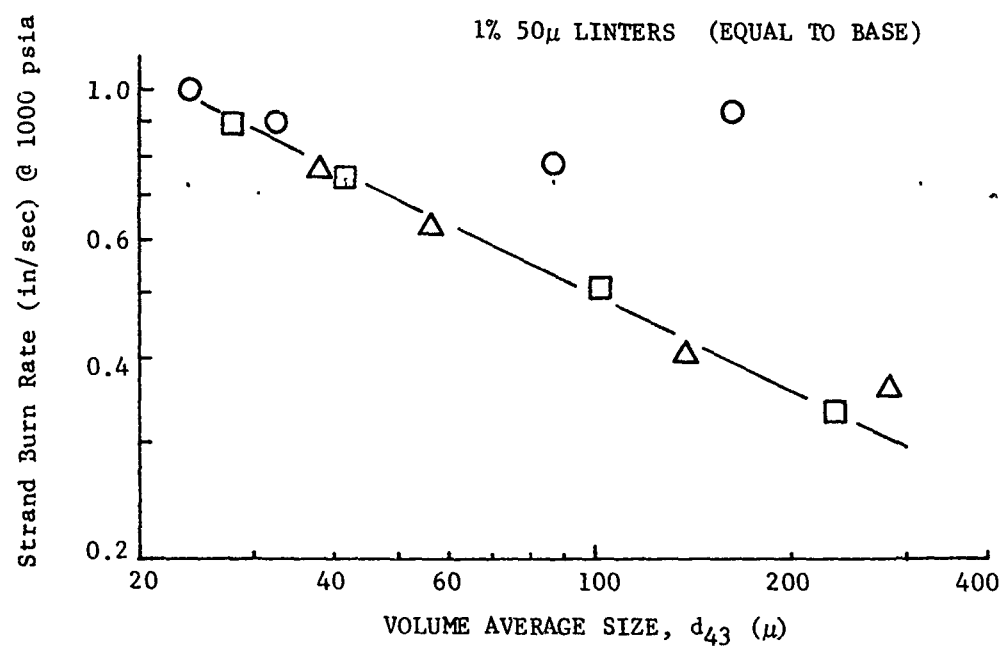


Figure A2. Attempted Burn Rate Correlation
Using Conventional Moment